11-2014

NARROWBAND AND WIDEBAND SPECTRUM SENSING FOR COGNITIVE RADIO NETWORKS IN A LOG-NORMAL SHADOWING ENVIRONMENT

Nedaa Yousef Mohammad Al Hussien

United Arab Emirates University

College of Engineering

Department of Electrical Engineering

NARROWBAND AND WIDEBAND SPECTRUM SENSING FOR COGNITIVE RADIO NETWORKS IN A LOG-NORMAL SHADOWING ENVIRONMENT

Nedaa Yousef Mohammad Al Hussien

This thesis is submitted in partial fulfillment of the requirements for the degree of Master of Science in Electrical Engineering

Under the Supervision of Dr. Mohammed Abdel-Hafez

November 2014

Declaration of Original Work

I, Nedaa Yousef Mohammad Alhussien, the undersigned, a graduate student at the United Arab Emirates University (UAEU), and the author of this thesis entitled "*Narrowband and Wideband Spectrum Sensing for Cognitive Radio Networks in a Log-normal Shadowing Environment"* hereby, solemnly declare that this thesis is an original research work that has been done and prepared by me under the supervision of Dr. Mohammed Abdel-Hafez, in the College of Engineering at UAEU. This work has not been previously formed as the basis for the award of any academic degree, diploma or a similar title at this or any other university. The materials borrowed from other sources and included in my thesis have been properly cited and acknowledged.

Student's Signature _____ Date _____

Approval of the Master Thesis

This Master Thesis is approved by the following Examining Committee Members:

1) Advisor (Committee Chair): Dr. Mohammed Abdel-Hafez

Title: Associate Professor

Department of Electrical Engineering

College of Engineering

Signature _____Date_____

2) Member: Dr. Atef Abdrabou

Title: Assistant Professor

Department of Electrical Engineering

College of Engineering

Signature _____Date_____

3) Member (External Examiner): Dr. Pavel Loskot

Title: Assistant Professor

College of Engineering

Institution: Swansea University (United Kingdom)

Signature _____Date_____

This Master Thesis is accepted by:

Dean of the College of Engineering: Prof. Mohsen Sherif

Signature _____Date_____

Dean of the College of Graduate Studies: Prof. Nagi Wakim

Signature _____Date_____

Copy ____ of ____

Abstract

The efficiency of cognitive radio networks mainly depends on the spectrum sensing stage, in which spectrum opportunities are exploited. However, one of the challenges facing spectrum sensing is the presence of fading and log-normal shadowing. Moreover, when the spectrum utilization is high and details regarding primary user activity are not available, a need to sense the whole spectrum arises. Hence, developing wideband spectrum sensing technique is a fundamental concern.

In this thesis a narrowband spectrum sensing in a log-normal shadowing environment is addressed, a closed-form expression for the probability of detection under shadowing is derived. The accuracy of the expression is tested using a MATLAB simulation. Collaborative spectrum sensing is addressed, and expressions for the probability of detection and false alarm in both AWGN channels and log-normal channels are derived for different fusion rules namely; soft fusion using square-law selection (SLS), square-law combining (SLC), hard fusion using OR, AND and Majority combining. The detection performance of these fusion rules is tested and compared. Simulation results showed that sensing performance is enhanced due to collaboration and better detection is achieved with more collaborative secondary users. Moreover, SLC outperforms SLS in terms of the probability of detection. OR-combining is found to outperform both AND-combining and Majority-combining from the primary user's point of view by providing higher protection for the primary user from any secondary user interference; while AND-combining is found to outperform the other two techniques, from the secondary user perspective, as it results in higher spectrum utilization and more spectrum opportunities.

Wideband spectrum sensing using wavelet-based detection is investigated. The performance of this method and the effect of parameters such as the scale factor of the wavelet smoothing function, collaboration between secondary users in edge detection and the presence of log-normal shadowing is investigated and analyzed using MATLAB simulation. Simulation results indicate that better edge detection was achieved at higher scale factor values. Log-normal shadowing affected the accuracy of edge detection since it attenuates the average power received at the secondary user, and adds random variations at the same time as detecting false edges.

Two approaches to wideband spectrum detection are investigated and compared. The first approach is the tunable bandpass filter (TBPF) filterbank. The second approach is a proposed model using wavelet-based detection. Simulation results indicate that the proposed approach performed better in terms of spectrum occupancy and utilization as it accurately detected the primary user signal. While the TBPF filterbank approach failed to detect the primary user at low probabilities of false alarm when it partially occupied the subbands, leading to more interference for the primary user.

Keywords: Cognitive radio, spectrum sensing, narrowband sensing, log-normal shadowing, collaborative sensing, soft fusion, hard fusion, wideband sensing, wavelet-based detection.

Title and Abstract (in Arabic)

استشعار الطيف الترددي للنطاق الضيق و الواسع في شبكات الراديو المعرفية في بيئة التظليل اللوغاريتمي

الملخص

تشكل ندرة الطيف الترددي عائقاً أمام تطوير شبكات الاتصال اللاسلكية من حيث تقديم خدمات جديدة أو تحسين الخدمات الموجودة. إضافة إلى ذلك فإن جدول توزيع الترددات القائم على فكرة تخصيص الترددات الموجودة للمستخدمين المرخصين (الأوليين) بشكل ثابت تزيد من مشكلة ندرة الطيف و عدم كفاءة استخدامه. لذلك تم طرح مبدأ الراديو المعرفي للتغلب على ذلك من خلال السماح للمستخدمين غير المرخصين (الثانويين) باستخدام الترددات المخصصة للمستخدمين الأوليين في الوقت الذي تكون فيه متاحة.

إن كفاءة و فعالية شبكات الراديو المعرفي تعتمد بشكل أساسي على مرحلة استشعار الطيف الترددي، و التي يتم خلالها الحصول على معلومات عن كثافة استخدام الترددات. لكن دقة استشعار الطيف تتأثر بوجود التظليل اللوغاريتمي. كذلك فإن عدم توفر معلومات كافية عن المستخدم الأولي يتطلب استشعار الطيف على النطاق الواسع، و لذلك فإن تطوير تقنيات استشعار للنطاق الواسع ضروري.

بداية تناولت هذه الأطروحة استشعار الطيف الترددي على النطاق الضيق باستخدام الاستشعار الفردي و درست تأثير التظليل اللوغاريتمي على دقة استشعار الطيف . حيث تم اشتقاق معادلة لحساب احتمال استشعار المستخدم الأولي في بيئة التظليل اللوغاريتمي و تم اختبار دقتها، و قد أظهرت النتائج أن دقة استشعار الطيف تتدنى في وجود التظليلي اللوغاريتمي. كذلك تناولت مبدأ الاستشعار التعاوني المستخدم للتغلب على تأثير التظليل اللوغاريتمي، حيث يتم استشعار الطيف من قبل أكثر من مستخدم ثانوي و من ثم تجميع نتائج الاستشعار لاتخاذ قرار نهائي بخصوص وجود المستخدم الأولي أو غيابه. و توجد عدة طرق مستخدمة للجمع بين نتائج الاستشعار التعاوني منها طرق التجميع اللينة و تتضمن القانون التربيعي للتجميع و القانون التربيعي للاختيار، و هناك طرق التجميع القاسية. و قد أظهرت النتائج التحسن في دقة استشعار الطيف نتيجة استخدام الاستشعار التعاوني خاصة مع زيادة عدد أجهزة الاستشعار الثانوية. كما أن طرق التجميع اللينة أظهرت تفوقها على طرق التجميع القاسية، إلا أن زيادة تكلفتها و تعقيدها تعطي الأفضلية لطرق التجميع القاسية.

و من ناحية أخرى، تمت دراسة استشعار الطيف الترددي على النطاق الواسع باستخدام طريقة المويجات القائمة على كشف الحواف الموجودة في الطيف. هذه الحواف تمثل الفواصل بين مناطق الطيف المستخدم من قبل المستخدم الأولي و الطيف المتاح للمستخدم الثانوي. و قد تم تفحص تأثير عدد من العوامل على أداء هذه الطريقة لاستشعار الطيف الواسع منها عامل القياس و شكل الطيف و كذلك وجود التظليل اللوغاريتمي. و قد أظهرت النتائج أن دقة الاستشعار باستخدام المويجات تزداد مع زيادة قيمة عامل القياس، كما

أن وجود التظليلي اللوغاريتمي يؤثر سلباً على دقة الاستشعار حيث يزيد من عدد الحواف الخاطئة و يقلل احتمالية اكتشاف الحواف الصحيحة.

و قد تم مقارنة أداء طريقتين لاستشعار الطيف الترددي على النطاق الواسع: الأولى باستخدام مجموعة من مرشحات تمرير الطيف، حيث يقوم كل مرشح باستشعار وجود المستخدم الأولي في جزء معين من الطيف الواسع. و الثانية باستخدام طريقة المويجات الموضحة سابقاً حيث يتم استشعار المستخدم الأولي في مناطق الطيف الواقعة بين الحواف المكتشفة. و قد أظهرت النتائج تفوق طريقة المويجات على طريقة مرشحات تمرير الطيف من خلال قدرتها على اكتشاف وجود المستخدم الأولي بدقة، بينما فشلت طريقة المرشحات في استشعار المستخدم الأولي في بعض مناطق الطيف المستخدمة بشكل جزئي.

Acknowledgements

First and foremost I would like to convey my deepest gratitude to my thesis advisor, Dr. Mohammed Abdel-Hafez, for introducing me to this topic, and for his guidance and support throughout my thesis. His knowledge and patience helped me overcome many difficult situations and finish this thesis. I wish that one day I would be a good advisor to my students as Dr. Mohammed has been to me.

Many thanks go to my thesis co-advisor, Dr. Khaled Shuaib. He generously gave me time to offer valuable comments toward improving my thesis. I would like to thank my examining committee members, Dr. Atef Abdrabou and Dr. Pavel Loskot for their time and precious feedback.

I wish to thank the Department of the Electrical Engineering for providing me a good working environment. To my friends who have been a good accompany and support for me throughout this journey.

Words cannot express who grateful I am to my family for their support and encouragement. My sincere gratitude to my parents, your prayer for me was what helped during my hardest times.

To my sweet angel and lovely daughter, Lamar. You are the light of my life, and the very core of my soul. Last but not least, I thank with deep love my beloved husband, Younes. You have been a constant source of love and strength for me during my good and bad times. Words fail me to express my appreciation for your confidence in me and your patience. Without your encouragement and support this accomplishment would not have been possible.

Dedication

I dedicate this thesis to my beloved husband, Younes, for his unconditional love and support during my graduate study and life. To my lovely daughter, Lamar, whose presence in my life kept me strong during the hard times. To my beloved parents for their boundless love, encouragement and payers.

Table of Contents

List of Tables

List of Figures

Acronyms and Abbreviations

ADC	Analogue-to-digital converter
AIC	Analogue-to-information converter
AoA	Angle of arrival
AOC	Area of coverage
AWGN	Additive white Gaussian noise
BPF	Bandpass filter
CAF	Cyclic autocorrelation function
CR	Cognitive radio
CROC	Complementary receiver operating characteristic
CS	Compressed sensing
CSD	Cyclic spectrum density
CWT	Continuous Wavelet transform
dB	Decibels
DSSS	Direct sequence spread spectrum
DTFT	Discrete-time Fourier transform
DTV	Digital television
ECC	Electronic communications committee
FC	Fusion center
FCC	Federal communications commission
FHSS	Frequency hopping spread spectrum
FT	Fourier transform
i.i.d	Independent and identically distributed
MAC	Medium access control
MGF	Moment generating function
MRC	Maximal ratio combining
MRS	Asynchronous multirate sampling
MRSS	Multi-resolution spectrum sensing
MWC	Modulated wideband converter
Ofcom	Office of communications
PDF	Probability density function
PHY	Physical
PSD	Power spectral density
PU	Primary user
QoS	Quality of service
RF	Radio frequency
RFE	Radio frequency front-end
RV	Random variable
SC	Selection combining
SLC	Square-law combining
SLS	Square-law selection
SMRS	Synchronous multirate sampling
SNR	Signal-to-noise ratio

STFT	Short-time Fourier transform
SU	Secondary user
TBPF	Tunable bandpass filter
TV	Television
TVWS	Television white spaces

Glossary

$r(t)$	Signal received by the secondary user
$R_r^{(\beta)}(\tau)$	Cyclic autocorrelation function
$E[.]$	Expectation operator
β	Cyclic frequency
$S(f,\beta)$	Cyclic spectrum density function
f_c	Center frequency
W	Signal bandwidth
T	Sensing interval
N_0	One-sided noise power spectral density
λ	Energy threshold
V	Test statistic
H_0	Hypothesis of the primary user's absence
H_1	Hypothesis of the primary user's presence
$s(t)$	Primary user transmitted signal
$n(t)$	Additive white Gaussian noise
σ^2	Variance of the random variable
σ_n^2	Variance of the AWGN
μ	Mean of the random variable
N_s	Half number of samples
P_d	Probability of detection
P_m	Probability of misdetection
P_f	Probability of false alarm
$\Gamma(.)$	Gamma function
$\Gamma(.,.)$	Upper incomplete gamma function
${}_0F_1(.,.)$	Confluent hyper-geometric function
$Q_N(.,.)$	Generalized Marcum-Q function
γ	Average signal-to-noise ratio of the primary user signal received by the secondary user
$h(t)$	Linear channel gain between the primary user and the secondary user
$P_{d,log}$	Probability of detection in a log-normal shadowing channel
$P_{m,log}$	Probability of misdetection in a log-normal shadowing channel
$I_{N_s-1}(.)$	Modified Bessel function of order (N_s-1)
M	Gauss-Hermite integration order
w_i	Gauss-Hermite integration weight
α_i	Gauss-Hermite integration abscissa
k	Number of collaborative secondary users
C_d	Collaborative probability of detection

C_m	Collaborative probability of misdetection
C_f	Collaborative probability of false alarm
$\binom{k}{l}$	l combinations out of k
$C_{d,AND}$	Collaborative probability of detection using hard fusion with AND-combining
$C_{d,OR}$	Collaborative probability of detection using hard fusion with OR-combining
$C_{d,MAJ}$	Collaborative probability of detection using hard fusion with Majority-combining
V_{SLS}	Test statistic in collaborative sensing using soft fusion with SLS combining scheme
$P_{d,SLS}$	Collaborative probability of detection using soft fusion with SLS combining scheme
$P_{f,SLS}$	Collaborative probability of false alarm using soft fusion with SLS combining scheme
$P_{d,SLS}^{log}$	Collaborative probability of detection in a log-normal shadowing channel using soft fusion with SLS combining scheme
V_{SLC}	Test statistic in collaborative sensing using soft fusion with SLC combining scheme
$P_{d,SLC}$	Collaborative probability of detection using soft fusion with SLC combining scheme
$P_{f,SLC}$	Collaborative probability of false alarm using soft fusion with SLC combining scheme
$P_{d,SLC}^{log}$	Collaborative probability of detection in a log-normal shadowing channel using soft fusion with SLC combining scheme
$\Psi(.)$	Moment generating function
$S_{rr}(f_i)$	Power spectral density of the received signal $r(t)$ in the *i*-th subband
N_f	Root-Nyquist filter order
f_s	Sampling rate
N	Number of frequency subbands in the wideband signal
B	Wideband signal total bandwidth
B_n	Bandwidth of the *n*-th subband
$f_{c,n}$	Center frequency of the *n*-th subband
$S_n(f)$	Power spectral shape within the *n*-th subband
$S_r(f)$	Power spectral density of the received wideband signal $r(t)$
$S_w(f)$	Power spectral density of the wideband additive white Gaussian noise $w(t)$
a_n^2	Power density within the *n*-th subband

s	Scale factor of the Wavelet function
$\phi(f)$	Wavelet mother function
$\mathcal{W}_s(S_r(f))$	Continuous Wavelet transform of $S_r(f)$
$\mathcal{W}_s'(S_r(f))$	First derivative of $\mathcal{W}_s S_r(f)$
$\mathcal{W}_s''(S_r(f))$	Second derivative of $\mathcal{W}_s S_r(f)$
$U_J(S_r(f))$	Multiscale wavelet product of J CWT gradients
β_n	Estimated power density within the *n*-th subband
$\mathcal{F}\{.\}$	Fourier transform operator
$R_r(\tau)$	Autocorrelation function of the received signal $r(t)$
$h_n(t)$	Linear channel gain between the primary user and secondary user in the *n*-th subband
$r_{log}(t)$	Signal received by the secondary user under log-normal shadowing

CHAPTER 1: INTRODUCTION

This thesis addresses spectrum sensing in cognitive radio networks. Spectrum sensing is the first and most important cognitive task upon which the entire operation of cognitive radio relies. Sensing can be performed either on narrowband or wideband levels. Narrowband sensing is performed when there is enough information about the primary user's signaling, center frequency and bandwidth. However, sensing performance on a narrowband level is affected by fading and log-normal shadowing.

On the other hand, wideband spectrum sensing obtains better utilization of the frequency spectrum, when the occupancy details of the primary users are unknown to cognitive network users. The design and implementation of wideband sensing systems are both difficult due to high implementation complexity and large energy consumption from high-rate analogue-to-digital converters (ADC).

1.1 Motivation

Radio frequency (RF) spectrum scarcity is the main challenge facing the development of wireless communication networks. The introduction of new services that require high data rates, the spread of smartphones and social networks and the wish of users to stay fully connected increased the demand on frequency spectrum. The allocation of frequency bands is controlled by government regulators such as the office of communications (Ofcom) in the United Kingdom, the federal communications commission (FCC) in the United States [1], and the telecommunication regulatory authority (TRA) in the UAE. Current allocation policies are characterized by static frequency allocation where the frequency bands are assigned to licensed networks and users on a long-term basis within a certain geographical area. However, measurements indicate that these bands are unused by the licensed users for significant periods of time, resulting in spectrum under-utilization [2]. For example experiments indicate that the maximal occupancy of the spectrum from 30 MHz to 3 GHz in New York city is only 13.1%, with an average occupancy (over six locations) of 5.2%, as was shown in Figure 1-1[3]. To overcome the issue of spectrum under-utilization and accommodate the growing demand,

cognitive radio (CR) networks were proposed. As a promising technology, cognitive radio networks allow unlicensed (secondary) users to access the licensed spectrum opportunistically without causing harmful interferences to the licensed (primary) users.

To achieve this spectrum sensing defines spectrum opportunities (holes) that can be used for opportunistic access as shown in Figure 1-2. It is crucial to perform spectrum sensing efficiently and rapidly to guarantee better spectrum utilization for the secondary users and higher interference protection for the primary users at the same time. Therefore, different spectrum sensing techniques have been developed to perform sensing based on available information about primary user signaling [4]. Throughout this thesis energy detection is used for spectrum sensing because of its generality and simplicity. However, sensing performance is affected by fading and log-normal shadowing where the secondary user cannot distinguish between a faded band and an empty band. To alleviate this degradation in sensing performance, collaborative spectrum sensing is used [5, 6], in which multiple secondary users sense the spectrum and share their sensing information to help make a more reliable decisions regarding the presence of the primary user within the frequency band. Different fusion rules are used to combine local decisions, including soft fusion and hard fusion rules, and each rule is associated with a certain sensing performance levels.

On the other hand, when spectrum utilization is low and information about the primary user is scarce, multiple frequency bands are sensed at the same time using wideband sensing. One of the wideband sensing approaches is the tunable bandpass filters (TBPF) bank, in which a parallel structure of tunable BPFs is used to sense multiple frequency bands at the same time with the center frequency and bandwidth of each BPF preset. However, this structure requires a large number of components resulting in high implementation complexity. Other wideband sensing techniques have been developed [7-15] such as the filter bank detection, multicoset sampling based detection, multirate sampling based detection, wavelet-based detection and compressed sensing (CS). In this thesis wavelet-based detection performs wideband sensing as it is simple and has the ability to adapt to a large dynamic spectrum range.

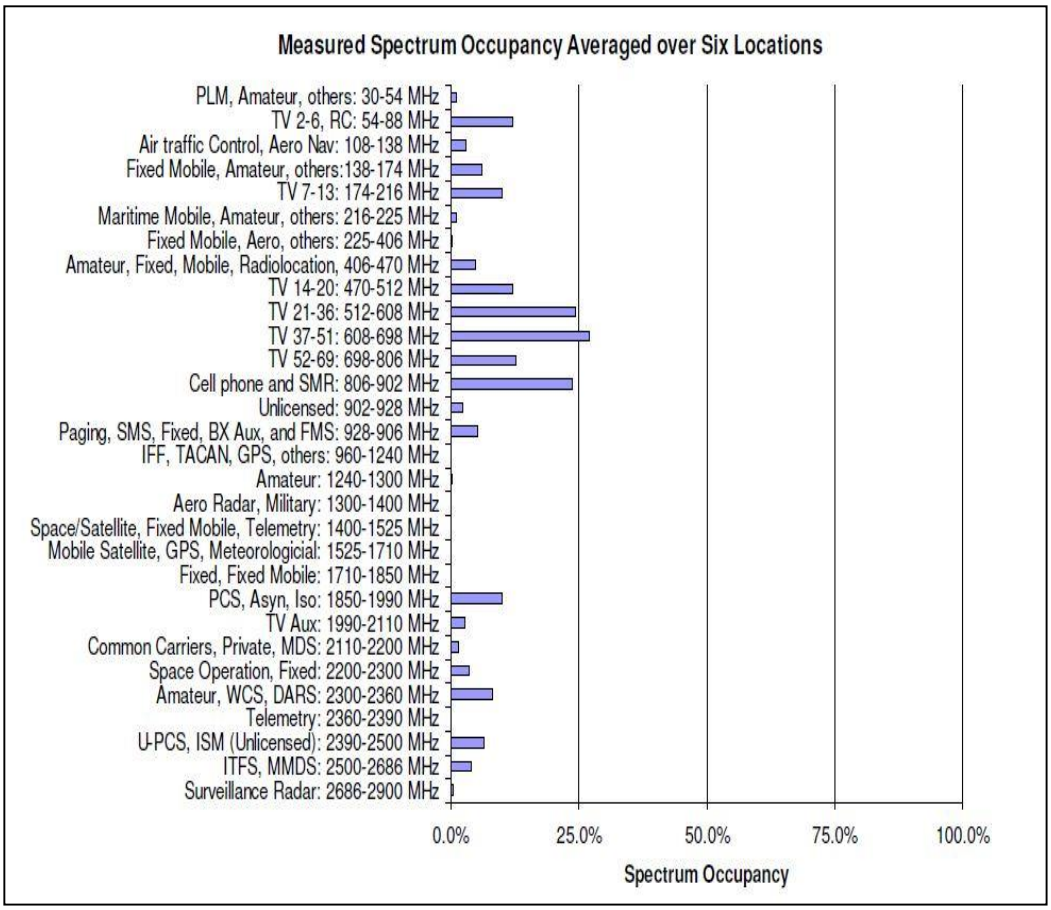

Figure 1-1: Spectrum occupancy measurement results averaged over six locations.

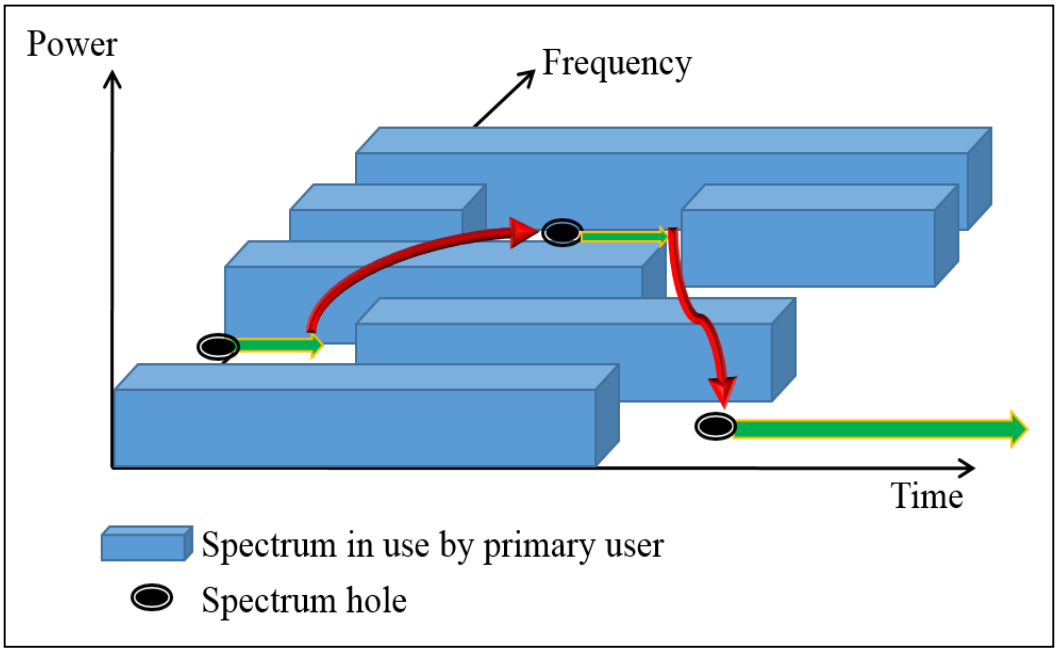

Figure 1-2: Spectrum holes used for opportunistic access.

The idea of wavelet-based detection is to identify the irregular structure in the power spectral density (PSD) function of the wideband signal. These irregularities, also called edges, carry information about the frequency boundaries of the non-overlapping frequency bands. Hence, the main goal is to identify the edges of those bands and classify the bands into black, gray, or white, based on whether the estimated PSD level within each band is high, medium, or low.

The performance of this sensing technique depends on different factors such as the scale factor of the smoothing wavelet function, the shape of the received PSD and the collaboration between secondary users in edge detection. Besides, the presence of log-normal shadowing affects sensing results due to attenuation in the signal power and the addition of random variations to signal received.

1.2 Objectives and Contributions

1.2.1 Objectives

This thesis aims to:

1. Study the performance of narrowband spectrum sensing in a log-normal shadowing environment in a non-collaborative mode.
2. Investigate the effect of collaborative sensing in a log-normal shadowing environment using different fusion rules.
3. Analyze the performance of wideband spectrum sensing using wavelet-based detection in both an AWGN channel and a log-normal channel.

1.2.2 Contributions

The contributions of this thesis are summarized as follows:

1. A closed-form expression of the probability of detection in a log-normal shadowing channel is derived based on the Gauss-Hermite integration method.
2. The performance of narrowband collaborative sensing in an AWGN channel and a log-normal channel using different fusion rules is derived. In particular,

soft fusion, using square-law selection (SLS); square-law combining (SLC) schemes and hard fusion using OR, AND and Majority combining are analyzed and compared under different parameters.

3. The performance of wavelet-based edge detection in wideband sensing is investigated. The system model is extended to include collaborative edge detection. In addition, log-normal shadowing is introduced and the performance of edge detection in log-normal shadowing environment is analyzed.

4. A wideband spectrum detection approach is proposed based on wavelet edge detection, and its performance is compared with the tunable bandpass filter filterbank approach in terms of spectrum occupancy.

1.3 Thesis Outline

The remainder of this thesis is divided into six chapters that are organized as follows:

Chapter 2

This chapter provides an overview of the cognitive radio concept, functionalities, applications and challenges. Common spectrum sensing techniques from the literature are addressed, with the advantages and disadvantages of each technique discussed. Finally, definitions of collaborative spectrum sensing, narrowband and wideband spectrum sensing are summarized.

Chapter 3

This chapter derives expressions for the probabilities of detection and false alarm in a log-normal shadowing channel. It also investigates the performance of these expressions in spectrum sensing under different constraints such as the average SNR, number of samples and a shadowing level represented by the dB-spread.

Chapter 4

In this chapter expressions for the probability of detection and false alarm under collaborative sensing in both an AWGN channel and a log-normal shadowing channel are derived. Collaboration using soft fusion (SLS and SLC) and hard fusion

is investigated and the collaborative probabilities of detection and false alarm are also given.

Chapter 5

This chapter presents an overview of wideband spectrum sensing and common wideband sensing techniques, with the advantages and disadvantages of each technique explained. A system model for wideband sensing, using wavelet-based detection, is investigated and the performance of this model in edge detection is analyzed. Also, the idea of collaborative edge detection is addressed, and the performance of wideband sensing using wavelet detection in a log-normal shadowing environment is also evaluated.

Chapter 6

This chapter investigates and analyzes two approaches to wideband spectrum detection. The first approach is the tunable bandpass filter (TBPF) filterbank in which a parallel structure of tunable narrowband bandpass filters is used to sense the spectrum on a wideband level. The second approach is a proposed wideband spectrum detection model using wavelet-based detection. Performance analysis of both approaches are studied and compared via a simulation.

Chapter 7

This chapter presents concluding remarks about the thesis, and provides suggestion to extend the work in certain directions.

CHAPTER 2: COGNITIVE RADIO - REVIEW

2.1 Introduction

The evolution in wireless communications has introduced new services and applications that require high data rates and a particular quality of service (QoS). This resulted in dramatically increasing demand on frequency spectrum to accommodate these new services or to enhance existing ones. However, frequency spectrum is characterized by static frequency allocation schemes that assign the existing frequency bands only to licensed users. This is the case despite that measurements indicate that the spectrum is underutilized by licensed users for significant periods of time [2]. This aggravates spectrum scarcity and make it more difficult to accommodate the need for a greater spectrum. Therefore, the concept of cognitive radio (CR) is a promising technology to alleviate frequency spectrum scarcity and under-utilization by allowing unlicensed (secondary) users to access the spectrum when it is not being used by licensed users. In this chapter an overview of the cognitive radio and spectrum sensing techniques will be discussed.

2.1.1 Features and Functionalities

The allocation of frequency spectrum is regulated by national regulatory bodies such as the Federal Communications Commission (FCC) in the United States. The FCC allocates spectrum to licensed users, also known as primary users (PU), which have the priority to use the spectrum on a long-term basis. However, this spectrum is under-utilized, since it is not used by the PUs for significant periods of time. This inefficient allocation of spectrum creates the need for new techniques that allows unlicensed users, also known as secondary users (SU), to access the spectrum whenever it is not being used by the PUs. Hence, the FCC adopted CR to overcome spectrum scarcity. According to the FCC; “Cognitive radio is a system that senses its operational electromagnetic environment and can dynamically and autonomously adjust its radio operating parameters to modify system operation, such as maximize throughput, mitigate interference, facilitate interoperability, access secondary markets.” [4].

This definition highlights the two main characteristics of cognitive radio, which are cognitive capability and reconfigurability. Cognitive capability enables CR devices to interact with the surrounding radio environment in a real-time manner and be aware of signal parameters such as waveform, RF spectrum, communication network type/protocols, geographical information, user needs and security policies, etc. CR devices then adjust their radio operating parameters according to the information sensed to achieve optimal performance. This is known as reconfigurability [16].

These characteristics are implemented via the three main functions of the cognitive radio cycle shown in Figure 2-1:

1. Spectrum sensing and analysis;
2. Spectrum management and handoff;
3. Spectrum allocation and sharing.

In the spectrum sensing and analysis stage, CR detects spectrum holes, known as white spaces, for opportunistic access and spectrum utilization, it also senses PU activity to avoid causing harmful interferences due to SU transmissions. Then the characteristics of the frequency bands sensed such as their capacity and reliability are estimated and later used in decision making.

After that the spectrum management and handoff function allows the SU to choose the best frequency band, or hop among multiple bands to meet QoS requirements. For example, when the PU reclaims its band, then the SU transmitting in that band has to move to another available frequency band according to the channel capacity, path loss, holding time, etc.

The SU in cognitive radio networks may coexist in a certain frequency band with a PU or other SUs. Therefore, the need for efficient spectrum allocation and sharing mechanism is fundamental to protect the licensed PU from SU interference and to minimize the collisions and interference between SUs sharing the same frequency band.

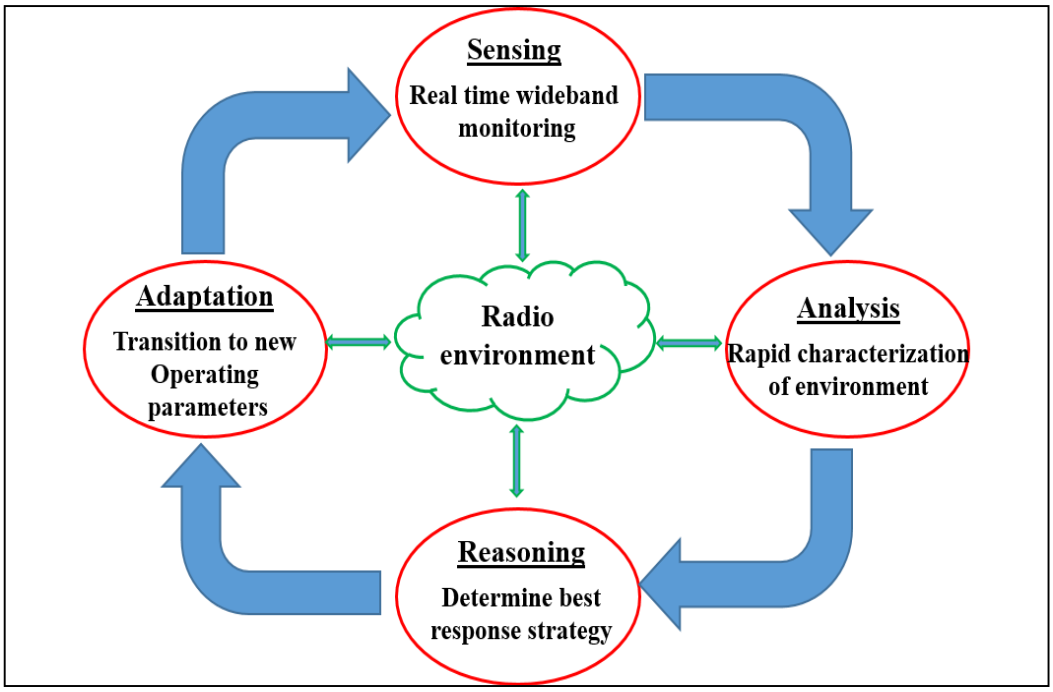

Figure 2-1: Cognitive radio cycle [16].

2.1.2 Applications

Advances in spectrum sensing and spectrum access techniques encouraged many applications of cognitive radio networks in different areas. Certain applications are explored in this section.

A. Cellular Networks

Smartphones, and the spread of social networks raised user expectations of being fully connected. This in its turn added a burden to the already overloaded cellular networks. But cognitive radio applications have been introduced to help overcome these challenges and accommodate traffic growth. For example, indoor coverage is one of the challenges facing cellular networks, where the concept of femtocells has been proposed. The femtocell unit performs as a typical BS (eNodeB in LTE) with a self-deployment property, however, this property make it difficult to overcome femtocells interference using centralized interference management.

The solution to this problem is using distributed spectrum planning, where each femtocell scans the spectrum to find available frequency bands, in order to maintain coverage and avoid interference with other femtocell, as shown in Figure 2-2.

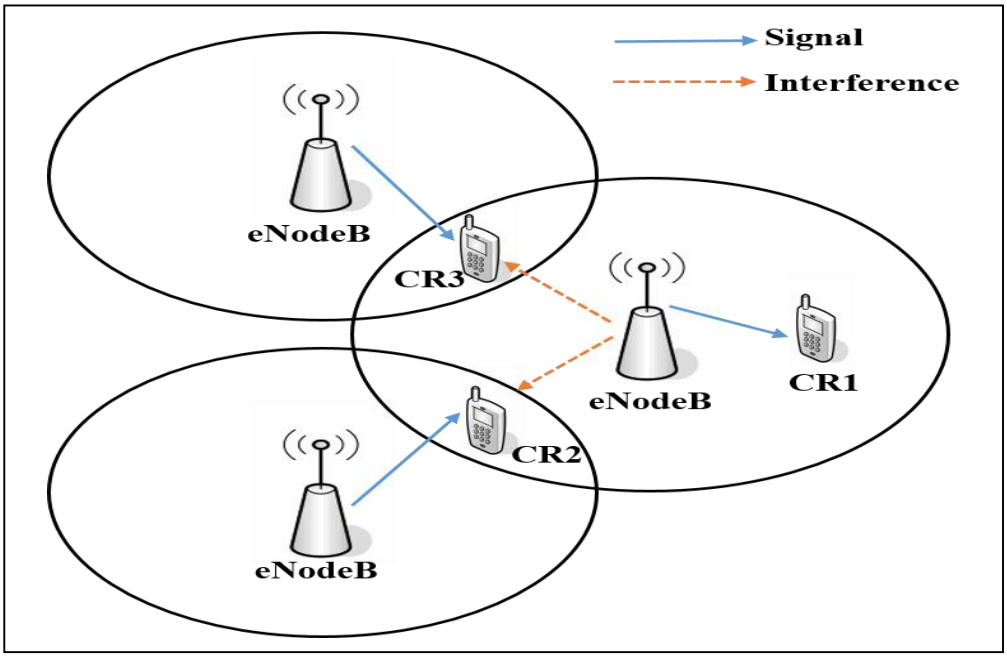

Figure 2-2: Femtocells interference [17].

B. TV White Spaces

TV White Spaces (TVWS) are unused frequency bands located within the VHF and UHF portions of the frequency spectrum. In most countries this spectrum is not allowed for unlicensed use, but after the conversion of TV broadcasts from analogue to digital transmission, large parts of analogue TV channels became completely vacant due to the higher efficiency of digital TV (DTV).

On the other hand, the transition to DTV leaves some channels in certain geographic areas unused by DTV stations due to the interference they cause to co- or adjacent channels. This resulted in more vacant bands that can be used by unlicensed users operating at a low power levels without causing interference to DTV stations. The FCC in the US, the Office of Communications (Ofcom) in the UK, and the Electronic Communications Committee (ECC) in Europe are the main regulatory agencies that allow unlicensed use for TV white spaces by cognitive users [1].

C. Public Safety Networks

The FCC allocated a 700 MHz (698-806 MHz) frequency band for emergency responders (i.e. police, fire and medical services) to prevent or respond to emergencies. However, this spectrum is not sufficient as public safety workers are increasingly equipped with wireless devices such as laptops and mobile video cameras, to improve the efficiency of emergency responses. Moreover, responders

from different agencies cannot communicate during emergencies due to the use of multiple frequency bands, incompatible radio devices and a lack of standardization [1].

To overcome these challenges cognitive radio networks have been proposed to utilize spectrum usage and increase the efficiency of emergency response. With cognitive radio, public safety workers can use other frequency bands such as TVWS for daily communication. Also, through spectrum sharing they can share the spectrum of other commercial operators in locations where public safety networks are unavailable, or where there is an operating public safety network but more capacity is needed to respond to an emergency more effectively.

Cognitive radio applications can be used in many other areas such as smart grid networks, the military and wireless medical networks [1].

2.1.3 Challenges

Several challenges are facing spectrum sensing in cognitive radio networks. Such as; hidden PU problem, spread spectrum PUs, hardware requirements and sensing parameters are addressed in this section.

A. Hidden Primary User Problem

Hidden primary user problem, shown in Figure 2-3, arises when the PU transmitter is located outside the SU area of coverage (AOC). In this situation the SU will cause unwanted interference to the PU receiver as the PU transmitted signal cannot be detected by the SU during spectrum scanning. The multipath fading and shadowing experienced by the PU are the main sources of this problem. Collaborative spectrum sensing is used to overcome this issue, where multiple SUs collaborate with each other to detect the presence of the hidden PU.

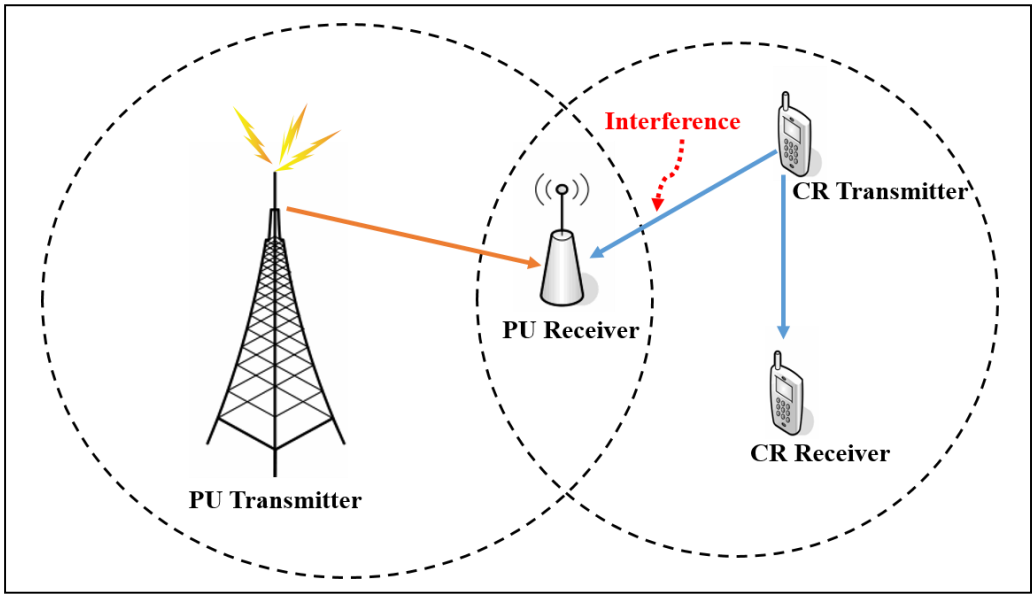

Figure 2-3: Hidden primary user in cognitive radio network.

B. Spread Spectrum Primary Users

There are two main spread spectrum technologies that can be used by the PU to access the frequency spectrum: frequency hopping spread spectrum (FHSS) and direct sequence spread spectrum (DSSS). In FHSS the PU changes its operating frequency according to a certain hopping sequence known by both the transmitter and receiver. While in DSSS the PU spreads its energy over a single frequency band.

Detection of a PU that uses spread spectrum techniques is difficult as its power is distributed over a large bandwidth and looks like a background noise. However, knowing the hopping sequence and achieving perfect synchronization between the SU and the PU transmissions allows simultaneous transmission without causing harmful interference to the PU.

C. Hardware Requirements

Searching for a spectrum opportunity requires scanning wide frequency bands by SUs at high resolutions. This requires RF receivers with components (antennas and power amplifiers) tuned over a large frequency range and high speed processors to accommodate the excessive computational demands with minimal processing delay and to perform noise/interference estimations efficiently.

Sensing architecture is another factor that should be taken into consideration. There are two different architectures that are implemented in cognitive radio networks: single-radio architecture and dual-radio architecture [18]. In a single-radio

architecture a limited time slot is allocated for sensing thus resulting in a limited sensing time, a less sensing accuracy and lower spectrum efficiency. This is the case since part of the time slot is used for sensing instead of data transmission. The advantages of this architecture are low implementation costs and simplicity.

In a dual-radio architecture, two radio channels are used, one for data communication and the other for spectrum sensing. This architecture increases sensing accuracy and spectrum efficiency, but on the other hand it increases the complexity, hardware costs and power consumption.

D. Sensing Parameters

Sensing parameters have to be chosen carefully to guarantee interference protection for the PUs while achieving maximum spectrum utilization for the SUs. Different sensing parameters have to be taken into consideration such as sensing time, sensing frequency and sensing accuracy.

Sensing time has to be selected carefully, because the licensed PU can use its channel anytime, and the SU should vacate this channel immediately. Hence, sensing time has to be sufficient to identify the presence of the PU, which adds constraints on the design of the sensing algorithms.

Another important parameter is sensing frequency that determines the number of times spectrum sensing is performed. The value of a sensing frequency is chosen based on the capabilities of the cognitive radio and the temporal characteristics of the PU in its environment [19]. If the status of the PU changes slowly, then spectrum sensing can be relaxed and performed less frequently, such as with the detection of TVWS. Where the allocation of the TV channels is almost fixed unless a new station comes into operation or an existing station goes offline.

PU interference tolerance is another factor that affects sensing frequency. For example, if the SU is using a public safety channel, then sensing should be performed more frequently and the SU should immediately vacate the channel for the licensed user.

2.1.4 Research Areas

The main objective of cognitive radio networks is utilizing the frequency spectrum, by allowing SUs to access available licensed frequency bands. However, it is crucial to protect the PU from any interference which might be caused by the SU. This adds limitations on the SU transmission power and the interference produced to guarantee PU protection. Hence, more research in power adaptation strategies is done to meet the QoS requirements of the PU and maximize both the SNR and capacity of the SU.

Another field that attracts researchers is spectrum sensing. It is the first and most important cognitive task, since it defines the vacant frequency bands and the state of the channel that will carry the transmission. There are many spectrum sensing techniques such as energy detection, waveform detection, matched filtering, etc. Significant research has been carried out in this area to study these different techniques and optimize their parameters for efficient spectrum sensing performance.

Research in cognitive radio networks also takes other directions i.e. energy efficiency, seamless spectrum handover, cross-layer design and optimized spectrum decision making [20].

2.2 Spectrum Sensing

Spectrum sensing is the most important function in the cognitive cycle. It provides the SU with the information required to access the spectrum accurately and efficiently at a certain time at a certain position on the spectrum. Spectrum sensing is performed across different dimensions including frequency, time, geographical area, code and angle. Significant research has been carried out in the field of spectrum sensing, to address the various spectrum sensing techniques, sensing dimensions and sensing challenges. In the following sections, a brief review of spectrum sensing techniques and dimensions is provided.

2.2.1 Spectrum Sensing Techniques

Different spectrum sensing techniques have been proposed in the literature. In this section the most common sensing techniques are explained and the advantages and drawbacks of each technique are presented.

A. Energy Detector

Energy detection, also known as radiometry or periodogram, is the most common spectrum sensing technique due to its computational and implementation simplicity [18]. The concept of energy detection is comparing the output of the energy detector with a certain energy threshold that depends on the noise floor to determine the presence of the PU signal [21]. Information about the PU signal is not necessary for the energy detector to perform sensing. However, many challenges are faced in this technique starting for the selection of the energy threshold, the inability to differentiate between noise and PU interference, performance degradation at low signal to noise ratio and the difficulty in detecting spread spectrum PUs. More details about energy detection techniques are presented in chapter 3.

B. Matched Filter Sensing

Matched filter is the optimal spectrum sensing technique when the SU has information about the PU signal such as its operating frequency, bandwidth, pulse shaping, modulation type and frame format. The signal received is correlated with a known primary signal and compared to a threshold in order to detect the presence of the PU and maximize the SNR in the presence of additive white noise.

The main advantage of the matched filter technique is the short sensing time required to achieve a good detection performance. However, when the SU has poor knowledge about the PU signal, matched filter performance degrades. Another drawback of this technique is that it requires a dedicated receiver for every PU signal type, resulting in high implementation complexity, and large power consumption as various receiver algorithms need to be evaluated.

C. Cyclostationary-Based Sensing

Cyclostationary-based sensing utilizes the cyclostationary features of the PU signal, due the periodicity of the signal or its mean, by analyzing the Cyclic Autocorrelation Function (CAF) of the received signal. The CAF of the received signal $r(t)$ can be expressed as [17]:

$$R_r^{(\beta)}(\tau) = E\left[r(t)r^*(t-\tau)e^{-j2\pi\beta t}\right] \tag{2.1}$$

where $E[\,.\,]$ is the expectation operator,$(.)^*$ is the complex conjugation, and β is the cyclic frequency.

Another representation of the CAF uses the Fourier series expansion, known as the Cyclic Spectrum Density (CSD) function:

$$S(f,\beta) = \sum_{\tau=-\infty}^{\infty} R_x^{(\beta)}(\tau)\, e^{-j2\pi f t} \tag{2.2}$$

The CSD function has peaks when the fundamental frequency of the PU signal equals the cyclic frequency, β, and it has no peak when there is no PU signal, as the noise is non-cyclostationary. The cyclostationary detector performs efficiently at a very low SNR, since it can distinguish between the PU signal and noise. The main drawback of this sensing technique is the computational complexity, as all cycle frequencies need to be calculated.

D. Waveform-Based Sensing

This sensing technique takes advantage of the special patterns sent with the PU signal such as preamble, mid-ambles, pilot patterns and spreading sequences. A preamble is a pattern transmitted at the beginning of the data sequence, while mid-amble is transmitted in the middle of the data sequence. These patterns are added to the signal intentionally for synchronization and detection purposes.

Sensing is performed by correlating the received signal with these known patterns, and comparing the output of the correlator with a certain threshold. This method is also known as coherent sensing and can be applied on systems with known signal patterns. It was found that waveform-based sensing outperforms energy detector with higher reliability and shorter sensing time [22]. However, this sensing technique is susceptible to synchronization errors, and it decreases spectrum efficiency since longer signal patterns are required for a more accurate sensing performance.

E. Wavelet-Based Sensing

Wavelet-based sensing uses the Wavelet transform to get time and frequency information simultaneously about the wideband signal. Unlike the traditional Fourier transform that provides only spectral information and works for a stationary signal. Short Time Fourier Transform (STFT) is also used for time-frequency analysis, however, the main problem with the STFT is the inability to obtain both high time and frequency resolutions simultaneously due to the constant window length used in STFT analysis.

Wavelet transform can be used to analyze signals with different frequencies at different resolutions and obtain high time resolutions and low frequency resolutions at high frequencies and vice versa at low frequencies. The main idea in wavelet-based sensing is using the wavelet transform to detect the edges in the Power Spectral Density (PSD) function of the wideband signal. These edges carry important information about transitions from an occupied subband to an empty subband. Locating these edges and estimating the power between every two edges helps to represent the wideband signal in a binary fashion and classify the subbands into occupied and vacant. This sensing technique will be addressed in detail in chapters 5 and 6.

2.2.2 Multi-dimensional Spectrum Sensing

Spectrum sensing is about finding opportunities to allow SUs access to the licensed spectrum. A spectrum opportunity is usually exploited in three main dimensions: time, frequency and geographical area, i.e. it can be defined as "A band of frequencies that are not being be used by the primary user of that band at a particular time in a particular geographic area" [23]. However, there are other dimensions that can be sensed to create new spectrum opportunities such as code and angle.

Code dimension includes signals that use spread spectrum, time or frequency hopping codes. The conventional sensing algorithms do not deal with this dimension, which creates challenges in spectrum sensing, as mentioned in the previous section. However, this dimension in spectrum sensing helps avoid these challenges and increases spectrum utilization by creating new opportunities.

Angle dimension is another dimension that is not usually taken into consideration in spectrum sensing. With new advances in antenna design such as beamforming, multiple users can use the same frequency band at the same time within the same geographic area. This in its turn creates new opportunities if the angle of arrival (AoA) is estimated during sensing.

Hence, it is very important to consider all dimensions when designing sensing algorithms, as each dimension creates new opportunities. Figure 2-4 depicts the main spectrum space dimensions.

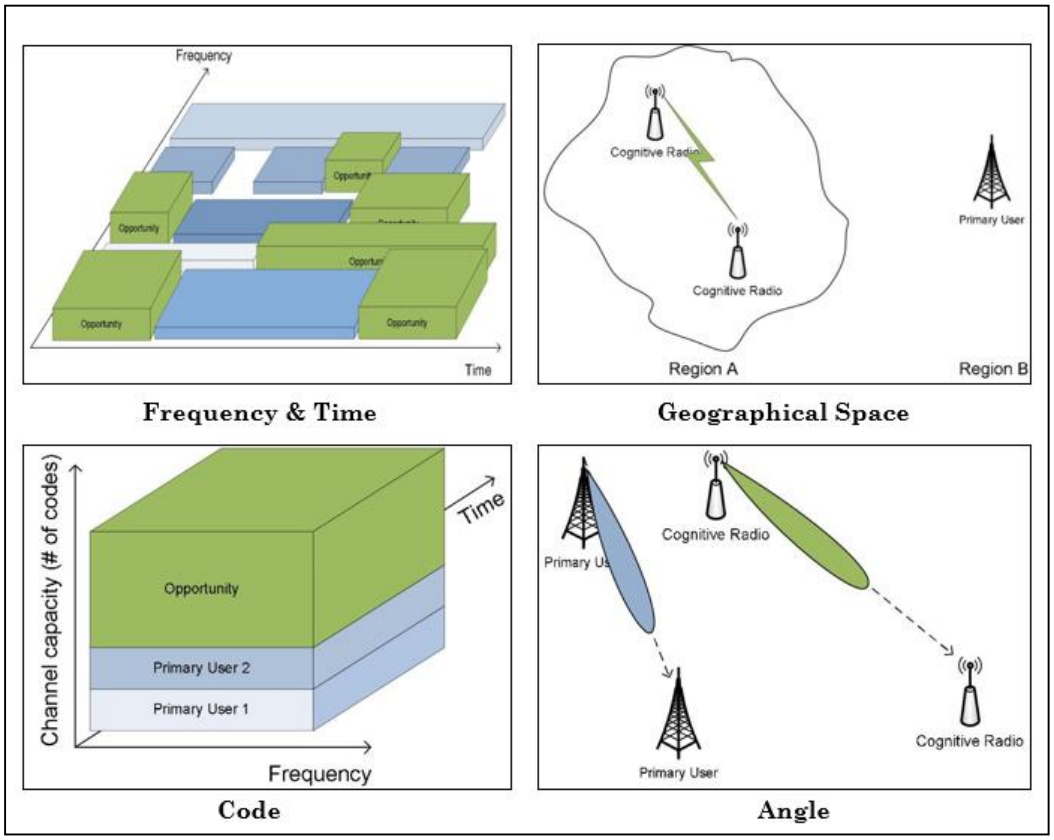

Figure 2-4: Multi-dimensional spectrum space [4].

2.3 Collaborative Spectrum Sensing

Collaborative sensing has been proposed to overcome the problems facing spectrum sensing such as, noise uncertainty, multipath fading and shadowing. It also alleviates hidden primary user problem and decreases sensing time [4]. In collaborative sensing multiple SUs sense the spectrum and share their sensing information to make the final decision regarding the presence of the PU within the frequency band. There are two approaches to perform collaborative sensing; centralized and distributed. These two approaches are addressed in the following sections.

2.3.1 Centralized Collaborative Sensing

In centralized sensing a central unit, called the fusion center (FC), gathers the local sensing information from all the SUs and decides whether the PU exists or not as shown in Figure 2-5. Different fusion algorithms can be used by the FC to combine local sensing information such as soft (data) fusion and hard (decision) fusion algorithms. These algorithms are investigated in detail in chapter 4. The FC then broadcasts the final decision to all SUs, or controls the traffic directly.

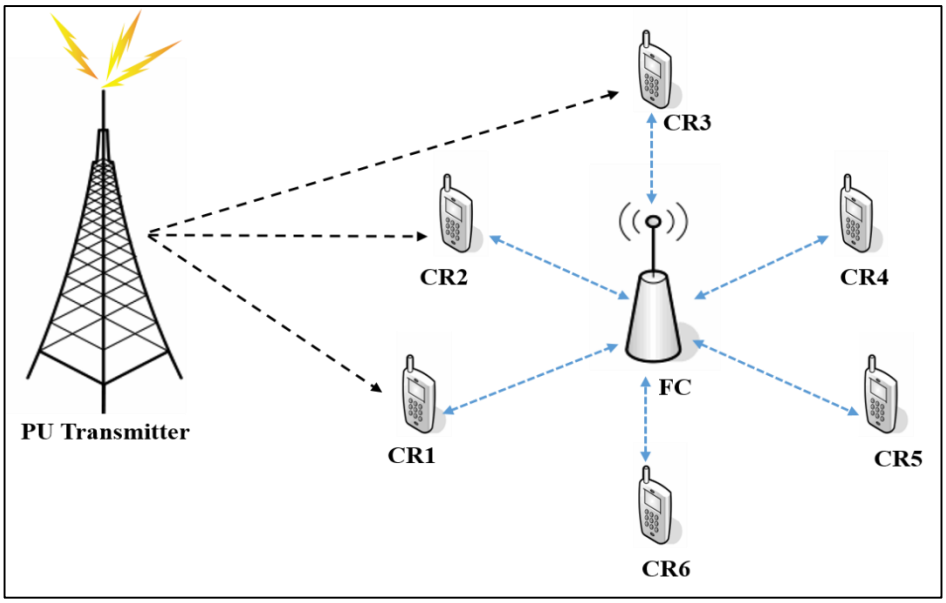

Figure 2-5: Centralized spectrum sensing.

2.3.2 Distributed Collaborative Sensing

In the case of distributed sensing, the SU receives sensing information from other SUs within its vicinity and based on its own sensing information and the information received from other SUs, it makes a decision regarding the presence of the PU. The main advantage of this approach is the reduced cost, since no backbone infrastructure (centralized fusion center) is required. However, every SU has to be equipped with an individual sensing unit. Figure 2-6 depicts a general distributed sensing architecture.

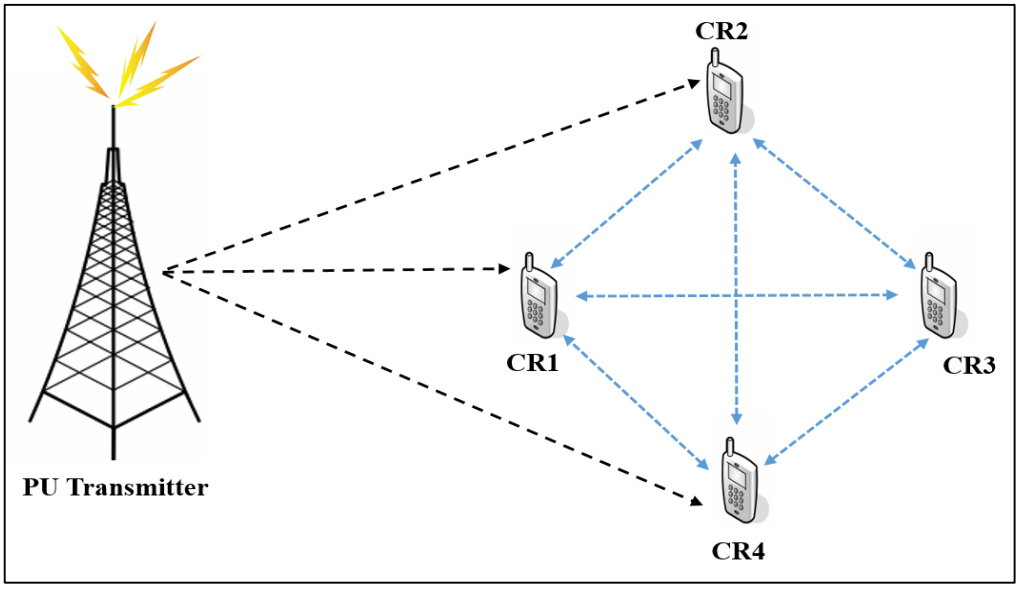

Figure 2-6: Distributed spectrum sensing.

2.3.3 External Sensing

External sensing can be considered as an alternative to centralized spectrum sensing. In this technique, an external agent performs spectrum sensing and reports the final decision to all the SUs. However, the difference between external sensing and centralized sensing is that the external agent is equipped with sensing capabilities and spectrum sensors, while the SUs do not need to have sensing capabilities, unlike in the centralized sensing method.

This method overcomes the hidden PU problem and uncertainty due to shadowing and fading. It is also efficient in terms of time, bandwidth and power consumption from the SU's point of view. Since the SUs do not have to spend time and power in sensing as this task is performed by an external agent [24].

2.4 Wideband and Narrowband Spectrum Sensing

In narrowband sensing, conventional spectrum sensing techniques, discussed earlier in this chapter, and collaborative sensing techniques are used. This implies that the SU knows the frequency band over which sensing will be performed, i.e. the radio front-end starts with a tunable bandpass filter (BPF) that scans one frequency band at a time. TV broadcasting is an example of narrowband sensing, where the center frequency and bandwidth of each band are pre-defined and sensing is performed band by band.

However, when the spectrum utilization is high, wideband sensing should be executed to explore more opportunities. In wideband sensing the SU has no information about the PU center frequency or bandwidth, hence multiple frequency bands should be scanned at the same time using a filterbank of parallel narrowband BPFs implemented at the radio front-end. But this architecture requires a large number of components and the filter range of each BPF is preset, which results in high implementation costs and complexity.

An alternative approach for wideband sensing has been proposed based on identifying the edges of the non-overlapping frequency bands and categorizing the bands detected into black, gray, and white based on estimated power spectral density (PSD) levels [25]. However, the detailed spectral shape of the wideband spectrum is not significant for the sensing process, therefore the wideband spectrum is modeled

as a train of consecutive frequency subbands with a smoothed PSD within each band, but with discontinuous changes between adjacent bands. The main objective is to identify these discontinuities within the spectrum, as they correspond to the frequency edges used to identify the subbands. Wavelet transform has been suggested as a powerful tool for wideband spectrum sensing, it is used to analyze spectrum singularities and detect frequency edges. Other algorithms have been developed for wideband spectrum sensing, these algorithms are addressed in detail in chapter 5.

In this thesis, narrowband spectrum sensing based on energy detection will be considered in an AWGN channel and a log-normal shadowing channel. Collaborative sensing will be addressed to overcome the effect of shadowing using different fusion rules that will be discussed in details in chapter 4. Also, wideband spectrum sensing using wavelet-based edge detection will be investigated for both an AWGN channel and a log-normal shadowing channel.

CHAPTER 3: NARROWBAND NON-COLLABORATIVE SPECTRUM SENSING

In this chapter narrowband spectrum sensing is addressed in a non-collaborative mode, where the secondary user (SU) senses a predetermined frequency band to decide on the presence of the primary user (PU). This decision is mainly affected by the channel model between the PU and the SU. In the first part of this chapter non-collaborative spectrum sensing in an AWGN channel is studied, where this channel model is considered as the ideal model. In the second part, non-collaborative sensing in a log-normal shadowing channel is investigated.

3.1 Spectrum Sensing in an AWGN Channel

An Additive White Gaussian Noise (AWGN) channel is very convenient for modeling real communication systems, where the AWGN represents background noise, or noise from other communication systems working in the same frequency band. The effect of this noise on spectrum sensing performance, in terms of the probability of detection and the probability of false alarm is explored in this section using the energy detection technique.

3.1.1 System Model

Energy detection is known for its simplicity and low computational complexity, therefore, it is commonly used for detecting unknown signals. A block diagram of an energy detector is depicted in Figure 3-1:

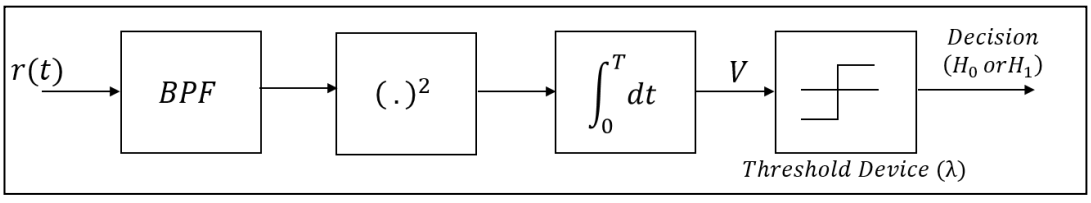

Figure 3-1: Energy detector block diagram.

The input signal $r(t)$ received by the SU passes through a band-pass filter (BPF) to eliminate the out-of-band noise at the center frequency, f_c, and bandwidth, W. The filtered signal then passes through a squaring device to determine its energy, followed by an integrator over a sensing interval $(0, T)$. Finally, the

output of the integrator, V, is compared with the energy threshold, λ, to decide whether the PU is present, H_1, or absent, H_0.

The input signal $r(t)$ is modeled as:

$$\begin{matrix} r(t) = n(t) & H_0 \\ r(t) = s(t) + n(t) & H_1 \end{matrix} \tag{3.1}$$

where $n(t)$ is the AWGN modeled as a zero-mean Gaussian random variable with variance σ_n^2, i.e. $n(t) \equiv \mathcal{N}(0, \sigma_n^2)$, and $s(t)$ is a PU transmitted signal ($s(t) = 0$ when the PU is not transmitting).

For the purpose of detection the signal $r(t)$ is sampled using N_s samples before processing, resulting in the discrete-time form:

$$r_i = s_i + n_i \qquad i = 0, \ldots, N_s - 1 \tag{3.2}$$

Then detection problem turns to a discrete-time binary hypothesis testing problem, by comparing the test statistic, V, with the energy threshold, λ. The test statistic, V, can be written as:

$$V = \frac{1}{N_s} \sum_{i=0}^{\lfloor N_s - 1 \rfloor} |r_i|^2 \tag{3.3}$$

where ($N_s = TW$) is the time-bandwidth product that can be either an integer or a non-integer, and W is the bandwidth of the signal.

Under the H_0 hypothesis, V follows a central chi-square distribution with $2N_s$ degrees of freedom, and a non-central chi-square distribution under the H_1 hypothesis with a non-centrality parameter of $2N_s\gamma$ and $2N_s$ degrees of freedom [21]. Hence, V can be modeled as:

$$V = \begin{cases} \chi^2_{2N_s} & H_0 \\ \chi^2_{2N_s}(2N_s\gamma) & H_1 \end{cases} \tag{3.4}$$

In AWGN channel the spectrum sensing performance is evaluated using two probabilities: the probability of false alarm, P_f, and the probability of detection, P_d. A high probability of detection provides high protection and less interference of the

PU, while a low probability of false alarm results in more spectrum opportunities for the SU, hence higher spectrum utilization, but lower protection for the PU.

The conditional probabilities, the probability of a false alarm, P_f, and the probability of detection, P_d, can be written as respectively:

$$P_f = P(V > \lambda | H_0) \tag{3.5}$$

$$P_d = P(V > \lambda | H_1) \tag{3.6}$$

The probability density function (PDF) of V under the two hypotheses can be expressed as [26]:

$$f_{V|H_0}(v) = \frac{v^{N_s-1}\, e^{-v/2}}{\Gamma(N_s) 2^{N_s}} \tag{3.7}$$

$$f_{V|H_1}(v) = \frac{v^{N_s-1}\, e^{-(v+2N_s\gamma)/2}}{\Gamma(N_s) 2^{N_s}} \;\; {}_0F_1\left(N_s, \frac{N_s \gamma v}{2}\right) \tag{3.8}$$

where $\Gamma(.)$ is the gamma function, and ${}_0F_1(.,.)$ is the confluent hyper-geometric limit function [27].

Closed-form expressions for the probability of false alarm and the probability of detection are given in [28]. The two probabilities can be expressed as:

$$P_f = \frac{\Gamma(N_s, \frac{\lambda}{2})}{\Gamma(N_s)} \tag{3.9}$$

$$P_d = Q_{N_s}\left(\sqrt{2\gamma}, \sqrt{\lambda}\right) \tag{3.10}$$

where γ is the SNR received at the SU, defined as $\gamma = \frac{P}{N_0 W}$ with P as the power of the PU signal received at the SU, and N_0 is the one-sided noise power spectral density. λ is the energy threshold, $\Gamma(.,.)$ is the upper incomplete gamma function, and $Q_{N_s}(.,.)$ is the generalized Marcum-Q function [29]. In real communication systems the value of λ is determined by solving (3.9) for a pre-assigned value of P_f.

The probability of misdetection is defined as:

$$P_m = 1 - P_d \tag{3.11}$$

3.1.2 Simulation Results in an AWGN Channel

Different factors affect spectrum sensing performance in an AWGN channel such as the number of samples, N_s, and the PU average SNR, γ. In this section sensing performance is investigated using a MATLAB simulation using the complementary receiver operating characteristic (CROC) curves [30]. CROC is a graphical representation of spectrum sensing performance for different values of energy threshold. It shows the relationship between the sensitivity, represented by the probability of misdetection, and the specificity, represented by the probability of false alarm.

A. Effect of the Number of Samples (N_s)

The number of samples, N_s, acquired from the signal received by the SU affects detection of the PU. When the number of samples increases the SU collects more information about the PU during a fixed sensing duration, T. Therefore, the probability of false alarm decreases [31]. However, in practical situations there is a predetermined probability of false alarm that is achieved. According to the inverse proportionality between the probability of misdetection and the probability of false alarm, increasing the number of samples results in a higher probability of misdetection, as shown in Figure 3-2.

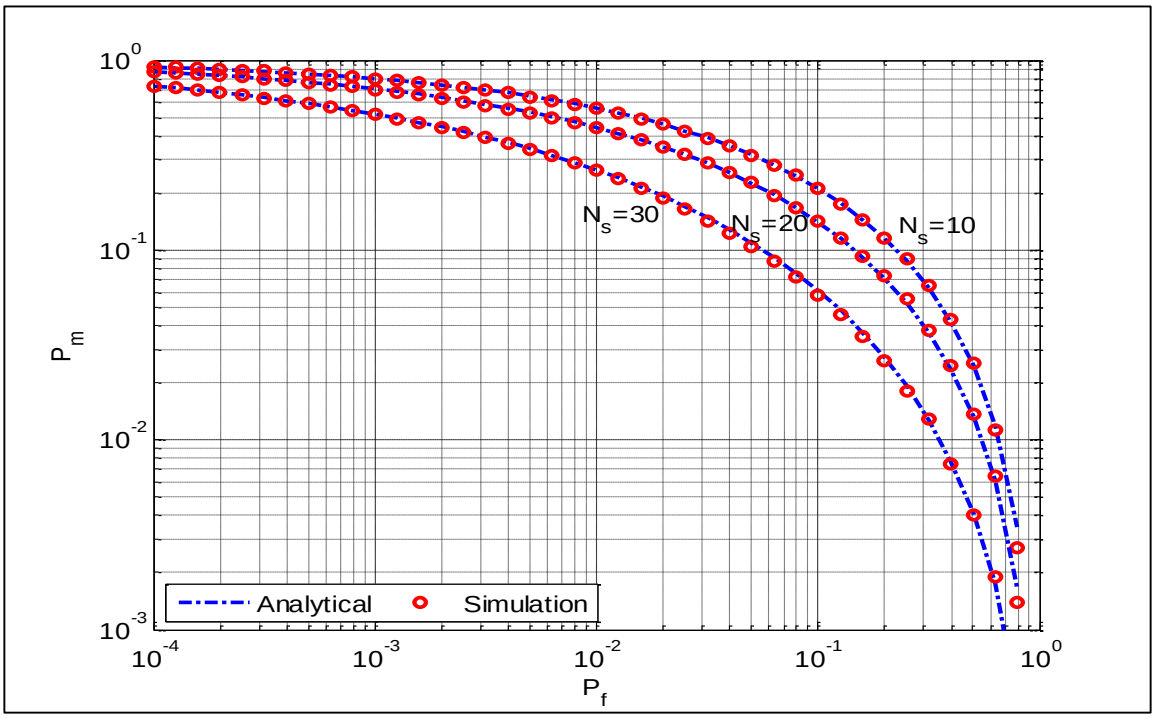

Figure 3-2: CROC in AWGN channel for different values of N_s at average SNR= 10dB.

B. Effect of Primary User Average SNR

The SNR of the PU signal received at the SU has a major influence on the performance of the energy detector. As the average SNR increases, the signal becomes immune to noise and hence easier to detect. This is obvious from the results shown in Figure 3-3, where the probability of misdetection, P_m, decreases as the average SNR increases from 5dB to 15dB. These results prove that the energy detector performs better at a high average SNR. Figure 3-4 further verifies this conclusion, where the probability of detection, P_d, grows as the average SNR increases from 0dB to 20dB.

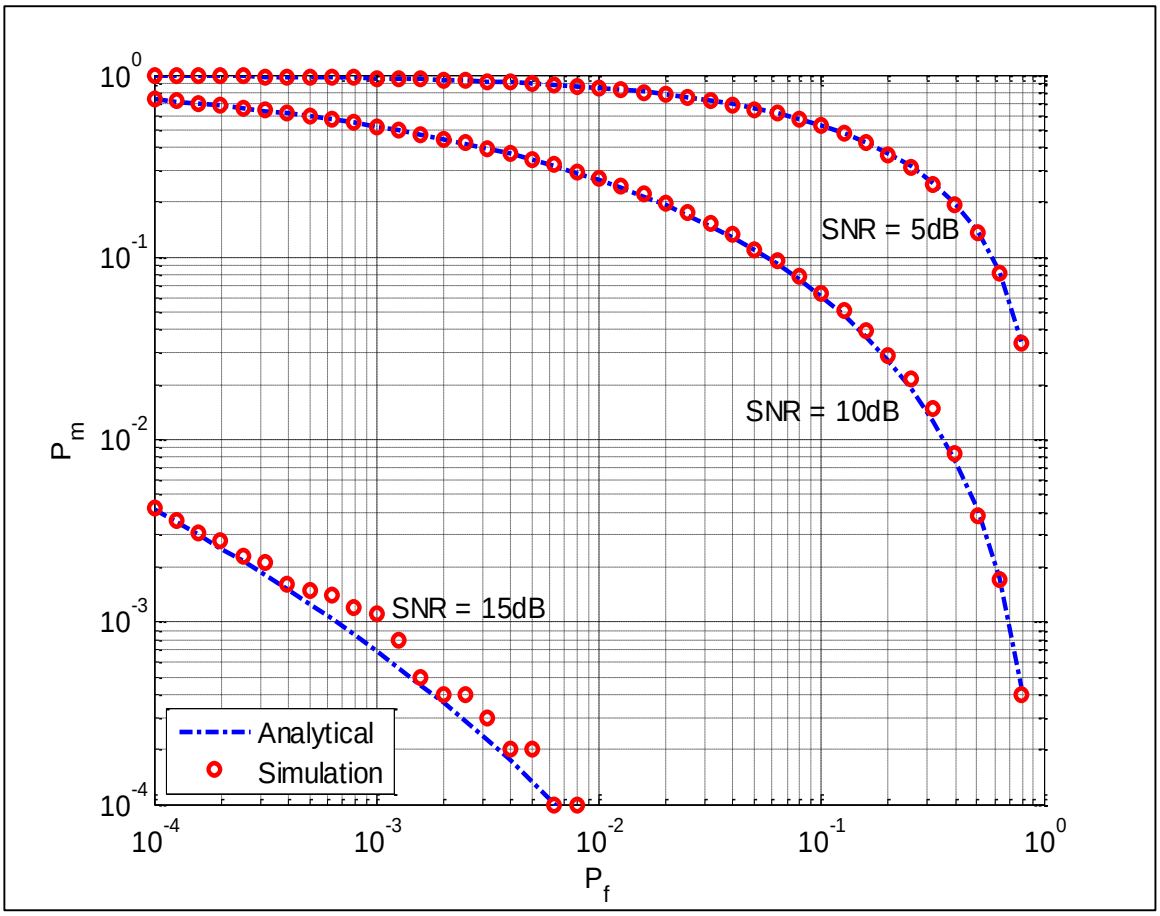

Figure 3-3: CROC in AWGN channel for different values of average SNR, and $N_s = 10$.

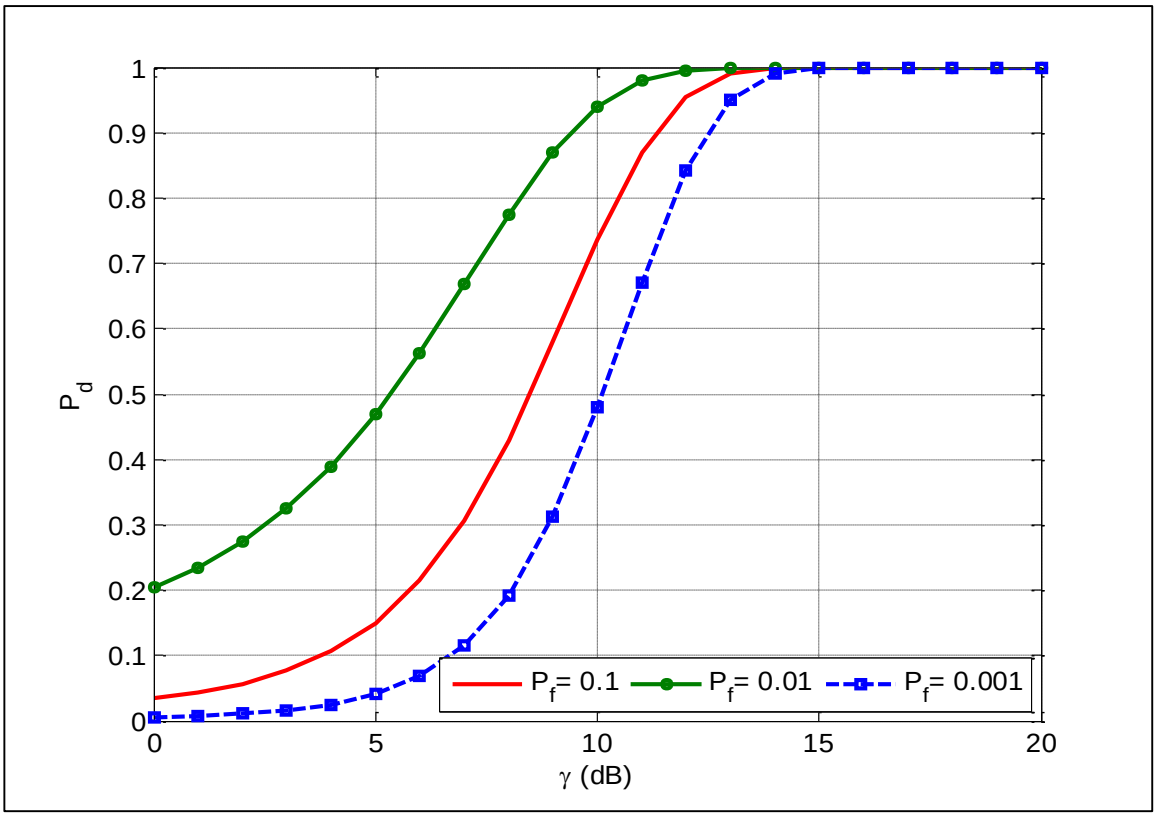

Figure 3-4: Probability of detection, P_d, vs. average SNR for N_s=10.

3.2 Spectrum Sensing in Log-normal Shadowing

In this section the effect of log-normal shadowing on spectrum sensing performance is investigated. In a log-normal shadowing, the signal received by the SU fluctuates randomly due to a blockage from an obstacle in the signal path as, shown in Figure 3-5 (a). These fluctuations affect the local-mean power of the signal, resulting in random variations of path loss at a given distance, as shown in Figure 3-5 (b). Since the location, size, and dielectric properties of the obstacle are usually unknown, a statistical model is used to describe these fluctuations. Empirical measurements indicate that the fluctuations in the local-mean power of the area-mean follow log-normal distribution, which means that they follow normal distribution when expressed in a logarithmic scale, decibel units [32].

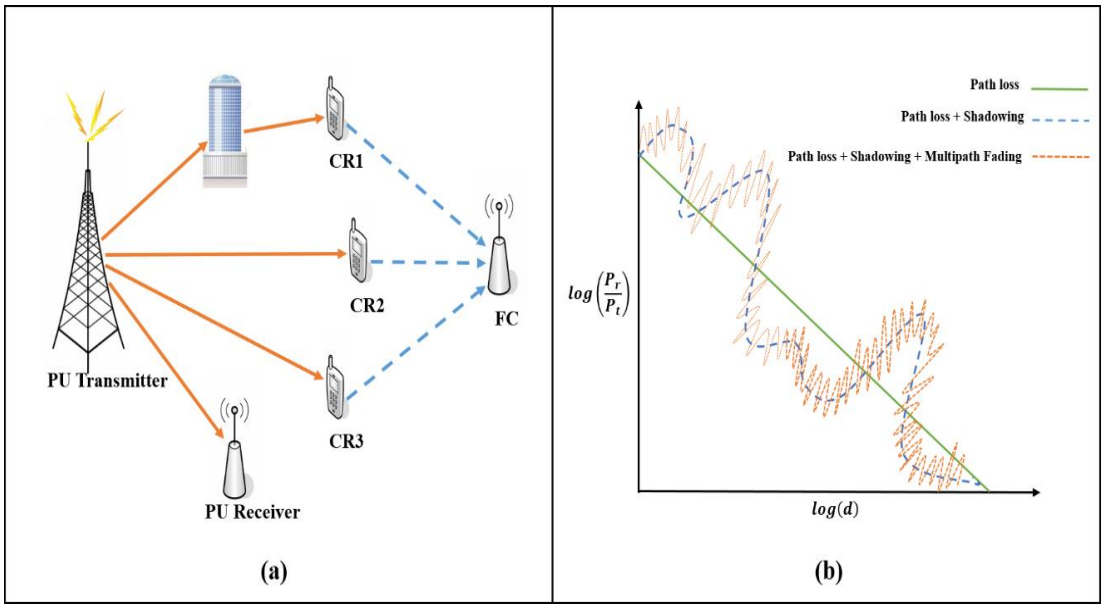

Figure 3-5: a) Illustration of log-normal shadowing, b) Path loss, shadowing and multipath fading vs. distance

3.2.1 Channel Model in Log-normal Shadowing

For the SU log-normal shadowing affects the average SNR of the signal received. Hence, the SNR, γ, is modeled as a log-normal random variable with a probability density function (PDF) expressed as [33]:

$$f_\gamma(\gamma) = \frac{\xi}{\gamma\sigma_{dB}\sqrt{2\pi}} exp \frac{-(\xi log_e\gamma - \mu_{dB})^2}{2{\sigma^2}_{dB}} \quad ,\gamma \geq 0 \tag{3.11}$$

where $\gamma \sim LN(\mu_{dB}, {\sigma^2}_{dB})$, $\xi = \frac{10}{log_e(10)}$, μ_{dB} and ${\sigma^2}_{dB}$ are the mean and the variance, both in dB, of $\xi log_e\gamma$ respectively.

A log-normal distribution is usually characterized in terms of the dB-spread, σ_{dB}. The value of σ_{dB} depends on the type of the obstacle blocking the signal travelling from the PU to the SU. For outdoor channels the value of σ_{dB} ranges from 5 to 12dB in macrocells and 4 to 13dB in microcells [34].

Log-normal shadowing affects sensing performance in cognitive radio networks. Due to shadowing, white spaces may result not only from the absence of the PU, but also due to a blockage of the signal transmitted by an obstacle in the signal path between the PU and the SU. Hence the SU has to be careful while sensing the spectrum to avoid confusion between a white space and heavy shadowing to

avoid interfering with the PU, while maintaining acceptable spectrum utilization levels.

3.2.2 Spectrum Sensing in Log-normal Shadowing

In the case of log-normal shadowing, spectrum sensing problem can be formulated as follows:

$$\begin{matrix} r(t) = n(t) & H_0 \\ r(t) = h(t)\, s(t) + n(t) & H_1 \end{matrix} \tag{3.12}$$

where $h(t)$ is the linear channel gain between the PU and the SU.

In the presence of shadowing, the probability of false alarm, P_f, is not affected, because it is defined under the H_0 hypothesis, where no PU signal is transmitted. On the other hand, the probability of detection under a log-normal shadowing, $P_{d,log}$, is calculated by averaging P_d in (3.10) over the pdf in (3.11), i.e.

$$P_{d,log} = \int_0^\infty P_d\,(\gamma, \lambda) f_\gamma\,(\gamma)\, d\gamma = \int_0^\infty Q_{N_s}\left(\sqrt{2\gamma}, \sqrt{\lambda}\right) f_\gamma\,(\gamma)\, d\gamma \tag{3.13}$$

or

$$P_{d,log} = \frac{\xi}{\sigma_{dB}\sqrt{2\pi}} \int_0^\infty Q_{N_s}\left(\sqrt{2\gamma}, \sqrt{\lambda}\right) \left(\frac{1}{\gamma}\right) exp\, \frac{-(\xi log_e \gamma - \mu_{dB})^2}{2\sigma_{dB}^2}\, d\gamma \tag{3.14}$$

The Generalized Marcum-Q function is defined as:

$$Q_{N_s}(a, b) = \int_b^\infty \frac{y^{N_s}}{a^{N_s - 1}} e^{\left(-\frac{y^2 + a^2}{2}\right)} I_{N_s - 1}(ay)\, dy \tag{3.15}$$

where $I_{N_s-1}(ay)$ is the modified Bessel function of order (N_s-1), and y is a dummy variable. Assuming $x = \frac{\xi log_e \gamma - \mu}{\sqrt{2}\sigma}$, then:

$$dx = \frac{\xi}{\gamma\sqrt{2\sigma}} d\gamma \tag{3.16}$$

and $P_{d,log}$ can be written as:

$$P_{d,log} = \frac{1}{\sqrt{\pi}} \int_{-\infty}^{\infty} Q_{N_s}\left(\sqrt{2\, exp\left(\frac{x\sigma\sqrt{2} + \mu}{\xi}\right)}, \sqrt{\lambda}\right) e^{-x^2}\, dx \tag{3.17}$$

Based on the Gauss-Hermite integration method in [35], the probability of detection in (3.16) can be written as:

$$P_{d,log} = \sum_{i=1}^{M} \frac{w_i}{\sqrt{\pi}} \, Q_{N_s}\left(\sqrt{2 \, exp\left(\frac{a_i \sigma \sqrt{2} + \mu}{\xi}\right)}, \sqrt{\lambda}\right) \tag{3.18}$$

where M is the Hermite integration order, w_i, and , α_i, are the weights and abscissas respectively [36].

The probability of misdetection in log-normal shadowing, $P_{m,log}$, is defined as:

$$P_{m,log} = 1 - P_{d,log} \tag{3.19}$$

or

$$P_{m,log} = 1 - \sum_{i=1}^{M} \frac{w_i}{\sqrt{\pi}} \, Q_{N_s}\left(\sqrt{2 \, exp\left(\frac{a_i \sigma \sqrt{2} + \mu}{\xi}\right)}, \sqrt{\lambda}\right) \tag{3.20}$$

The newly derived expression of the probability of misdetection in (3.20) is a closed-form expression that can be evaluated easily. The precision of this expression is investigated by calculating the probability of misdetection using three methods: the Gauss-Hermite approximation in (3.20), Monte Carlo simulation for (3.13) and numerical integration for (3.17).

Figure 3-6 and Figure 3-7 depict the CROC curves in a log-normal shadowing channel using the three methods for average SNR = 10dB, $\sigma_{dB} = 2$dB, and N_s = 10 samples, the AWGN curve is provided as a reference. It is obvious from the figures that spectrum sensing performance degraded due to shadowing, resulting in a higher probability of misdetecting the PU. Also, comparing the three curves of $P_{m,log}$ proves that the Gauss-Hermite approximation provides an accurate formula for calculating the probability of misdetection in a log-normal shadowing channel.

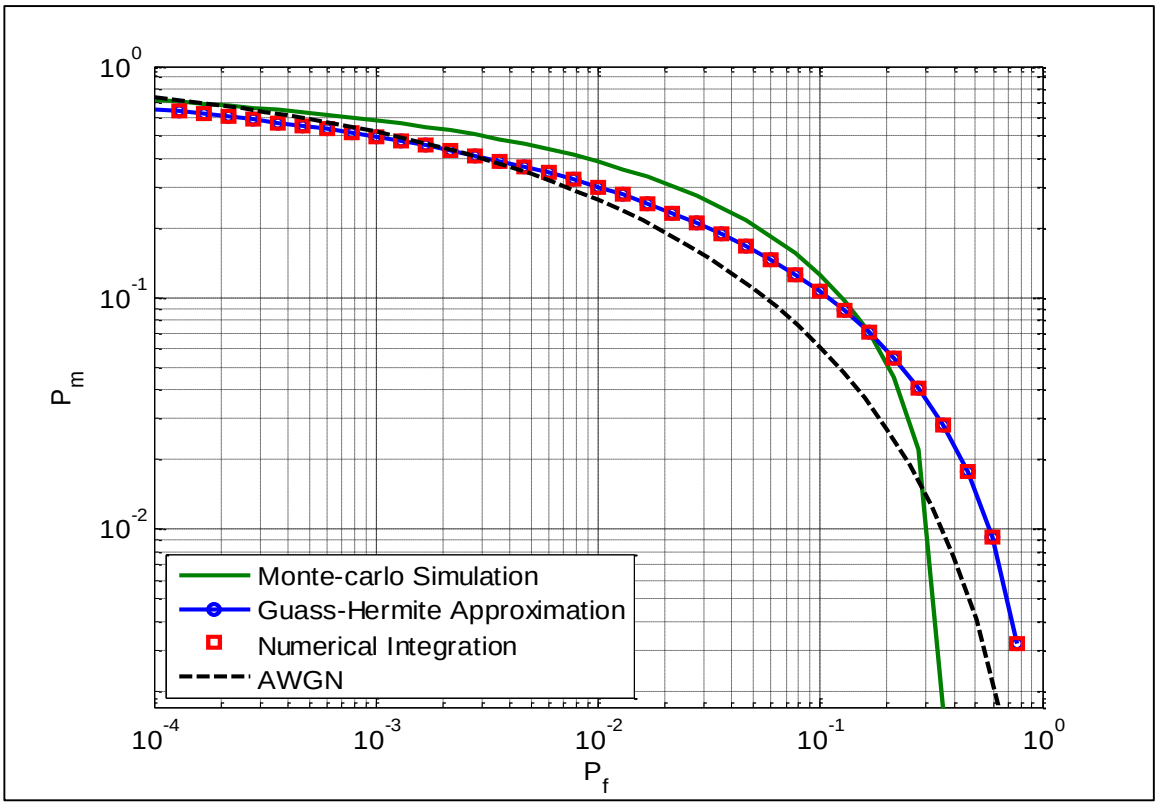

Figure 3-6: CROC in log-normal channel for 10 simulation runs where $N_s = 10$, average SNR$= 10dB$, and $\sigma_{dB} = 2$dB.

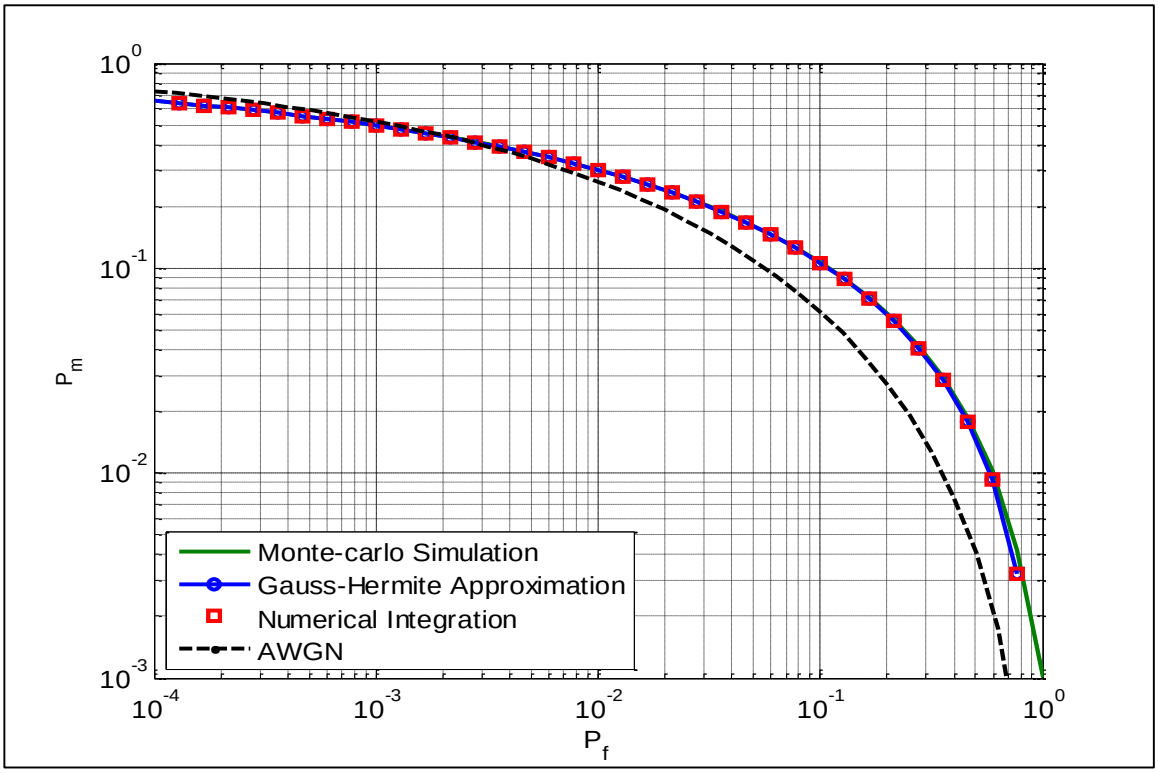

Figure 3-7: CROC in log-normal channel for 1000 simulation runs where N_s=10, average SNR$= 10$dB, and $\sigma_{dB} = 2$dB.

3.2.3 Simulation Results in Log-normal Shadowing

The effect of log-normal shadowing on sensing performance is investigated in this section. There are many factors that can be a major influence on sensing performance such as the dB-spread, σ_{dB}, the PU average SNR and the number of samples, N_s.

A. Effect of dB-spread (σ_{dB})

The severity of shadowing is represented by the value of the dB-spread, σ_{dB}, where higher values of σ_{dB} result in more intensive shadowing. As shown in Figure 3-8, the probability of misdetection increases as the value of σ_{dB} grows from 2dB to 12dB. This is a result of the attenuation experienced by the received signal, making it more difficult to detect. This in its turn affects sensing performance and make the PU more susceptible to interference from the SU.

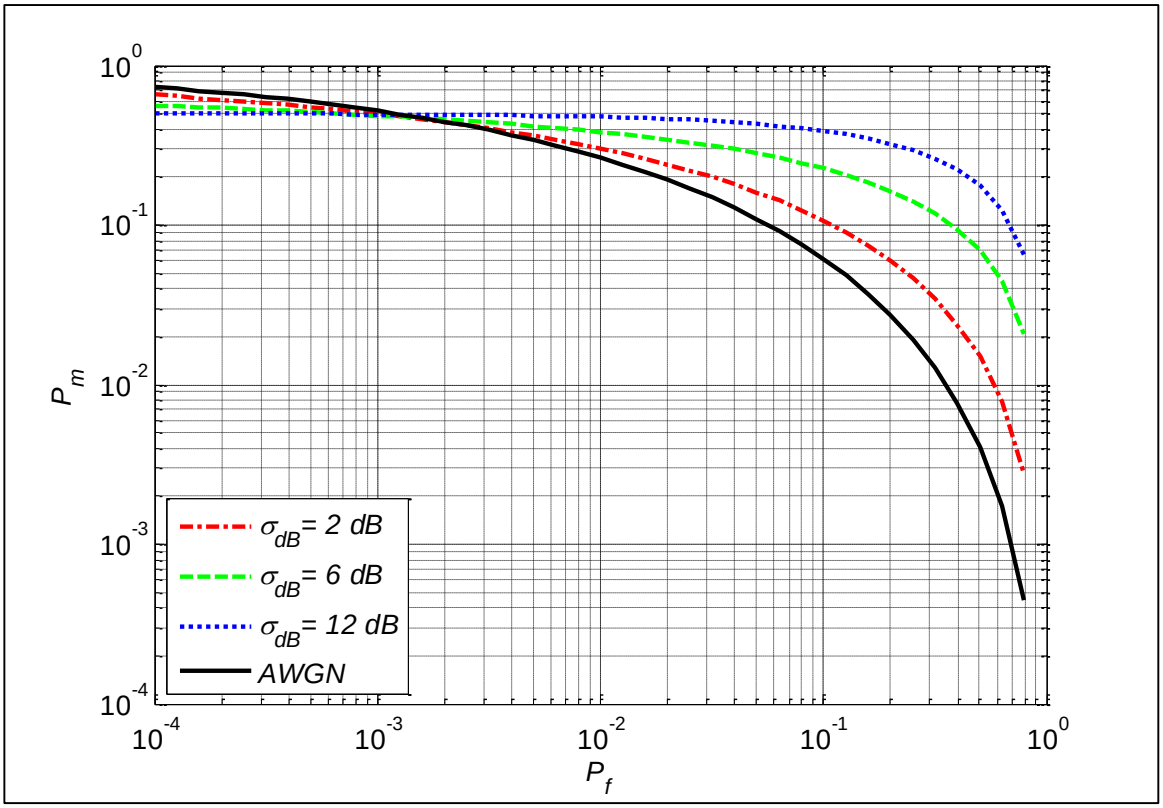

Figure 3-8: CROC in log-normal channel for different values of dB-spread at average SNR=10dB, $N_s = 10$.

B. Effect of the Primary User Average SNR

In energy detection based spectrum sensing the average SNR of the PU signal received by the SU is a major influence on sensing performance. However, due to

shadowing, the average power of the signal received by the SU will be attenuated, hence the probability of misdetection will increase. This degradation in performance grows as the average SNR of the PU signal decreases, as shown in Figure 3-9, where the probability of misdetection increased as the average SNR decreased from 15dB to 5dB.

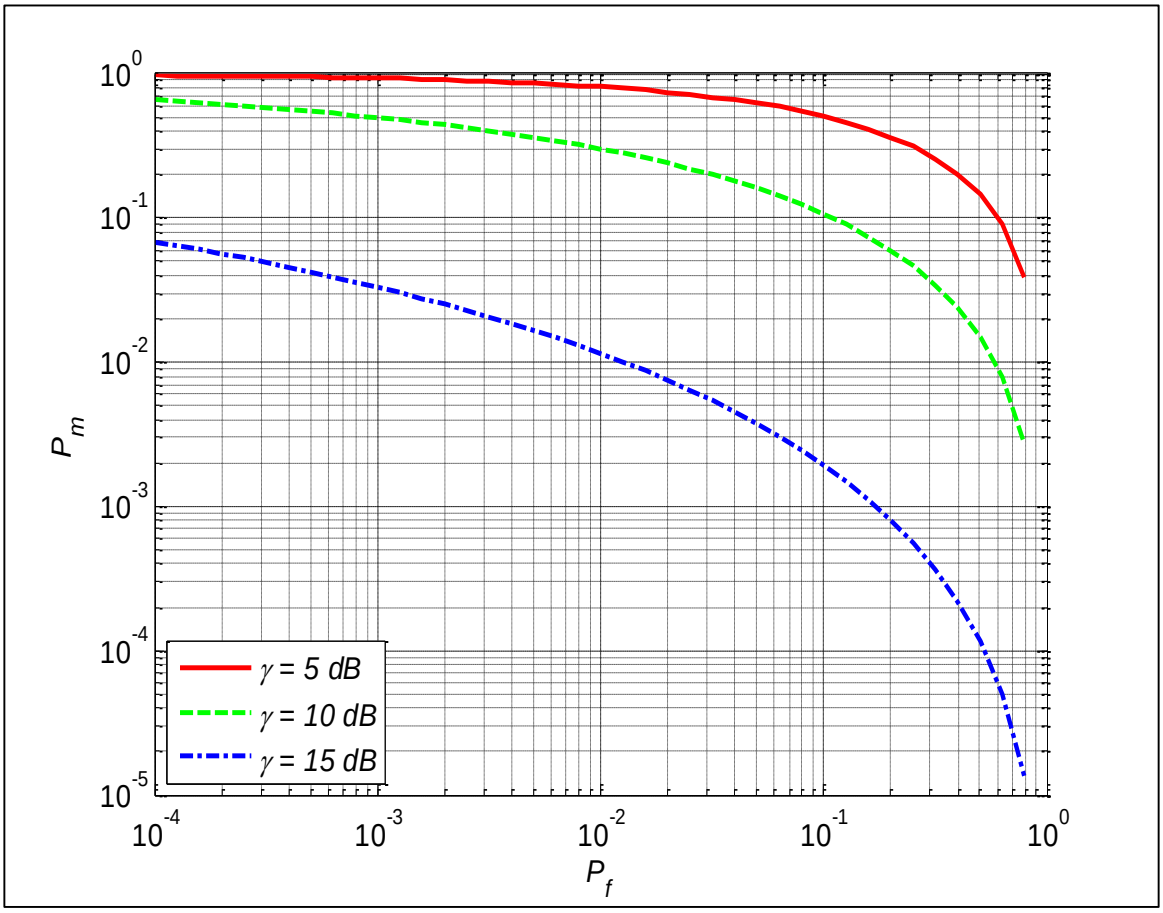

Figure 3-9: CROC in log-normal channel for different values of average SNR at $\sigma_{dB} = 2\text{dB}, N_s = 10$.

C. Effect of the Number of Samples (N_s)

As discussed previously in the AWGN channel, acquiring fewer samples from the signal received by the SU results in a higher probability of detection for a given probability of false alarm, as shown in Figure 3-10.

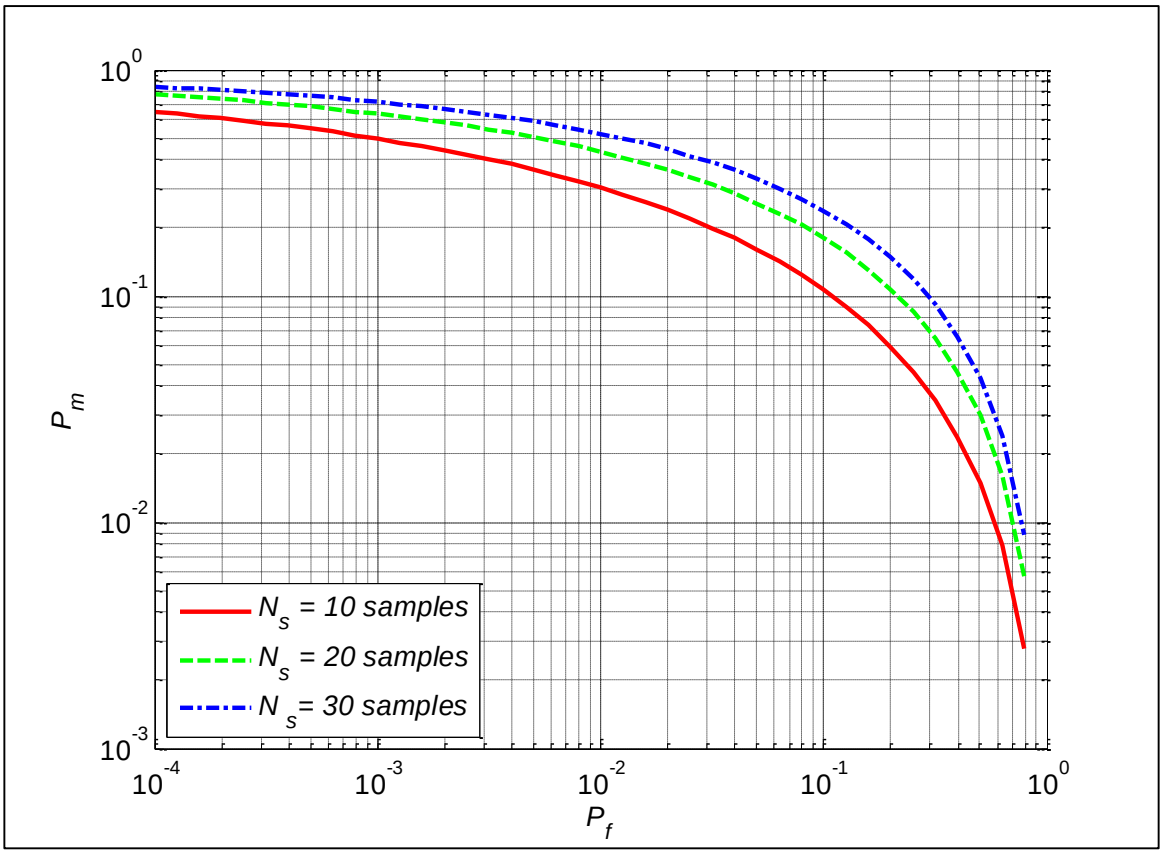

Figure 3-10: CROC in log-normal channel for different values of N_s at average SNR=10dB, $\sigma_{dB} = 2$dB.

In conclusion, a narrowband spectrum sensing model using energy detection in a non-collaborative mode was investigated both in an AWGN channel and a log-normal shadowing channel. It was found that the energy detector performs better at higher average SNR values with a smaller number of samples (N_s) and vice versa. A new closed-form expression for the probability of detection in a log-normal shadowing channel was derived based on the Gauss-Hermite integration. This expression proved its accuracy in calculating the probability of detection under shadowing. Moreover, the degradation in sensing performance due to the presence of shadowing was obvious, as the average power of the signal received is attenuated due to signal blockage by an obstacle. The higher the value of σ_{dB}, the worse the detection of the PU, as shadowing is more severe at higher σ_{dB} values.

CHAPTER 4: NARROWBAND COLLABORATIVE SPECTRUM SENSING

4.1 Introduction

Collaborative spectrum sensing is addressed in this chapter, where the secondary users (SUs) share their sensing information with each other to make decisions about the status of the frequency band. Collaborative sensing provides a diversity that is important to alleviate the degradation in sensing performance due to the presence of log-normal shadowing.

Collaboration in spectrum sensing can be implemented using one of the two main architectures: centralized or distributed. In this chapter centralized collaborative sensing is assumed, where a central data fusion center (FC) receives sensing information from the SUs, and makes decision about the presence of the primary user (PU) in a certain frequency band. Two main fusion rules can be used by the FC to combine local sensing information: hard fusion (also called decision fusion), and soft fusion (also called data fusion).

The following scenario is considered: there are k independent and identically distributed (i.i.d) SUs within the reception area of the PU. Without loss of generality, all SUs are assumed to experience identical shadowing, i.e. signal statistics are assumed to be the same for all SUs, and all control channels used for reporting sensing information and final decisions between the SUs and the FC are assumed to be ideal noiseless channels as shown in Figure 4-1.

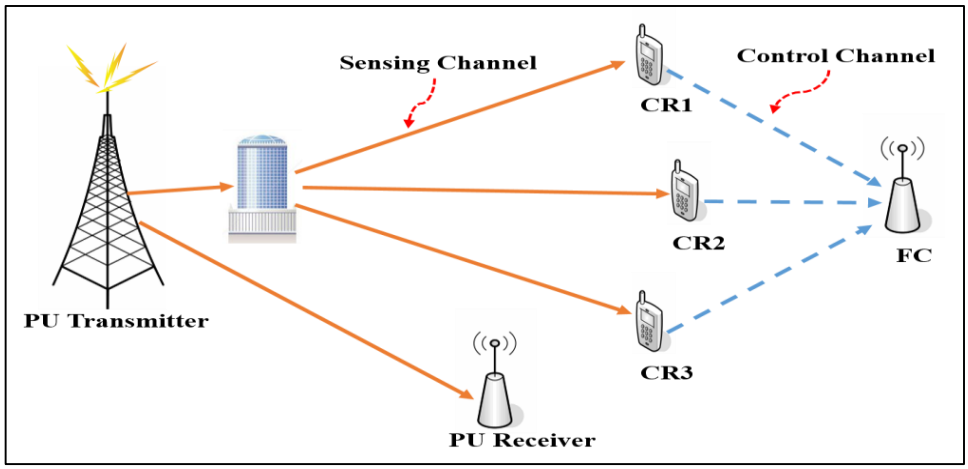

Figure 4-1: Collaborative sensing scenario in a log-normal shadowing channel.

4.2 Hard (Decision) Fusion

In hard fusion all SUs sense the same frequency band, and each SU makes its own decision regarding the presence of the PU. All SUs then transmit their binary local decisions (1 or 0) over a common control channel to the FC, and the FC in its turn combines these local decisions and diffuses the final decision back to every SU. The main advantages of using hard decision combining are reducing the computational complexity at the FC and using low communication overheads, since each SU transmits one-bit hard decision. There are three main decision fusion rules that can be used to combine the local decisions at the FC: AND, OR and Majority combining.

4.2.1 Collaborative Probability of Detection

If we assume that the FC needs m out of k SUs to decide, then the independent local decisions of the SUs follow binomial distribution based on Bernoulli trials. The collaborative probability of detection, C_d, and the collaborative probability of false alarm, C_f, calculated at the FC can be expressed as follows [37]:

$$C_d = \sum_{l=m}^{k} \binom{k}{l} {P_d}^l (1 - P_d)^{k-l} \tag{4.1}$$

and

$$C_f = \sum_{l=m}^{k} \binom{k}{l} {P_f}^l \left(1 - P_f\right)^{k-l} \tag{4.2}$$

where P_f and P_d are defined in (3.9) and (3.10) respectively for an AWGN channel, and P_d is defined in (3.18) for a log-normal shadowing channel.

The collaborative probability of misdetection, C_m, can be written as:

$$C_m = 1 - C_d \tag{4.3}$$

Based on the fusion rule used by the FC to make the final decision, the number of SUs, m, is determined. The collaborative probability of detection can be calculated as follows:

AND-combining: k out of k SUs are needed to decide the collaborative probability of detection, C_d, in (4.1):

$$C_{d,AND} = \sum_{l=k}^{k} \binom{k}{l} {P_d}^l (1 - P_d)^{k-l} \tag{4.4}$$

For k i.i.d SUs, $C_{d,AND}$ can be written as:

$$C_{d,AND} = (P_d)^k \tag{4.5}$$

OR-combining: Here 1 out of k SUs is needed to make the collaborative decision, i.e.

$$C_{d,OR} = \sum_{l=1}^{k} \binom{k}{l} {P_d}^l (1 - P_d)^{k-l} = 1 - \binom{k}{l} {P_d}^l (1 - P_d)^{k-l}\Big|_{l=0} \tag{4.6}$$

In the case of i.i.d users, $C_{d,OR}$ can be expressed as:

$$C_{d,OR} = 1 - (1 - P_d)^k \tag{4.7}$$

Majority-combining: $\left(\left\lfloor \frac{k}{2} \right\rfloor + 1\right)$out of k SUs are required to make the decision:

$$C_{d,MAJ} = \sum_{l=\left\lfloor \frac{k}{2} \right\rfloor + 1}^{k} \binom{k}{l} {P_d}^l (1 - P_d)^{k-l} \tag{4.8}$$

4.2.2 Simulation Results Using Hard Fusion

Figure 4-2 shows sensing performance in a collaborative mode using different decision fusion rules. These results represent the performance in a log-normal channel for $k = 3$ i.i.d SUs, average SNR $= 10$dB , $\sigma_{dB} = 2$dB, and $N_s = 10$ samples. It is obvious that using the OR-combining results in the lowest probability of misdetection (C_m) for a fixed probability of false alarm (C_f), while using the AND-combining results in the highest probability of misdetection. This means that higher protection for the PU from SU interference is guaranteed using OR-combining, since it is sufficient that one of the collaborative SUs declares the presence of the PU in the frequency band. However, from the SU perspective, using the AND-combining increases spectrum utilization and creates more opportunities, because it requires that all collaborative SUs agree on the presence of the PU to decide if a certain frequency band is busy and can't be accessed by the SUs.

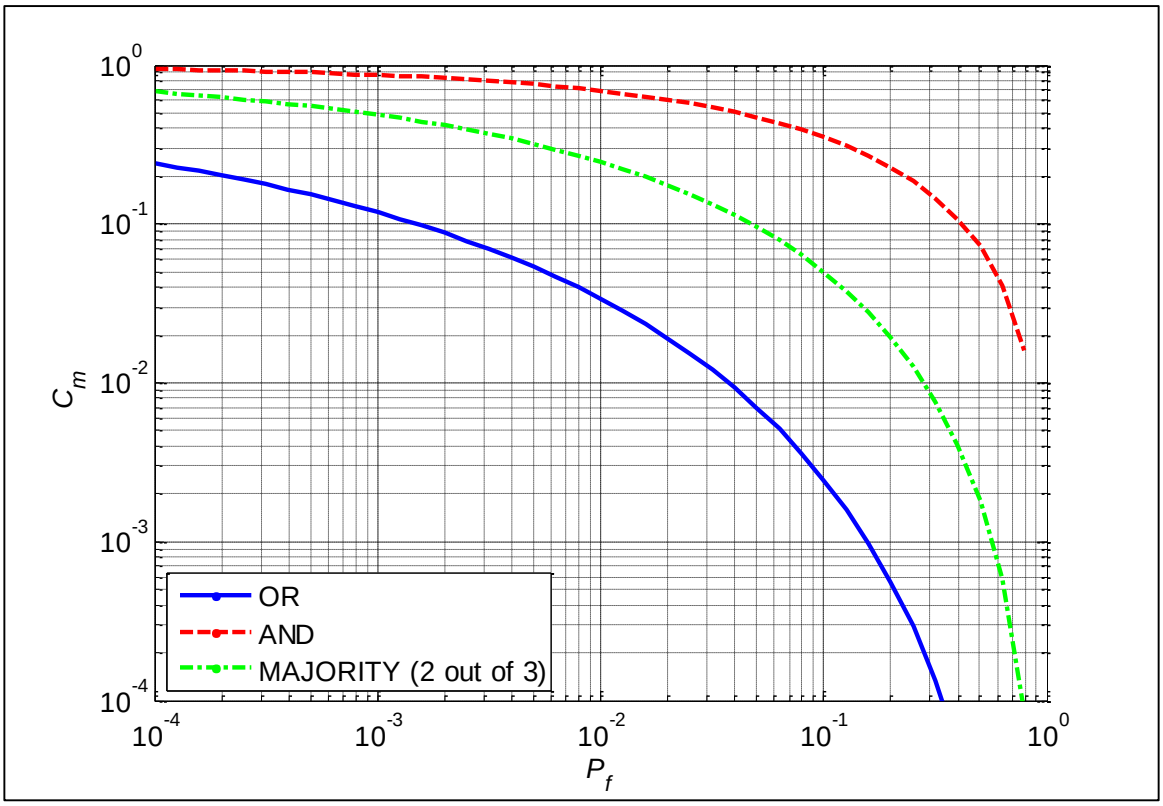

Figure 4-2: CROC in log-normal channel using different hard fusion rules at average SNR=10dB, $\sigma_{dB} = 2\text{dB}, N_s = 10, k = 3$.

4.3 Soft (Data) Fusion

In soft (data) fusion, SUs send their measured energy, or a function of it, to the FC to make the final decision about the presence of the PU. Different soft fusion schemes can be used [38] such as: square-law selection (SLS), square-law combining (SLC), maximal ratio combining (MRC) and selection combining (SC). The block diagram of these soft fusion schemes is depicted in Figure 4-3. In this section the SLS and SLC schemes are addressed in detail.

4.3.1 Square-Law Selection (SLS)

In the square-law selection scheme the energies measured by every SU are sent to the FC and the SU with the highest measured energy is selected. Assuming that k identically distributed SUs are performing sensing, then the test statistics of the energy measured by the FC can be expressed as:

$$V_{SLS} = max(V_1, V_2, \dots, V_k) \tag{4.9}$$

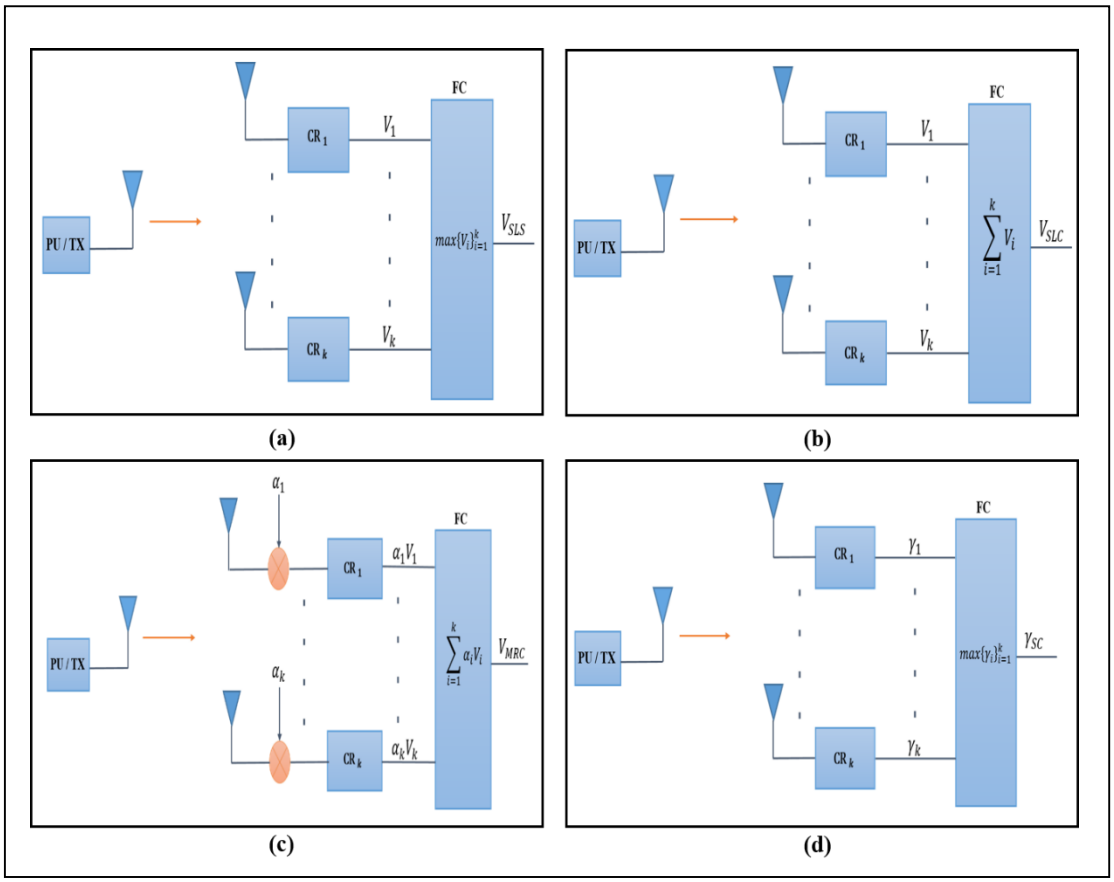

Figure 4-3: Block diagrams of different soft fusion rules: a) SLS, b) SLC, c) MRC, d) SC.

A. SLS in AWGN Channel

In a non-fading AWGN channel, the probability of false alarm, $P_{f,SLS}$, and the probability of detection, $P_{d,SLS}$, using the SLS scheme are given respectively as [39]:

$$P_{f,SLS} = 1 - \left(1 - P_f\right)^k \tag{4.10}$$

$$P_{f,SLS} = 1 - \left(1 - \frac{\Gamma(N_s, \frac{\lambda}{2})}{\Gamma(N_s)}\right)^k \tag{4.11}$$

$$P_{d,SLS} = 1 - \prod_{i=1}^{k}\left(1 - Q_{N_s}\left(\sqrt{2\gamma_i}, \sqrt{\lambda}\right)\right) \tag{4.12}$$

Assuming k i.i.d SUs, $P_{d,SLS}$ can be written as:

$$P_{d,SLS} = 1 - \left(1 - P_d(\gamma, \lambda)\right)^k \tag{4.13}$$

$$P_{d,SLS} = 1 - \left(1 - Q_{N_s}\left(\sqrt{2\gamma}, \sqrt{\lambda}\right)\right)^k \tag{4.14}$$

where $= \{\gamma_i\}_{i=1}^{k}$, and represents the SNR received at the SU.

B. SLS in a Log-normal Shadowing Channel

In a log-normal shadowing channel, the probability of false alarm is not affected by shadowing, while the probability of detection is calculated using the following formula:

$$P_{d,SLS}^{log} = \int_0^{\infty} P_{d,SLS}(\gamma_1, \gamma_2, \dots, \gamma_k, \lambda)\, f_{\gamma_1\gamma_2\dots\gamma_k}(\gamma_1, \gamma_2, \dots, \gamma_k)\, d\gamma_1 d\gamma_2 \dots d\gamma_k \tag{4.15}$$

For k independent SUs, $P_{d,SLS}^{log}$ can be written as:

$$P_{d,SLS}^{log} = 1 - \int_0^{\infty} \dots \int_0^{\infty} \prod_{i=1}^{k} \left[1 - Q_{N_s}\left(\sqrt{2\gamma_i}, \sqrt{\lambda}\right)\right] f_{\gamma_i}(\gamma_i)\, d\gamma_i$$

$$= 1 - \prod_{i=1}^{k} \int_0^{\infty} \left[1 - Q_{N_s}\left(\sqrt{2\gamma_i}, \sqrt{\lambda}\right)\right] f_{\gamma_i}(\gamma_i)\, d\gamma_i \tag{4.16}$$

where $f_{\gamma_i}(\gamma_i)$ is given by:

$$f_{\gamma_i}(\gamma_i) = \frac{\xi}{\gamma_i \sigma_{i,dB}\sqrt{2\pi}} exp \frac{-\left(\xi log_e \gamma_i - \mu_{i,dB}\right)^2}{2{\sigma^2}_{i,dB}} \quad , \gamma_i \geq 0 \tag{4.17}$$

Substituting (4.12) and (4.17) in (4.16) yields the following expression for the probability of detection in log-normal channel using the SLS scheme, $P_{d,SLS}^{log}$:

$$P_{d,SLS}^{log} = 1 - \prod_{i=1}^{k} \left(1 - P_{d,log}(\gamma_i, \lambda)\right)$$

$$= 1 - \prod_{i=1}^{k} \left(1 - \sum_{j=1}^{M} \frac{w_j}{\sqrt{\pi}}\, Q_{N_s}\left(\sqrt{2\, exp\left(\frac{a_j \mu_{i,dB}\sqrt{2} + \mu_{i,dB}}{\xi}\right)}, \sqrt{\lambda}\right)\right) \tag{4.18}$$

For the case of k i.i.d SUs, $P_{d,SLS}^{log}$ can be written as:

$$P_{d,SLS}^{log} = 1 - \left(1 - P_{d,log}\right)^k \tag{4.19}$$

$$P_{d,SLS}^{log} = 1 - \left(1 - \sum_{j=1}^{M} \frac{w_j}{\sqrt{\pi}}\, Q_{N_s}\left(\sqrt{2\, exp\left(\frac{a_j \sigma_{dB}\sqrt{2} + \mu_{dB}}{\xi}\right)}, \sqrt{\lambda}\right)\right)^k \tag{4.20}$$

4.3.2 Simulation Results Using SLS Scheme

Collaborative sensing performance using the SLS scheme is depicted in Figure 4-4. The CROC curves are evaluated in a log-normal shadowing channel at average SNR= 10dB, $\sigma_{dB} = 2$dB and $N_s = 10$ samples. The improvement in sensing performance due to collaboration is obvious from the simulation results, where the probability of misdetection, $P_{m,SLS}^{log}$, decreases as the number of collaborative SUs increases from $k = 1$ SU to $k = 7$ SUs.

In Figure 4-5, the probability of misdetection in a log-normal channel using the SLS scheme, $P_{m,SLS}^{log}$, is presented with respect to the average SNR at $P_f = 0.01$, $\sigma_{dB} = 2$dB and $N_s = 10$ samples. The probability of misdetection decreases with the increase in the average SNR. Moreover, as the number of collaborative SUs, k, increases the probability of misdetection decreases for a given average SNR.

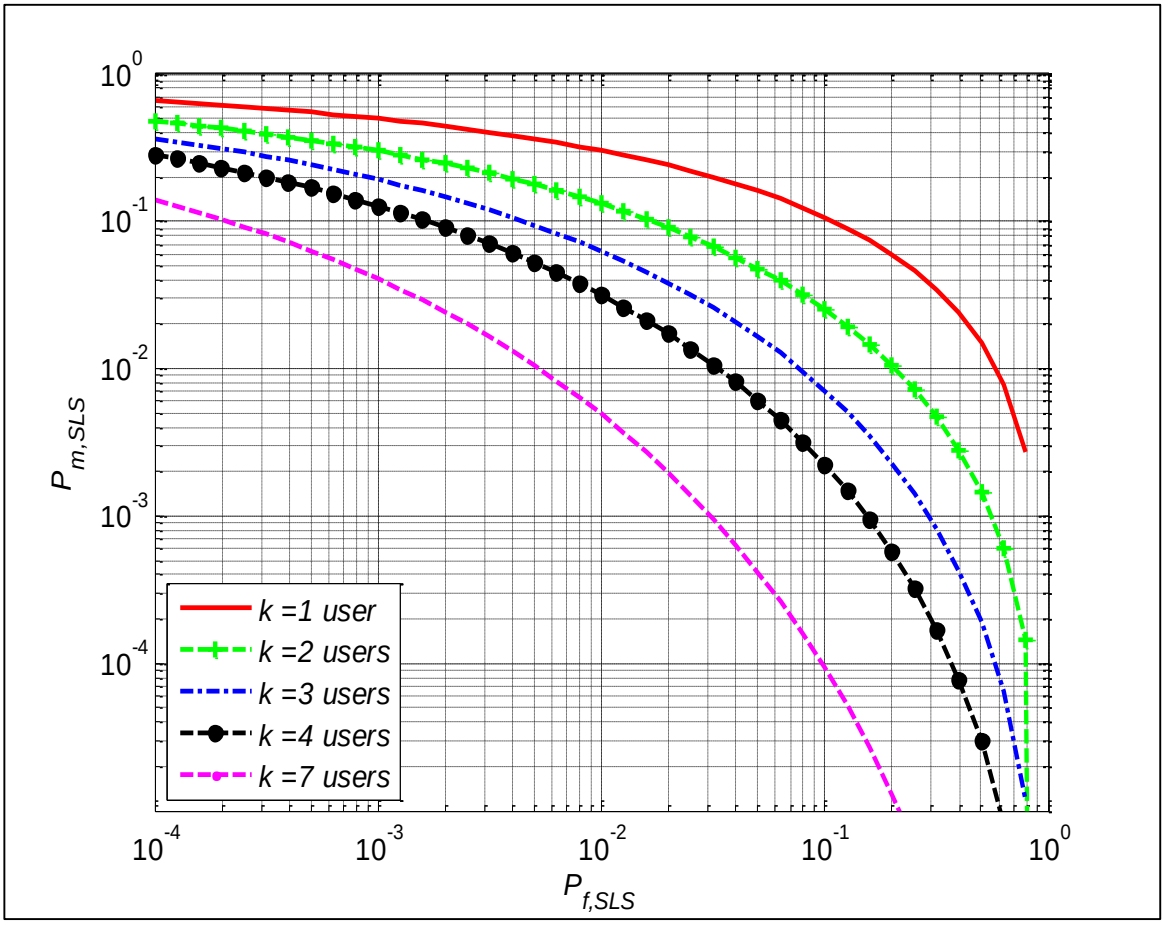

Figure 4-4: CROC in log-normal channel using SLS scheme for different values of k at average SNR=10dB, $\sigma_{dB} = 2$dB, $N_s = 10$.

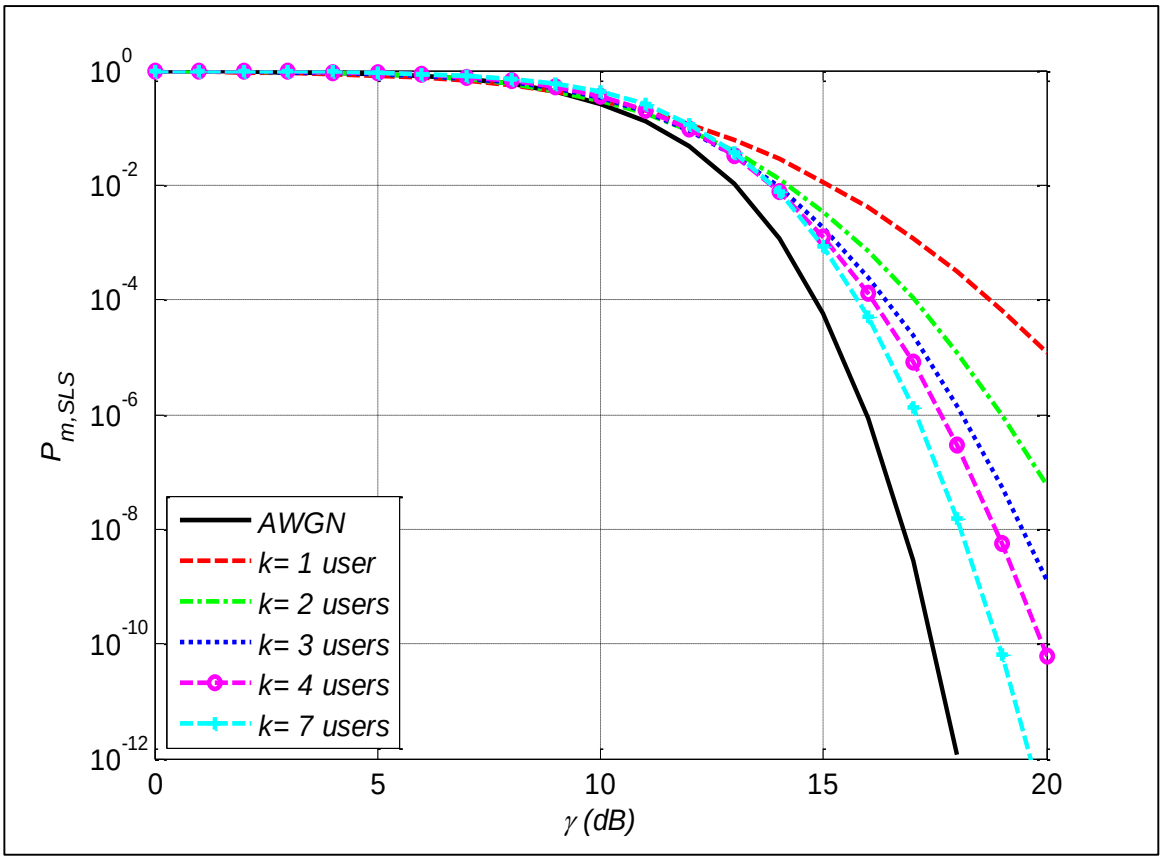

Figure 4-5: $P_{m,SLS}^{log}$ vs. the average SNR in log-normal channel using SLS scheme at $P_f = 0.01, \sigma_{dB} = 2\text{dB}, N_s = 10$.

4.3.3 Square-Law Combining (SLC)

In the SLC scheme, the test statistics (measured energies) of the k SUs are combined at the FC as follows [39]:

$$V_{SLC} = \sum_{i=1}^{k} V_i \tag{4.21}$$

A. SLC in AWGN Channel

In an AWGN channel, the new test statistic V_{SLC} under the H_0 hypothesis is a sum of k central chi-square variables each with $2N_s$ degrees of freedom. Under the H_1 hypothesis, it is a sum of k non-central chi-square variables each with $2N_s$ degrees of freedom and a non-centrality parameter of $2\gamma_i$. Therefore, V_{SLC} can be modeled as a central chi-square variable with $2kN_s$ degrees of freedom under H_0, and a non-central chi-square variable with $2kN_s$ degrees of freedom and a non-centrality parameter of $2\gamma_t$ under H_1.i.e.

$$V_{SLC} = \begin{cases} \chi^2_{2kN} & H_0 \\ \chi^2_{2kN}(2\gamma_t) & H_1 \end{cases} \tag{4.22}$$

where $\gamma_t = \sum_{i=1}^{k} \gamma_i$, and $\gamma_i$is the SNR received at the *i*-th SU.

The probability of false alarm, $P_{f,SLC}$, and the probability of detection, $P_{d,SLC}$, using the SLC scheme in an AWGN channel can be expressed by an analogy to equations (3.9) and (3.10) respectively as:

$$P_{f,SLC} = \frac{\Gamma\left(kN_s, \frac{\lambda}{2}\right)}{\Gamma(kN_s)} \tag{4.23}$$

$$P_{d,SLC} = Q_{kN_s}\left(\sqrt{2\gamma_t}, \sqrt{\lambda}\right) \tag{4.24}$$

For k i.i.d SUs, $P_{d,SLC}$ can be written as:

$$P_{d,SLC} = Q_{kN_s}\left(\sqrt{2k\gamma}, \sqrt{\lambda}\right) \tag{4.25}$$

B. SLC in Log-normal Shadowing Channel

If the SUs experience a log-normal shadowing, then the probability of detection is calculated by averaging $P_{d,SLC}$ in (4.24) over the PDF of γ_t $\left(f_{\gamma_t}(\gamma_t)\right)$.i.e.

$$P_{d,SLC}^{log} = \int_0^{\infty} P_{d,SLC}(\gamma_t, \lambda)\, f_{\gamma_t}(\gamma_t)\, d\gamma_t \tag{4.26}$$

C. Sum of Log-normal Random Variables

The problem that arises here is that there is no exact closed-form expression for the PDF of the sum of the log-normal random variables, $f_{\gamma_t}(\gamma_t)$. According to [35, 40, 41] many analytical approximations have been proposed based on the assumption that the sum of log-normal RVs is a log-normal RV with new mean and variance. Which means that γ_t can be modeled as a log-normal RV with mean $\mu_{t,dB}$, and variance $\sigma^2{}_{t,dB}$. In [41] Schwartz-Yeh presented a method for evaluating the mean and variance of γ_t using exact expressions for the sum of two independent summands. An iterative procedure for the sum of more than two summands, by matching the moments of γ_t in the logarithmic domain with the moments of the individual summands. This method is accurate in calculating the first two moments

within the practical range of the dB-spread i.e. $(2dB \leq \sigma_{dB} \leq 14dB)$ and up to 30 summands. However, it is less accurate outside this range.

Another method for calculating $\mu_{t,dB}$ and ${\sigma^2}_{t,dB}$ is proposed in [35] using the moment generating function (MGF). The MGF of γ_t is defined as:

$$\Psi_{\gamma_t}(s) = \int_0^{\infty} e^{-s\gamma_t} f_{\gamma_t}(\gamma_t)\, d\gamma_t \tag{4.27}$$

where $f_{\gamma_t}(\gamma_t)$ is the PDF of γ_t:

$$f_{\gamma_t}(\gamma_t) = \frac{\xi}{\gamma_t \sigma_{t,dB}\sqrt{2\pi}} exp \frac{-\left(\xi log_e \gamma_t - \mu_{t,dB}\right)^2}{2{\sigma^2}_{t,dB}} \quad , \gamma_t \geq 0 \tag{4.28}$$

Using the Gauss-Hermite integration, the MGF of the log-normal RV γ_t can be written in a series expansion form as:

$$\Psi_{\gamma_t}(s) = \sum_{i=1}^{M} \frac{w_i}{\sqrt{\pi}} exp\left[-s\, exp\left(\frac{\sqrt{2}\sigma_{t,dB}\alpha_i + \mu_{t,dB}}{\xi}\right)\right] \tag{4.29}$$

where *M* is the Hermite integration order. The weights , w_i, and the abscissas, α_i, are tabulated in [36].

Taking advantage of the fact that the MGF of a sum of independent RVs is the product of their individual MGFs [33].i.e.

$$\Psi_{\gamma_t}(s) = \prod_{i=1}^{k} \Psi_{\gamma_i}(s) \tag{4.30}$$

The moments $\mu_{t,dB}$ and $\sigma_{t,dB}$ can be obtained by solving (4.29) numerically by using standard functions such as fsolve in MATLAB for any pair of positive real values of (s). The accuracy of this method increases by increasing the Hermite integration order, M, but this will be at the cost of increasing computational complexity. It is found that $M = 12$ is sufficient to accurately determine the values of $\mu_{t,dB}$ and $\sigma_{t,dB}$.

Following the same procedure used to derive $P_{d,log}$ in (3.18), and using the Schwartz-Yeh method to calculate the moments of γ_t, the collaborative probability

of detection in a log-normal shadowing using the SLC scheme in (4.26) can be written as:

$$P_{d,SLC}^{log} = \sum_{i=1}^{M} \frac{w_i}{\sqrt{\pi}} \, Q_{kN_s}\left(\sqrt{2 \, exp\left(\frac{a_i \sigma_{t,dB}\sqrt{2} + \mu_{t,dB}}{\xi}\right)}, \sqrt{\lambda}\right) \tag{4.28}$$

The performance of this formula in (4.28) is investigated using simulation in the following section.

4.3.4 Simulation Results Using SLC Scheme

The effect of collaboration using the SLC scheme in spectrum sensing performance is evaluated in Figure 4-6 for average SNR$=10$dB, $\sigma_{dB} = 2$dB and $N_s = 10$ samples. The enhancement in performance, due to collaboration between SUs, is obvious, where increasing the number of collaborative SUs, k, results in a significant reduction in the probability of misdetection, $P_{m,SLC}^{log}$.

These results are further proven in Figure 4-7, where the probability of misdetection, $P_{m,SLC}^{log}$, is plotted versus the average SNR for $P_f = 0.01$, $\sigma_{dB} = 2$dB, and $N_s = 10$ samples. Higher values of γ guarantee better detection of the PU, moreover, increasing the degree of collaboration by increasing the number of collaborative SUs, k, results in increasing the probability of detection, $P_{d,SLC}^{log}$ for a certain value of average SNR.

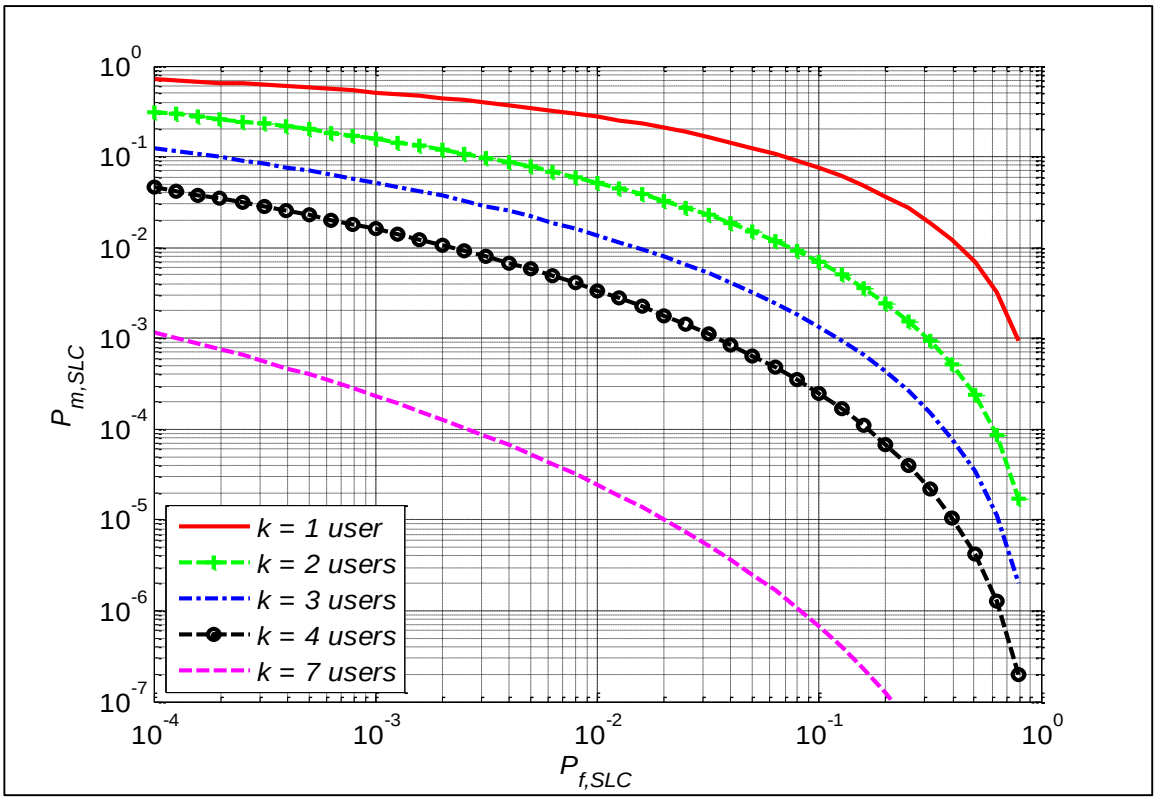

Figure 4-6: CROC in log-normal channel using SLC scheme for different values of k at average SNR=10dB, $\sigma_{dB} = 2\text{dB}, N_s = 10$.

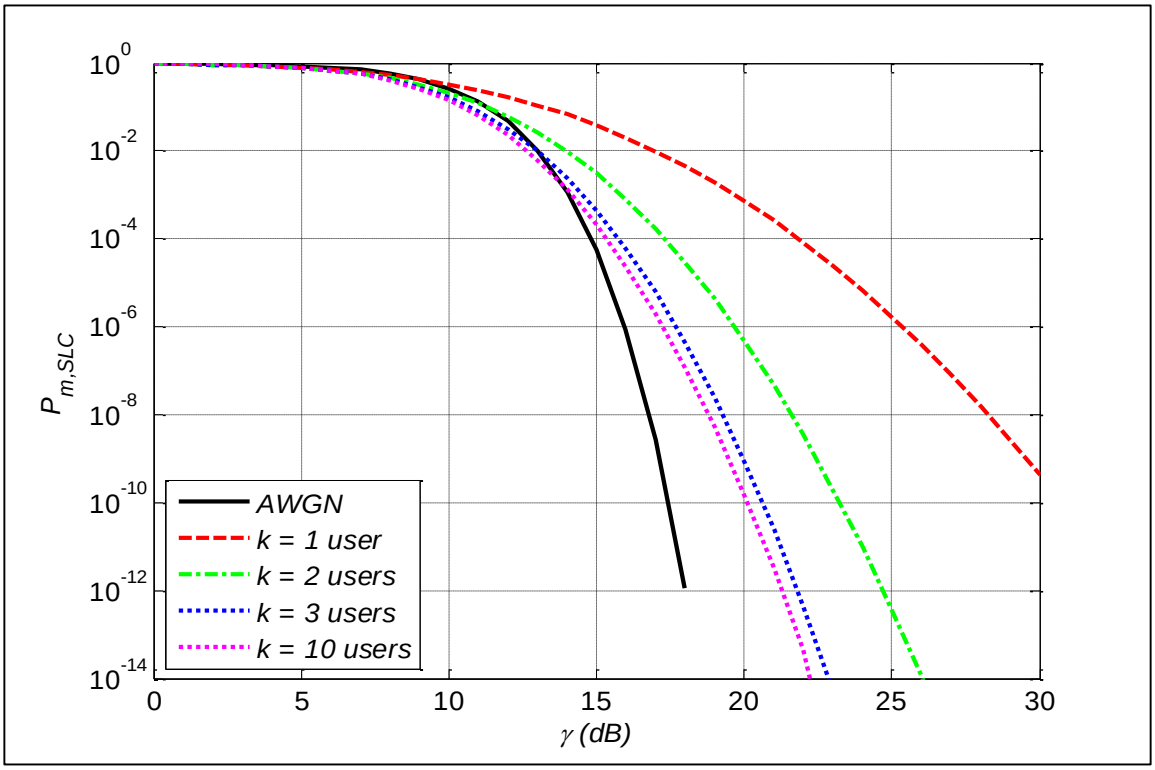

Figure 4-7: $P_{m,SLC}^{log}$ vs. the average SNR in log-normal channel using SLC scheme at $P_f = 0.01, \sigma_{dB} = 2\text{dB}, N_s = 10$.

4.3.5 Comparison

In this section a comparision between the two soft fusion schemes discussed earlier is drawn. In Figure 4-8, CROC for both the SLS and the SLC schemes is evaluated in a log-normal channel for avearge SNR$= 10$dB$\,, \sigma_{dB} = 2$dB and $N_s = 10$ samples. It is obvious that the SLC scheme outperforms the SLS scheme by providing lower probability of misdetection for the same number of collaborative SUs, k. This is because the FC in the SLC scheme accumulates the energies of every SU to make a final decision, in contrast to the SLS scheme where the energy of only one branch is used to make the decision.

Also, the SLS scheme requires estimating the energies of each collaborative SU to choose the branch with the maximum energy. While in the SLC scheme no estimation is required as the energies are added together at the FC. This in its turn gives the SLC scheme an advantage over the SLS scheme in terms comutational complexity.

In Figure 4-9, the probability of midetection is plotted versus the dB-spread for both the SLS and the SLC schemes at average SNR$= 10$dB, $P_f = 0.01$, $k = 3$ SUs, $N_s = 10$ samples. Again it is obvious from the simulation results that the SLC scheme outperforms the SLS scheme with less probability of misdetection at a certain σ_{dB} value for the same number of collaborative SUs. Also, the degredation in perfromance due to a log-normal shadowing is clear, since the probability of misdetection increases as σ_{dB} grows from 2dB to 12dB. However, increasing the number of collaborative SUs, k, mitigates the effect of shadowing as discussed earlier.

A comparison between hard fusion and soft fusion (using the SLC scheme) is depicted in Figure 4-10 at average SNR$= 10$dB, $\sigma_{sB} = 2$dB, $k = 3$ SUs, $N_s = 10$ samples. It is obvious that the SLC scheme outperforms hard fusion rules for the same number of collaborative SUs, by providing the lowest probability of misdetection for a certain probability of false alarm. However, using the SLC consumes more bandwidth, since each SU needs to send the energy measured. While in hard fusion a one-bit binary decision is sent to the FC, resulting in less bandwidth required and lower computational complexity at the FC.

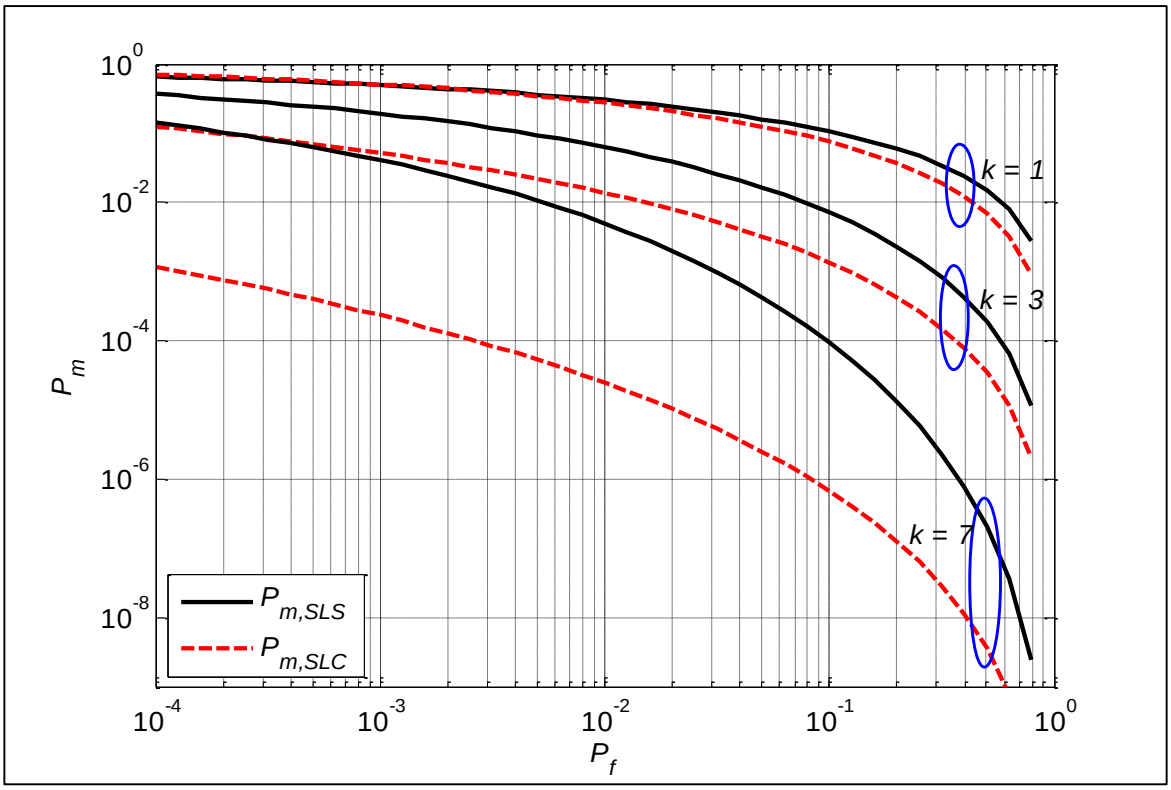

Figure 4-8: CROC in log-normal channel for both SLC and SLS schemes at average SNR=10dB , $\sigma_{dB} = 2\text{dB}, N_s = 10$.

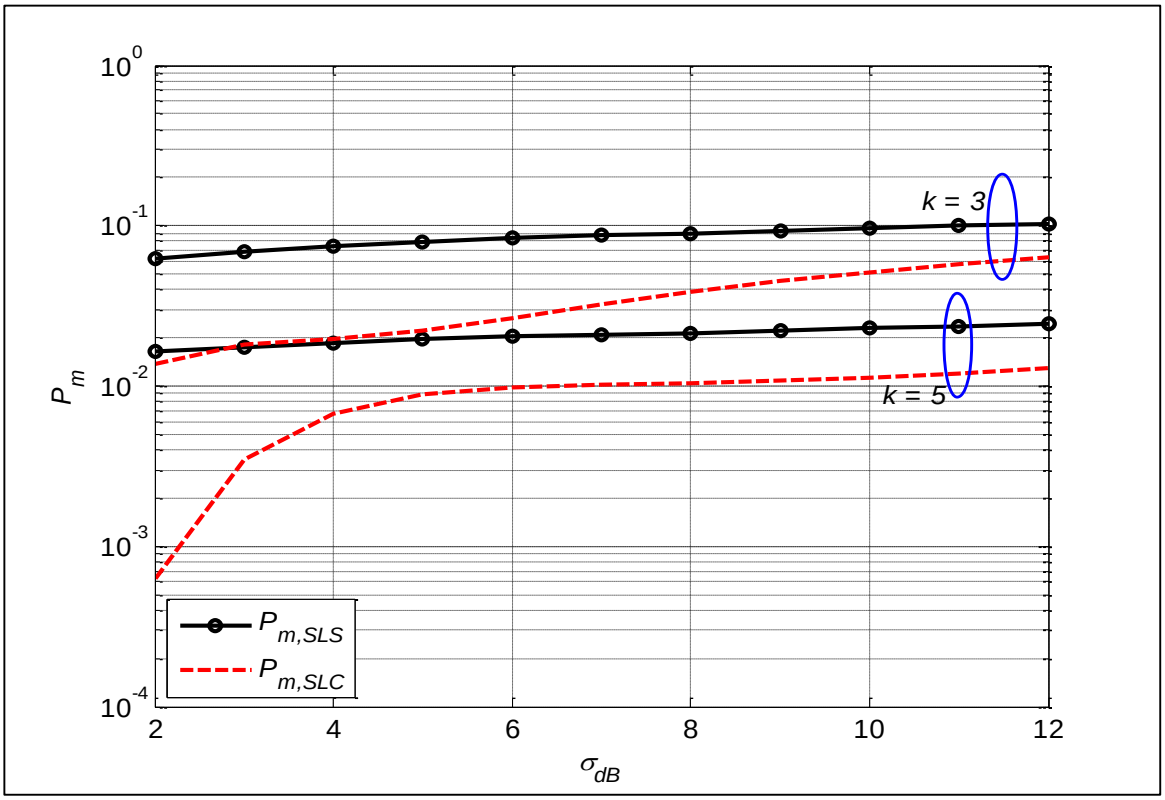

Figure 4-9: P_m vs. σ_{dB} for both SLC and SLS schemes at average SNR=10dB, $P_f = 0.01, N_s = 10, k = 3$.

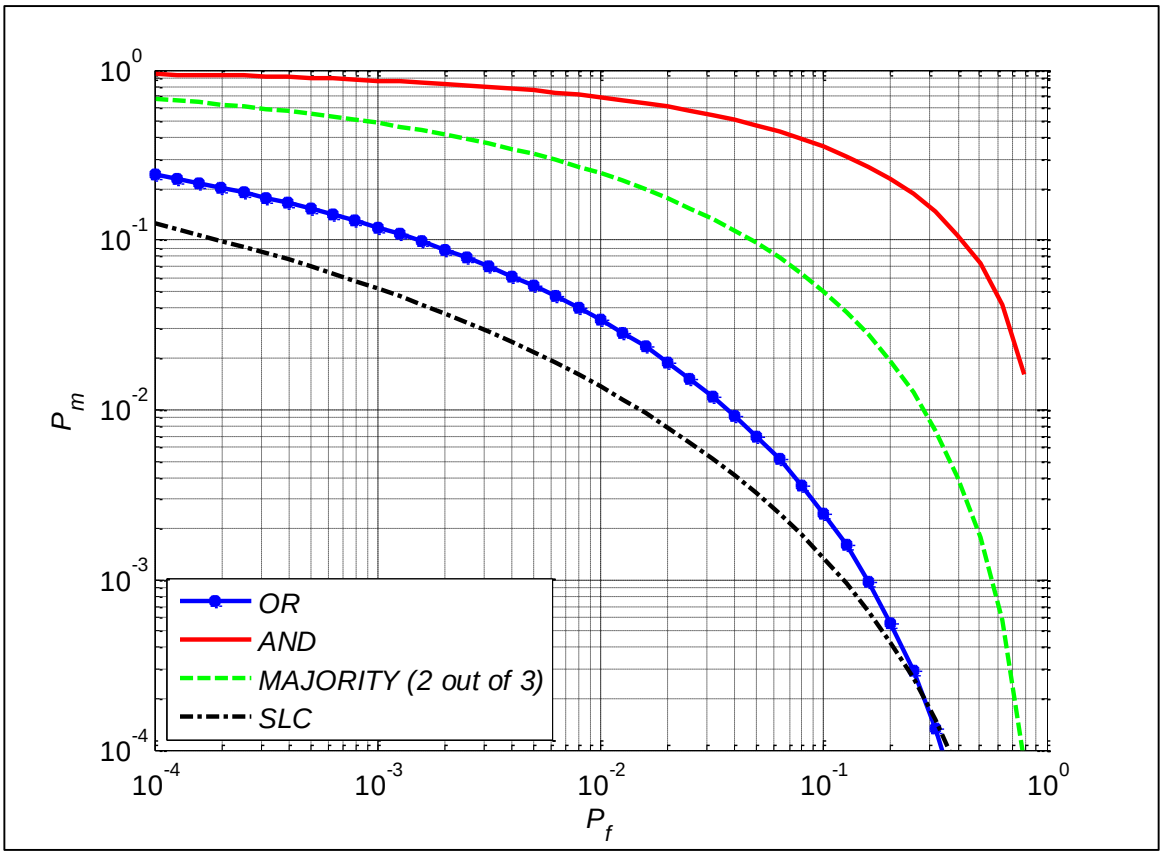

Figure 4-10: Comparison between hard fusion and soft fusion (using SLC) at average SNR=10dB, $\sigma_{dB} = 2$ dB, $k = 3, N_s = 10$.

In conclusion, the performance of spectrum sensing is enhanced due to collaborative sensing. Different fusion rules can be used by the fusion center to combine the local sensing information such as, soft fusion and hard fusion techniques. In soft fusion, the SLC scheme outperforms the SLS scheme and requires fewer computations at the fusion center. In hard fusion, OR-combining guarantees better protection for the PU from SU interference, while AND-combining results in higher spectrum utilization and more spectrum opportunities. In general, soft fusion provides better sensing performance than hard fusion, but it requires more bandwidth overhead and higher computational complexity at the FC. A trade-off between the available resources and the desired detection level should be evaluated when choosing a fusion rule.

CHAPTER 5: WIDEBAND SPECTRUM EDGE DETECTION

5.1 Introduction

Due to the development in wireless communication, average spectrum occupancy has increased, resulting in high spectrum scarcity. Under these circumstances, the secondary users (SUs) need to scan larger dynamic ranges of the frequency spectrum, up to several GHz, to explore spectrum opportunities. This leads to wideband sensing, where multiple frequency bands are sensed at the same time. In this case traditional spectrum sensing techniques such as energy detection, matched filter sensing and cyclostationary-based sensing are impractical, since they are designed for multi-band (narrowband) sensing. In narrowband sensing a tunable bandpass filter (TBPF) is used for sensing one frequency band at a time using one of those traditional techniques. However, this is not the case in wideband sensing, since the SU has to scan multiple frequency bands at the same time. Moreover, the SU usually has no information about the PU activity, such as the center frequency and the bandwidth. In this chapter wideband sensing will be addressed, and in particular wideband sensing using wavelet-based edge detection will be investigated.

5.2 Wideband Sensing Methods

Wideband spectrum sensing is still in its early stages of research. There are six main wideband sensing methods discussed in the literature. They are: filter bank detection [7, 8]; multi-resolution sampling based detection [10, 15]; multicoset sampling based detection [11]; compressed sensing based detection [13, 15]; multirate sampling based detection [9, 42] and wavelet-based detection [14]. A brief overview of these methods is presented in the following sections.

5.2.1 Filter Bank Detection

Boroujeny in [7] proposed a wideband sensing method based on a filter bank. The main idea is to implement a pair of matched root-Nyquist filters at the PU transmitter and the SU receiver, respectively, in a multicarrier cognitive radio network. The filter bank is implemented based on a prototype filter that is used to estimate the baseband (zeroth band). Other frequency bands are obtained by

modulating the prototype filter, as shown in Figure 5-1. Sensing is performed in each subcarrier through converting the corresponding spectrum portion into the baseband, and filtering using lowpass filters as shown in Figure 5-2. The power spectral density (PSD) of the filtered output signal in the *i*-th subcarrier, $S_{y_i,y_i}(f)$, can be written as:

$$S_{y_i y_i}(f) = S_{rr}(f + f_i)\left|H\left(e^{2\pi jf}\right)\right|^2 \approx S_{rr}(f_i)\left|H\left(e^{2\pi jf}\right)\right|^2 \tag{5.1}$$

where $S_{rr}(f_i)$ is the PSD of the received signal $r(t)$ in the *i*-th subband, and $H\left(e^{2\pi jf}\right)$ is assumed to be narrowband and designed as a root-Nyquist (N_f) filter. The expression in (5.1) can be written in terms of z-transform as:

$$\psi_{y_i y_i}(z) = S_{rr}(f_i)H(z)H(z^{-1}) = S_{rr}(f_i)G_{N_f}(z) \tag{5.2}$$

where $G_{N_f}(z)$ is called the Nyquist (N_f) filter, and N_f is the maximum number of subcarriers in the filter bank. In time domain $G_{N_f}(z)$ satisfies:

$$g_{N_f}(n) = \begin{cases} 1 & n = 0 \\ 0 & n = mN_f, m \neq 0 \end{cases} \tag{5.3}$$

Assuming that $\psi_{y_i y_i}(u)$ represents the correlation coefficients of $y_i(n)$ when performing inverse z-transform on $\psi_{y_i y_i}(z)$, the correlation matrix of the measured vectors, $\mathbf{R}_{y_i y_i}$, can be written as:

$$\mathbf{R}_{y_i y_i} = S_{rr}(f_i)\mathbf{A} \tag{5.4}$$

where **A** is the Teoplitz matrix, and each element of **A** is from the sequence $g_{N_f}(n)$.

It is found that $S_{rr}(f_i)$ follows a chi-square distribution, so estimating the degree of freedom is critical for the hypothesis test of $S_{rr}(f_i)$. By finding the eigenvalues of matrix **A**, the degree of freedom can found, and the estimated $S_{rr}(f_i)$ can be obtained using observation vectors, eigenvalues and degree of freedom.

The filter bank method performs well at low PSD values, due to a better response from the prototype filter. However, this method involves high implementation complexity since a large number of RF components are required. This method is not flexible because the range and number of the narrowband filters

are preset. Moreover, it is built based on the assumption that the pair root-Nyquist filters at the PU transmitter and the SU receiver are matched, but this is not practical because in cognitive networks it is hard to get information about the PU.

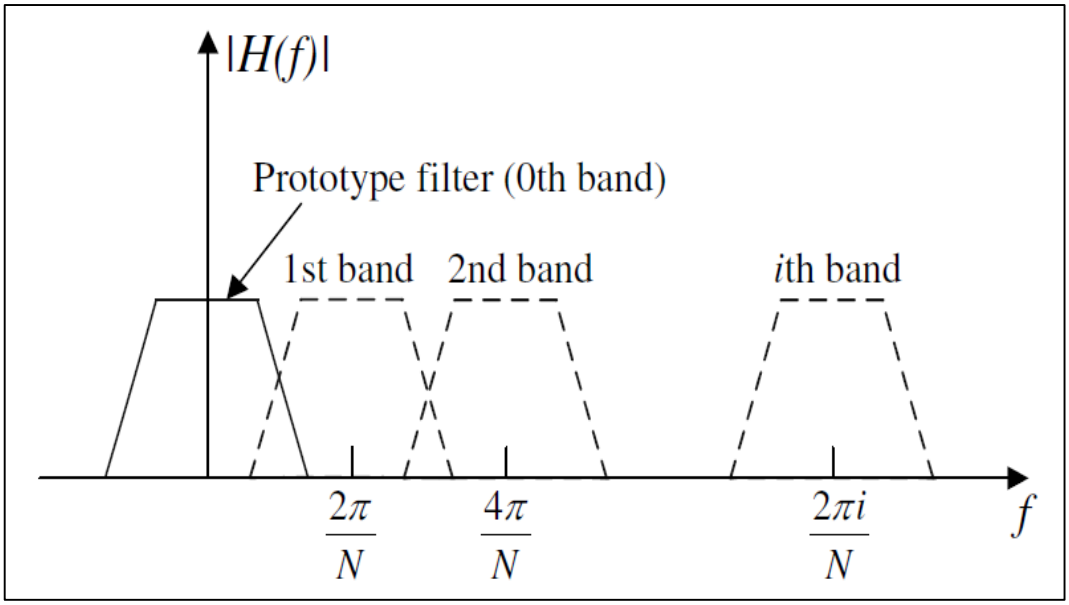

Figure 5-1: Graphical illustration of a filter bank [7].

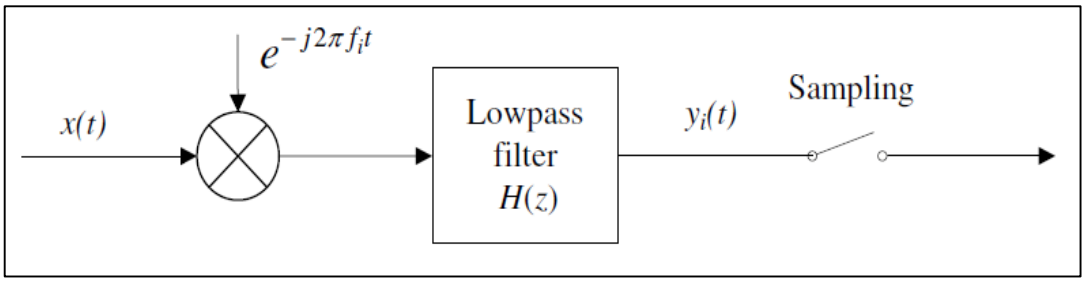

Figure 5-2: Demodulation process in the *i*-th subcarrier [7].

5.2.2 Multi-resolution Sampling Based Sensing

The main challenge in wideband sensing is the high sampling rate required to sense the whole spectrum, which has to be at or above the Nyquist rate. On the other hand, to achieve efficient sensing and high spectrum utilization, sensing should be performed rapidly. Which means that only a limited number of samples can be acquired from the received signal, leading to inaccurate sensing results.

To overcome this problem, sensing is divided into two stages, the first stage is coarse sensing and the second stage is fine sensing. This approach is known as multi-resolution spectrum sensing (MRSS) [15], and it is used to alleviate the high sampling requirements of wideband sensing. In the coarse sensing stage edges of the

non-overlapping frequency bands in the wideband spectrum are detected, then classified based on PSD level within each band into black, gray and white. Then, fine sensing is performed to estimate the spectral shape within the white spaces, which in turn transforms sensing to narrowband mode and reduces sampling requirements.

Figure 5-3 shows the functional block diagram of a CR access system based on MRSS [10]. It consists of:

a) Wideband antennas:
   i. Omni-directional antenna (for spectrum sensing).
   ii. Directive antenna (for the CR link).
b) Frequency-agile RF front-end (RFE) block.
c) Dual-stage wideband spectrum sensing block.
d) Physical (PHY) layer block.
e) Medium Access Control (MAC) block.

The first step in this architecture is coarse sensing, which is performed with a wide resolution bandwidth, to classify the frequency bands into vacant and free bands. Sensing results are then reported to the MAC block, and fine sensing is performed over the free bands. If the band is confirmed as unused, the MAC block allocates this band to the CR link. Fine sensing is repeated over on another band. The main advantage of the MRSS approach is its ability to be implemented in analogue fashion, which provides lower power and real-time sensing processes.

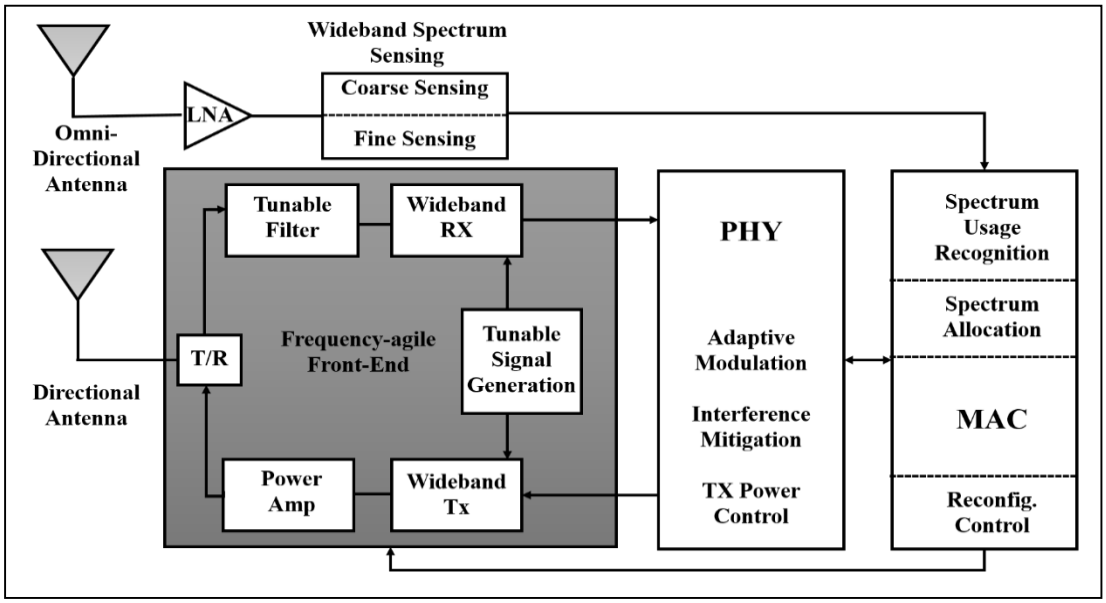

Figure 5-3: Functional block diagram of a CR access system architecture [10].

5.2.3 Multicoset Sampling Based Detection

Multicoset sampling is a wideband sensing method based on a sub-Nyquist sampling rate [11]. In this method some samples are selected from a uniform grid, which can be obtained by uniformly sampling the signal, $r(t)$, at a sampling rate f_s greater than the Nyquist rate. The uniform grid is divided into blocks of L consecutive samples, and v $(v < L)$ samples are acquired from each block while the rest of the samples $(L - v)$ are discarded. This method is implemented using v sampling channels with a sampling rate $\frac{f_s}{L}$, and the *i*-th sampling channel is offset by $\frac{t^i}{f_s}$ from the origin:

$$r^i[n] = \begin{cases} r\left(\frac{n}{f_s}\right) & n = mL + t^i \;\; m \in \mathbb{Z} \\ 0 & otherwise \end{cases} \tag{5.5}$$

where t^i is the index of the *i*-th sample. The indices of the v samples are stored in a constant set called a sampling pattern (C). The sampling pattern is defined as:

$$C = \{t^i\}_{i=1}^{v}, \quad 0 \le t^1 < t^2 < \cdots < t^v \le L - 1 \tag{5.6}$$

The discrete-time Fourier transform (DTFT) of the samples can be linked to the unknown Fourier transform (FT) of the signal $r(t)$ as follows:

$$\vec{Y}(f) = \Phi \vec{R}(f) \tag{5.7}$$

where $\vec{Y}(f)$ is a vector of DTFT of the measurements from the v channels, $\vec{R}(f)$ is a vector of the FT of $r(t)$, and Φ is the measurement matrix with elements determined by the sampling pattern C. Hence, sensing is about recovering $\vec{R}(f)$ from $\vec{Y}(f)$ by solving (5.7). The advantage of multicoset sensing is that the sampling rate of each sampling channel is lower than the Nyquist rate. Also, the number of samples acquired is less than those in the Nyquist case. However, the drawbacks of this method are requiring accurate timing offset between the sampling channels, and the need for a large number of sampling channels to obtain accurate sensing.

5.2.4 Compressed Sensing Based Detection

Compressed sensing (CS) is a novel technique that has been suggested to overcome the high sampling requirements of wideband sensing. Taking advantage of

the fact that wireless signals are sparse, due to low spectrum occupancy by licensed users, signals can be reconstructed using samples taken at a sub-Nyquist rate. In [15] the author proposed a CS technique based on the MRSS mentioned earlier. However, in this method the coarse sensing stage is performed using wavelet-based edge detection to detect the frequency edges of the non-overlapping bands in the PSD of the wideband signal. Figure 5-4 shows a block diagram of the proposed CS method.

Assume that the time required for sensing is $t \in [0, MT_o]$, with T_o as the Nyquist sampling rate, and M is the number of samples required to recover the signal without aliasing. The continuous-time signal received by the SU $r(t)$ is converted to a discrete signal x_t of length K. The sampling process can then be expressed as follows:

$$x_t = S^T r_t \tag{5.8}$$

where S is an $(M \times K)$ projection matrix , and r_t is an $(M \times 1)$ vector with samples taken from $r(t)$. The elements of x_t are the projection of $r(t)$ onto the basis.

Briefly, a multi-step compressed sensing is performed using the following steps:

a) A discrete signal x_t is generated from $r(t)$ using compressed random sampling.

b) The frequency response r_f is reconstructed from x_t via a basis pursuit technique, where $r_f = \mathrm{F}_M r_t$, and F_M is the *M*-point unitary discrete Fourier transform matrix.

c) A number of frequency bands *N*, and the frequency locations $\{[f_i, f_{i+1}]\}_{i=0}^{N-1}$ are estimated based on $\hat{\mathrm{r}}_f$ using wavelet-based edge detection.

d) The PSD average amplitude within each band is estimated to classify the bands into black, gray or white.

One-step compressed sensing is also proposed to reduce the implementation complexity of coarse sensing, where the frequency band locations are detected from x_t without recovering the frequency response r_f.

Other CS methods are presented in the literature. In [13, 43] the authors suggested using an analogue-to-information converter (AIC) for compressing the analogue signal in the analogue domain. However, the drawback of this approach is

the high computational complexity represented by the large size of the measurement matrix. Also, the AIC model is affected by design imperfections.

In [12] a parallel AIC model is proposed, known as a modulated wideband converter (MWC). The advantages of this method are the reduced measurement matrix size and robustness to design imperfections and noise. On the other hand, this method requires large numbers of parallel sampling channels leading to an increased computational complexity.

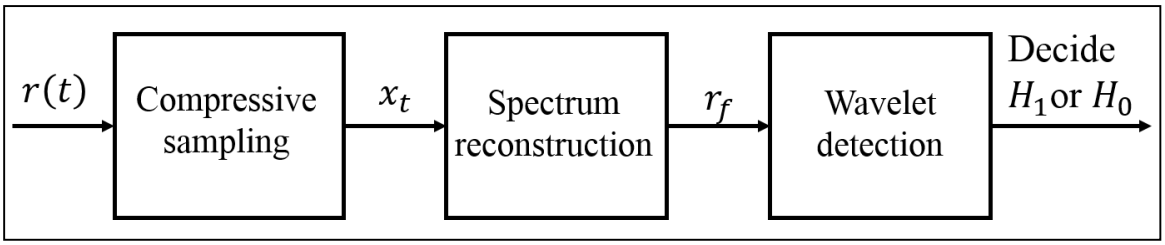

Figure 5-4: A block diagram for compressed sensing based detection.

5.2.5 Multirate Sampling Based Detection:

This method also uses the concept of compressing the wideband signal in the analogue domain. A sparse multiband signal can be reconstructed using asynchronous multirate sampling (MRS) [9], or synchronous multirate sampling (SMRS) [42]. In the MRS approach the signal can be reconstructed without synchronization of the sampling channels. However, the signal should possess certain properties to be reconstructed using MRS such as a minimal number of bands or uniqueness.

In the SMRS approach, the signal is reconstructed from linear equations relating the Fourier transform of the received signal to that of the samples. The number of sampling channels, v, required to reconstruct a k-sparse signal is $v \geq 2k$. However, applying the multirate sampling approach in cognitive radio networks involves high implementation complexity due to the number of sampling channels required, and the difficulty of having a spectrum with the special properties mentioned earlier for the MRS.

5.2.6 Wavelet-based Detection

Wavelet-based detection is a wideband sensing approach based on edge detection [14]. Edge detection is used to identify the irregular structure in the PSD

function of the received wideband signal. These irregularities, also called edges, carry information about the frequency boundaries of the non-overlapping bands. Hence, the main goal is to identify the edges of those bands, and classify the bands into black, gray or white, based on whether the estimated PSD level within each band is high, medium or low.

Continuous Wavelet transform (CWT) of the PSD function of the wideband signal is used to locate the singularities and irregularities. As shown in Figure 5-5 the PSD is modeled as a train of consecutive frequency subbands, where the PSD is smooth within the subbands but exhibits irregularities on the borders of any two neighboring subbands. The first and second derivatives of the CWT of the PSD are used to identify the edges. The local maxima of the first derivative or the zeroes of the second derivative are used to locate the boundaries (edges) of the consecutive subbands. The advantage of this approach is its ability to adapt to a dynamic frequency range by controlling the wavelet smoothing function. However, the high sampling rate analogue to digital converter (ADC) that is required to analyze wideband signals, and the energy cost of that ADC, are concerning issues.

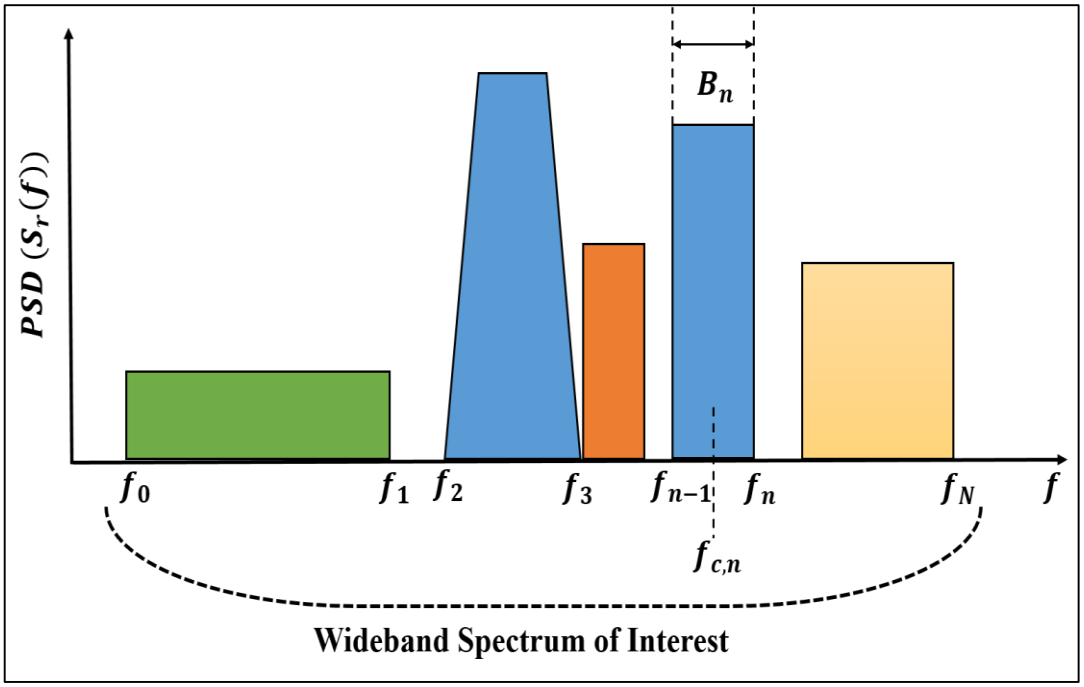

Figure 5-5: Power spectral density (PSD) of the wideband spectrum of interest.

Table 5-1 summarizes the advantages and disadvantages of the wideband sensing methods discussed above [44].

Table 5-1: Advantages and disadvantages of different wideband sensing methods.

Sensing Method	Advantages	Disadvantages
Filter Bank Detection	Low sampling rate High spectral dynamic range	Large implementation complexity Not flexible as filters are preset
Multicoset Sampling	Low sampling rate Less measurements	Requires accurate time offsets Requires too many sampling channels
Compressed Sensing	Low sampling rate Less processed data	High implementation complexity Matrix storage & transmission
Multirate Sampling	Low sampling rate Less sampling channels	Stringent requirements on devices
Wavelet-based Detection	Flexibility in adapting to dynamic spectrum	Requires high sampling rate ADC High energy consumption

5.3 System Model of Wavelet-based Detection

If we assume a wideband signal consisting of N consecutive subbands lies within the frequency range $[f_0, f_N]$ with a total bandwidth of B Hz. Frequency locations and PSD levels for each subband need to be detected by the SU, where the n-th subband is defined by $B_n: \{f \in B_n, f_{n-1} < f < f_n\}, n = 1, 2, \cdots, N$. The number of subbands and the frequency locations are unknown to the SU, however, the boundaries f_0 and f_N are known. Also, the PSD is assumed to be smooth within the subbands as shown in Figure 5-5.

Based on this scenario [14], the power spectral shape of each subband, $S_n(f)$, can be defined as:

$$S_n(f) = \begin{cases} 1, & \forall f \in B_n \\ 0, & \forall f \notin B_n \end{cases} \tag{5.9}$$

And the PSD of the signal received by the SU, $S_r(f)$, can be written as:

$$S_r(f) = \sum_{n=1}^{N} a_n^2 \, S_n(f) + S_w(f) \qquad f \in [f_0, f_N] \tag{5.10}$$

where a_n^2 is the power density within the n-th subband. The time domain signal is:

$$r(t) = \sum_{n=1}^{N} a_n \, p_n(t) + w(t) \tag{5.11}$$

where $p_n(t)$ is the signal occupying B_n with PSD $S_n(f)$, and $w(t)$ is the AWGN with zero-mean and two-sided PSD $S_w(f) = N_0/2, \ \forall f$.

The continuous wavelet transform (CWT) of $S_r(f)$ can be expressed as [14]:

$$\mathcal{W}_s\big(S_r(f)\big) = S_r(f) * \phi_s(f) \tag{5.12}$$

where * is the convolution operator, $\phi_s(f)$ is the wavelet smoothing function dilated by a scale factor s and is defined as:

$$\phi_s(f) = \frac{1}{s} \, \phi\left(\frac{f}{s}\right) \tag{5.13}$$

The scale factor s takes dyadic scales, i.e. $s = 2^j, j = 1, 2, \cdots, J$. $\phi(f)$ is the mother wavelet function, usually a Gaussian or Haar wavelet.

As mentioned earlier, edges are defined using the first and second derivatives of $\mathcal{W}_s\big(S_r(f)\big)$, since they correspond to the local sharp variations within the PSD function, $S_r(f)$. The first and second derivatives of $\mathcal{W}_s\big(S_r(f)\big)$ can be written respectively as:

$$\mathcal{W}_s'\big(S_r(f)\big) = s\frac{d}{df}(S_r(f) * \phi_s)(f) = S_r(f) * \left(s\frac{d\phi_s}{df}\right)(f) \tag{5.14}$$

$$\mathcal{W}_s''\big(S_r(f)\big) = s^2\frac{d^2}{df^2}(S_r(f) * \phi_s)(f) = S_r(f) * \left(s^2\frac{d^2\phi_s}{df^2}\right)(f) \tag{5.15}$$

By finding the local extrema of the $\mathcal{W}_s' S_r(f)$, the local maxima in particular, since they correspond to sharp variation points, or the zeros of $\mathcal{W}_s'' S_r(f)$, frequency edges can be realized as follows:

$$\hat{f}_n = \text{maxima}_f \left\{\left|\mathcal{W}_s'\big(S_r(f)\big)\right|\right\}, \qquad f \in (f_0, f_N) \tag{5.16}$$

$$\hat{f}_n = \text{zeros}_f \left\{\left|\mathcal{W}_s''\big(S_r(f)\big)\right|\right\}, \qquad f \in (f_0, f_N) \tag{5.17}$$

By setting the scale factor s to the dyadic scale, only modulus maxima or zero-crossings that propagate to larger scales are taken, while others are discarded as noise. Moreover, multiscale wavelet products can be used to enhance multiscale peaks due to the edges, while suppressing noise. The multiscale wavelet product of J CWT gradients can be defined as:

$$U_J(S_r(f)) = \prod_{j=1}^{J} \mathcal{W}'_{s=2^j}(S_r(f)) \tag{5.18}$$

where $\mathcal{W}'_s S_r(f)$ is defined in (5.14). Edges can be then acquired by finding the local maxima of $U_J S_r(f)$, i.e.

$$\hat{f}_n = \text{maxima}_f\{|U_J(S_r(f))|\}, \qquad f \in (f_0, f_N) \tag{5.19}$$

After identifying the frequency edges, the PSD levels within subbands, $\{a_n^2\}_{n=1}^N$, are estimated. The estimated PSD level within the *n*-th subband, B_n, can be computed as:

$$\beta_n = \frac{1}{f_n - f_{n-1}} \int_{f_{n-1}}^{f_n} S_r(f)\, df \tag{5.20}$$

The estimated PSD level β_n can be related to a_n^2 as:

$$\beta_n \approx a_n^2 + N_0/2 \tag{5.21}$$

where $N_0/2$ can be estimated from any empty subband. Hence the estimated PSD of the *n*-th subband can be written as:

$$\hat{a}_n^2 = \beta_n - \min_n \beta_n, \qquad n = 1, \cdots, N \tag{5.22}$$

According to the value of $\hat{a}_n^2$, detected frequency subbands can be classified to black, gray or white. A block diagram of the wavelet-based detection approach is depicted in Figure 5-6.

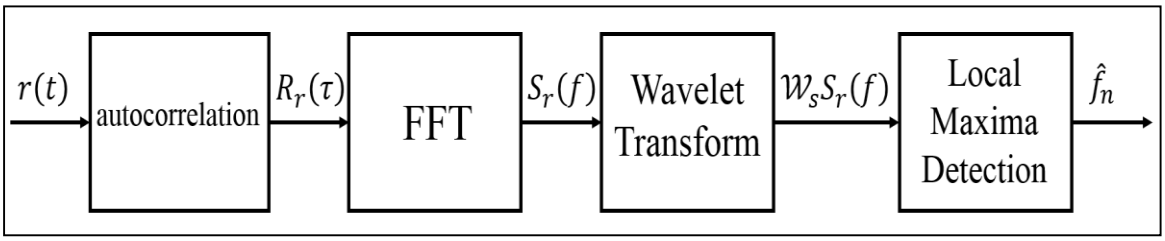

Figure 5-6: Wavelet-based edge detection block diagram.

The pseudo code for the wavelet-based edge detection technique described above is proposed in Algorithm 1.

Algorithm 1: Wavelet-based Detection

Input: $f_0, f_N, \ \phi_s(f), r(t)$

Output: $N, \{f_n\}_{n=1}^{N-1}, \{a_n^2\}_{n=1}^{N}$

$R_r(\tau) \leftarrow E\{r(t)r(t+\tau)\}$

$S_r(f) \leftarrow \mathcal{F}\{R_r(\tau)\}$

$\mathcal{W}_s(S_r(f)) \leftarrow (S_r(f) * \phi_s(f))$

$\mathcal{W}'_s(S_r(f)) \leftarrow s\dfrac{d\mathcal{W}_s S_r(f)}{df}$

$\{f_n\}_{n=1}^{N-1} = \textbf{maxima}_{\ f}\ \{|\mathcal{W}'_s(S_r(f))|\}$

for i**= (1) to (**N**) do**

$a \leftarrow f_{i-1}$

$b \leftarrow f_i$

$h = \frac{b-a}{y}$

$\beta_i = 0$

for j**= (1) to (**$y-1$**) do**

$\beta_i \leftarrow \beta_i + hS_r(a+jh)$

end for

$\beta_i \leftarrow \beta_i + \frac{h}{2}S_r(a) + \frac{h}{2}S_r(b)$

end for

$x \leftarrow \min_n\{\beta_n\}_{n=1}^{N}$

for n**= (1) to (**N**) do**

$a_n^2 \leftarrow \beta_n - x$

end for

5.4 Wavelet-based Detection in Log-normal Shadowing

The system model described in the previous section is for AWGN channel. In this section the system model is modified to include log-normal shadowing. Log-normal shadowing causes random variations in the average power of the signal in the order of tens of wavelengths. The level of shadowing depends on the type of the obstacle blocking the signal travelling from the transmitter to the receiver. It is measured by the value of dB-spread, σ_{dB}, as mentioned in Chapter 3.

Log-normal shadowing results in degradation in the power magnitude, adds more variations to the signal and leads to abrupt changes. This in its turn affects edge detection and results in more unwanted edges.

In log-normal shadowing, the time domain signal received by the SU can be expressed as:

$$r_{log}(t) = \sum_{n=1}^{N} a_n \, h_n(t) p_n(t) + w(t) \tag{5.23}$$

where $h_n$is the channel gain between the PU and SU in the *n*-th subband.

The PSD of the signal $r_{log}(t)$ is:

$$S_{r,log}(f) = \sum_{n=1}^{N} H_n(f)\left(a_n^2 S_n(f)\right) + S_w(f) \qquad f \in [f_0, f_N] \tag{5.24}$$

where $H_n(f)$ is the *n*-th subband impulse response. In the case of slow and flat fading, (5.24) can be written as:

$$S_{r,log}(f) = \sum_{n=1}^{N} H_n \, a_n^2 \, S_n(f) + S_w(f) \qquad f \in [f_0, f_N] \tag{5.25}$$

In the previous section a system model was built under the assumption that the number of subbands, N, is unknown to the SU, but remains unchanged within a time burst. However, in the presence of slow fading the number of subbands changes from burst to burst. The effect of log-normal shadowing on edge detection will be investigated in the next section.

5.5 Simulation Results & Discussion

In this section the performance of wavelet-based edge detection will be investigated. The effect of certain factors on edge detection accuracy such as, the scale factor (s), collaboration between SUs and spectrum shape will be discussed. Also, the performance of edge detection in the presence of log-normal shadowing will be investigated.

5.5.1 The Effect of Scale Factor (s)

For a wideband signal with total bandwidth $B = 750\ MHz$, located over the frequency range $[f_0 = 50\ MHz,\ f_N = 800\ MHz]$, the PSD $S_r(f)$ is depicted in Figure 5-7. Using a Gaussian mother wavelet, and scale factor over dyadic scale $s = 2^j, j = 1, 2, 3, 4$, it is obvious that the larger the value of s, the smoother the wavelet transform within the subbands. This means that the edges are retained at coarser scales, while the noise is suppressed as shown in Figure 5-8. Moreover, better edge detection is obtained using the multiscale wavelet product, where the exact edges are kept while edges due to noise vanished as illustrated in Figure 5-9.

The histogram of the detected edges using wavelet transform is shown in Figure 5-10 for 100 simulation runs. It can be observed that as the scale factor gets coarser (larger), more accurate detection is obtained. Furthermore, using the multiscale product enhances edge detection as discussed earlier.

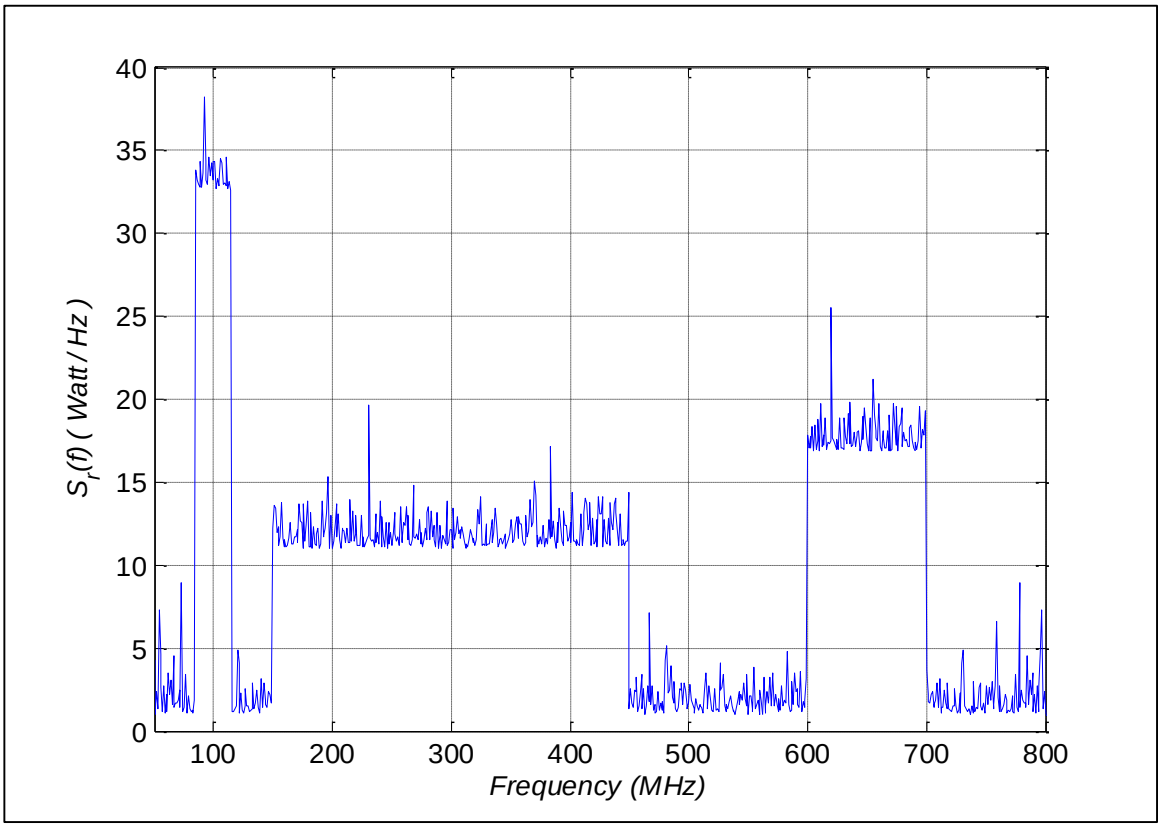

Figure 5-7: Power spectral density (PSD) of the received wideband signal.

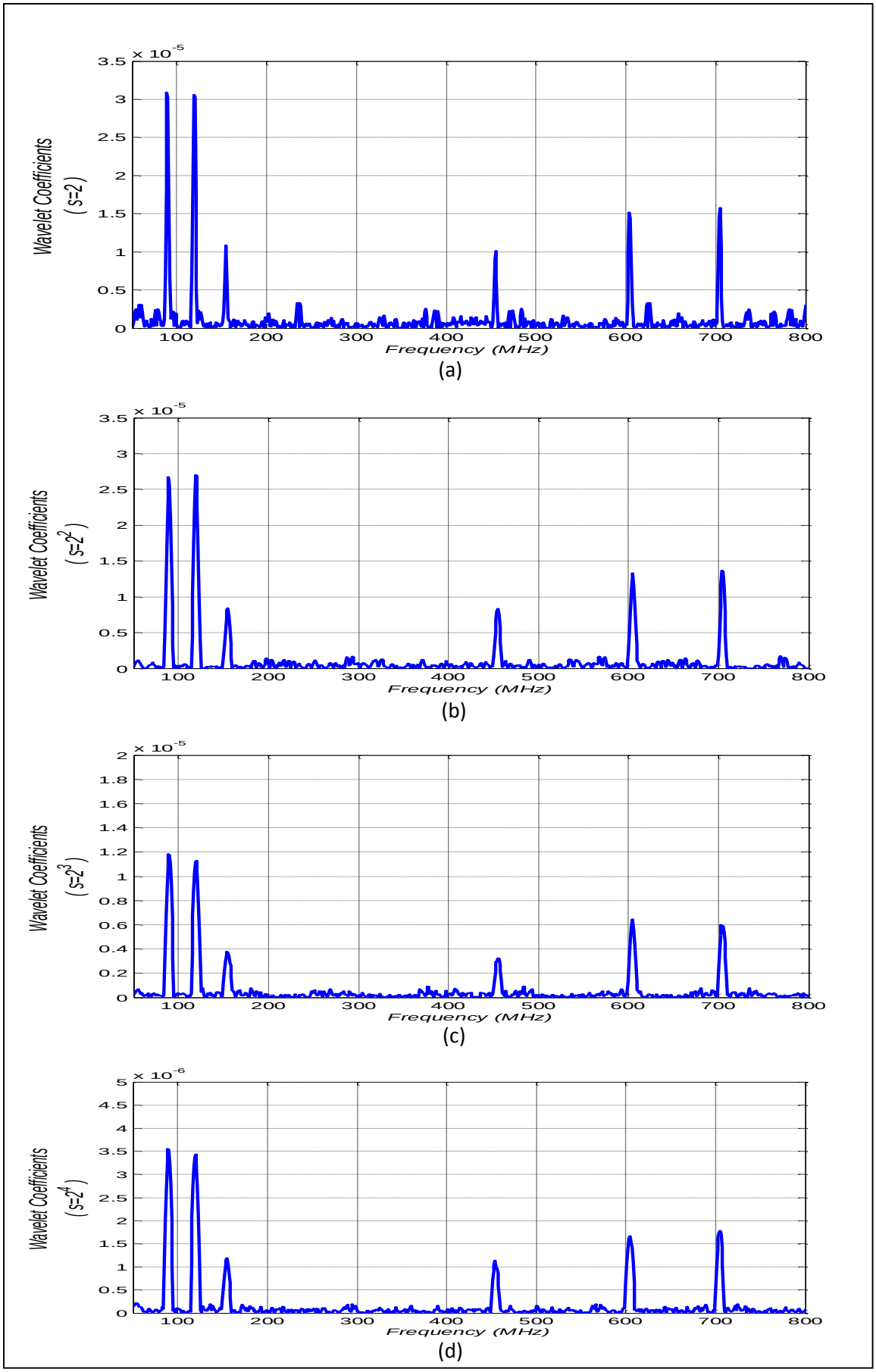

Figure 5-8: Wavelet coefficients at different scales: a) s = 2, b) s = 4, c) s = 8, d) s = 16.

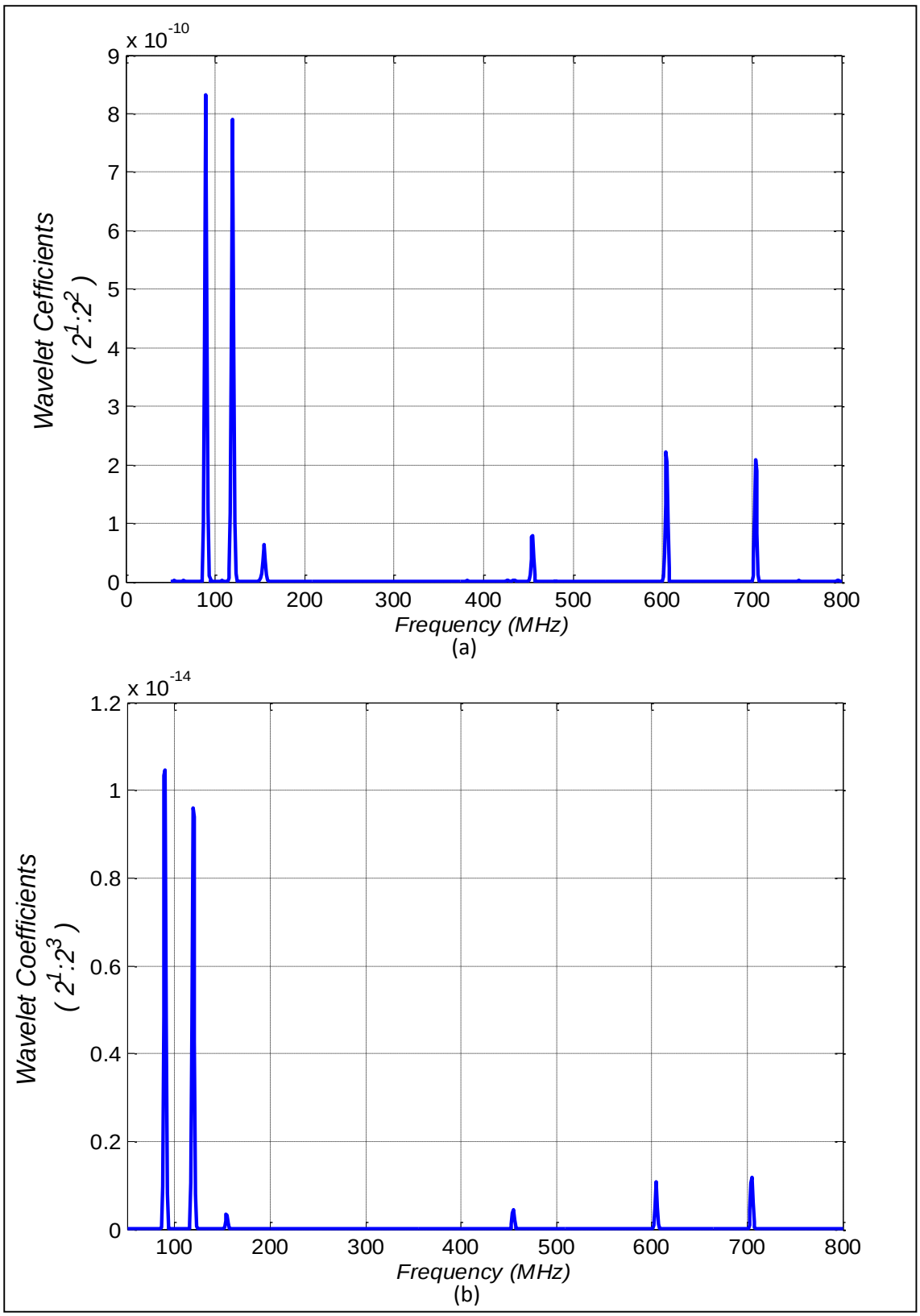

Figure 5-9: Wavelet coefficients at multiscale wavelet product.

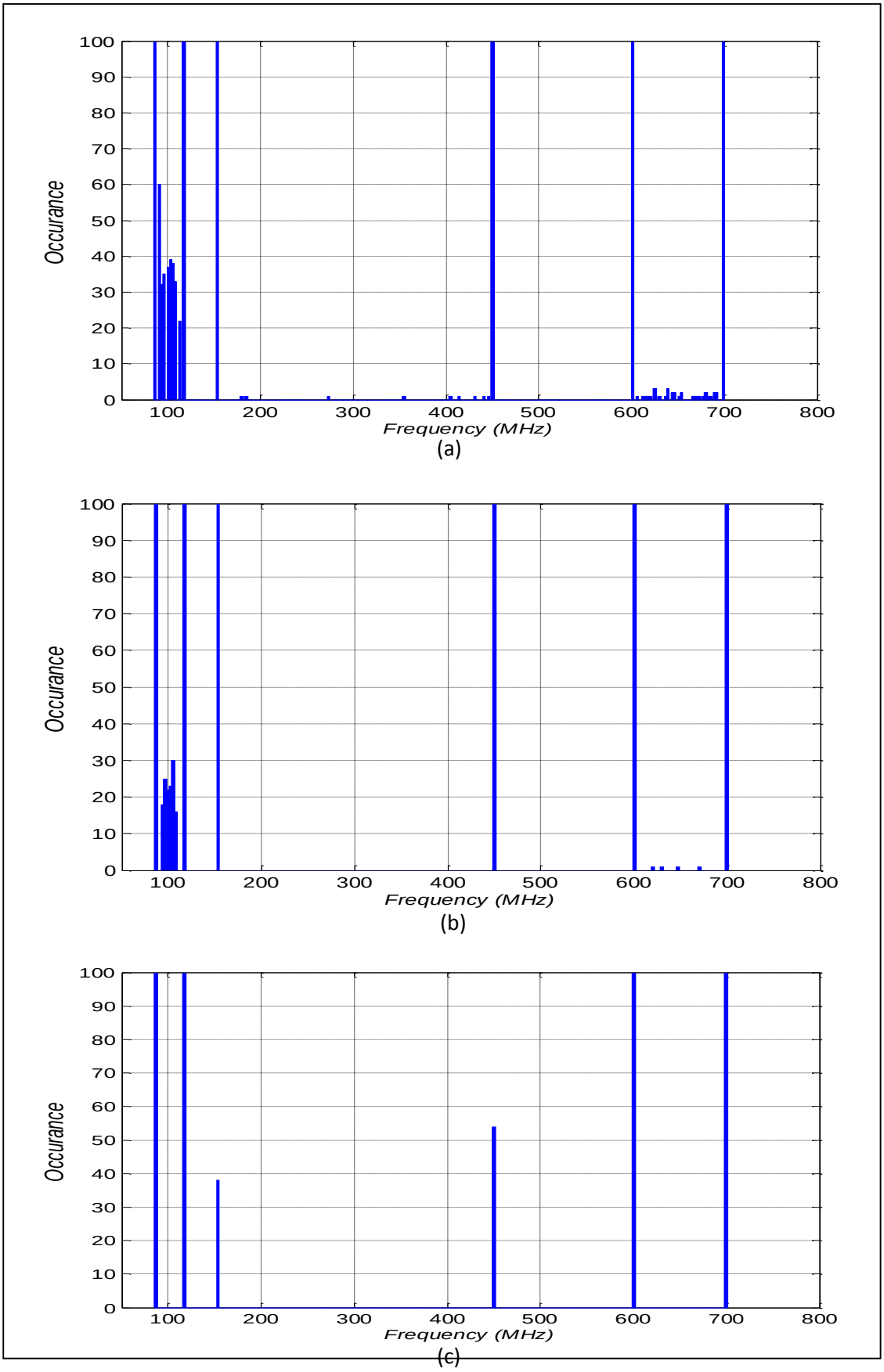

Figure 5-10: Histogram of the detected edges for 100 simulation runs at: a) $s = 2$, b)$s = 4$, c) multiscale product $s = 2{:}\,4$.

5.5.2 Collaborative Edge Detection

In this section the system model described in section 5.3 is extended to include collaborative edge detection, where the effect of collaboration between SUs in wavelet-based edge detection is investigated. Assuming k collaborative SUs where each SU performs wavelet edge detection and reports the detected edges to a fusion center (FC), the FC then combines the information received using one of the fusion rules, OR, AND or Majority, and takes the final decision regarding the edges and their corresponding locations. For the wideband signal shown in Figure 5-11, collaborative edge detection is performed using $k = 5$ SUs at a scale factor $s = 2$. Simulation results depicted in Figure 5-12 (c) show that collaborative edge detection using AND-combining outperforms the OR and Majority combining in terms of accuracy, since only the exact edges are detected. While in OR-combining (Figure 5-12 (b)) more edges are detected than detected by one SU in the non-collaborative detection (Figure 5-12 (a)), resulting in inaccurate edge detection.

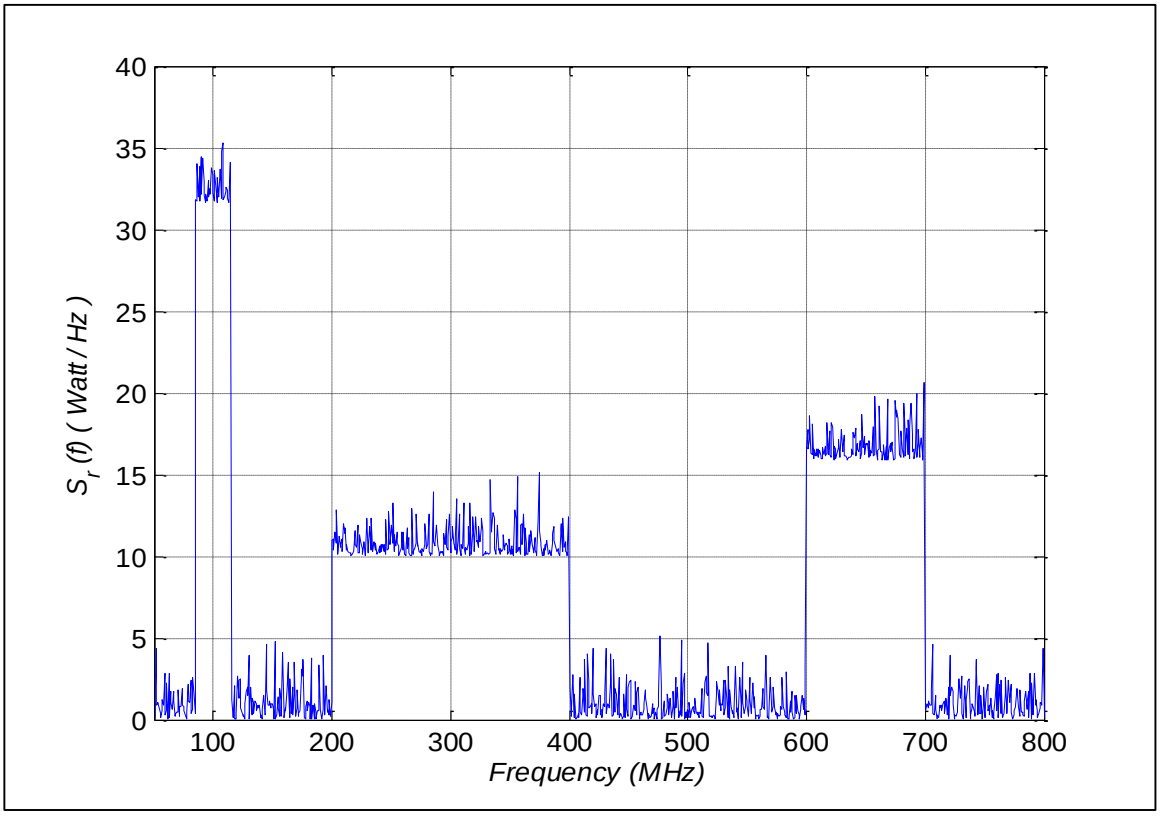

Figure 5-11: Power spectral density (PSD) of the received wideband signal.

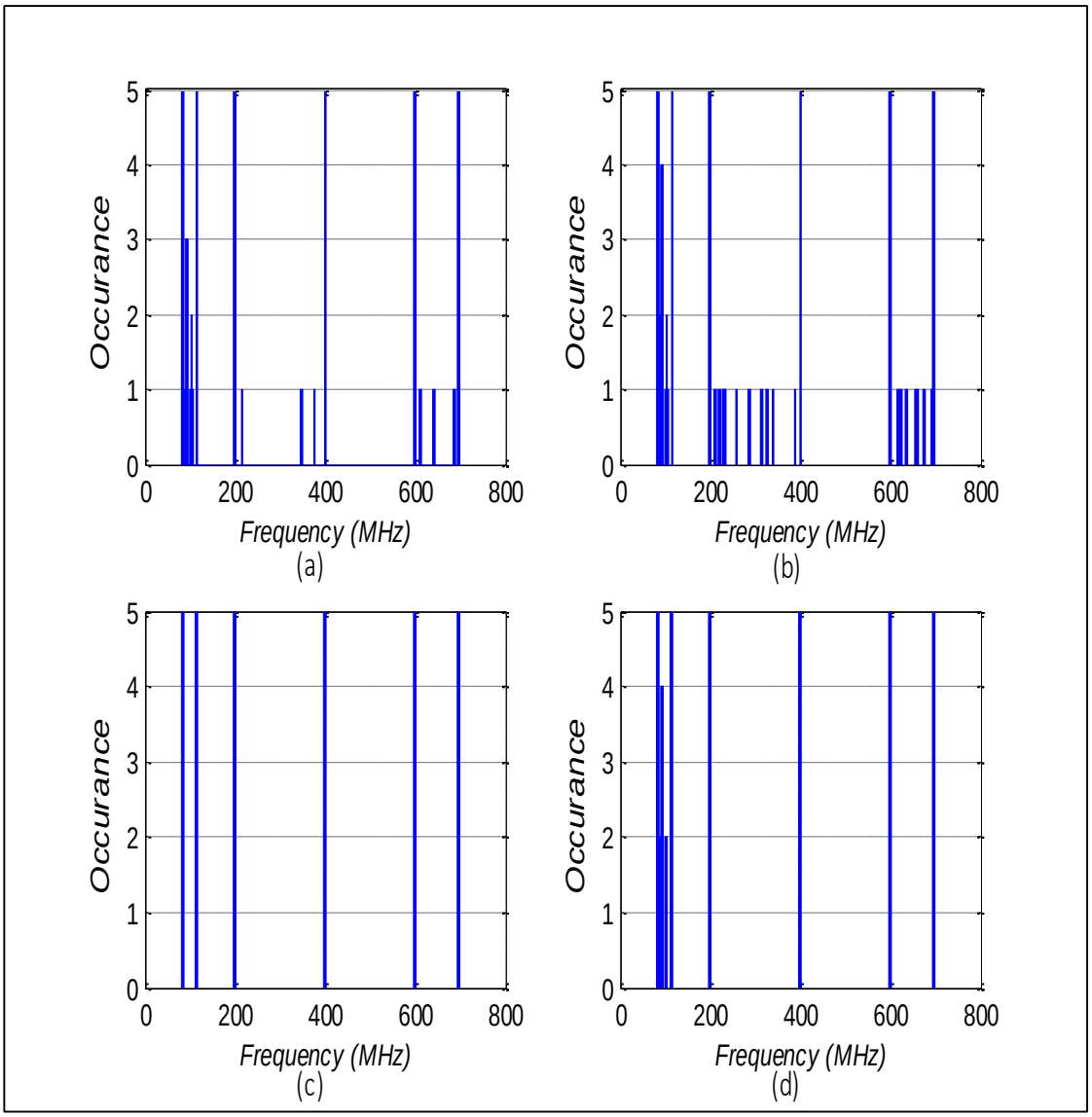

Figure 5-12: Histogram of the detected edges using collaborative edge detection for $k = 5$ SUs using: a) non-collaborative, b) OR (1 out of 5), c) AND (5 out of 5), d) Majority (2 out of 5).

In a case of sensing the presence of a PU with a low SNR level, as in the second subband in Figure 5-13 (a), the PU can be misdetected. Hence, using collaborative edge detection can help overcome this problem. It is obvious from Figure 5-14 (a) that the band occupied by the PU with low SNR, $f \in [200,400]$MHz, is not detected by the SU in non-collaborative edge detection. However, in Figure 5-14 (b) this band was detected using OR-combining, while AND-combining in Figure 5-14 (c), and Majority-combining in Figure 5-14 (d) failed to detect this band.

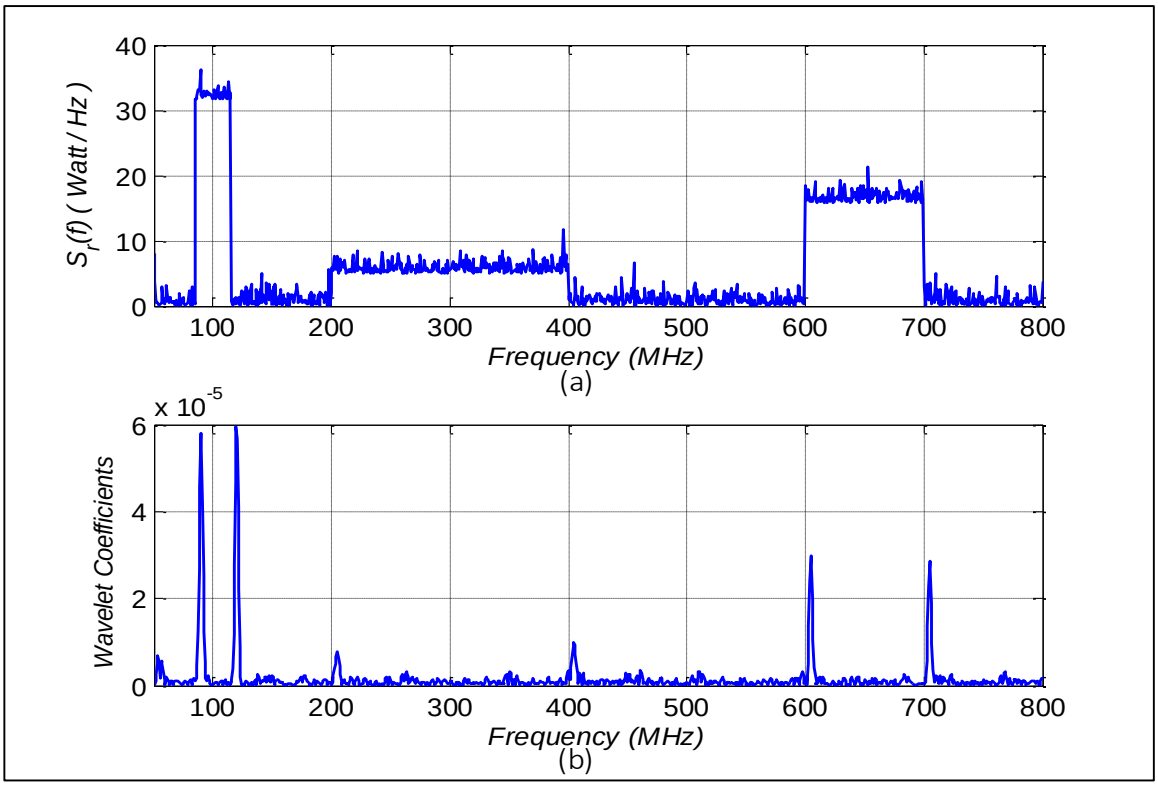

Figure 5-13: a) PSD of the received wideband signal, b) Wavelet coefficients at scale s = 2.

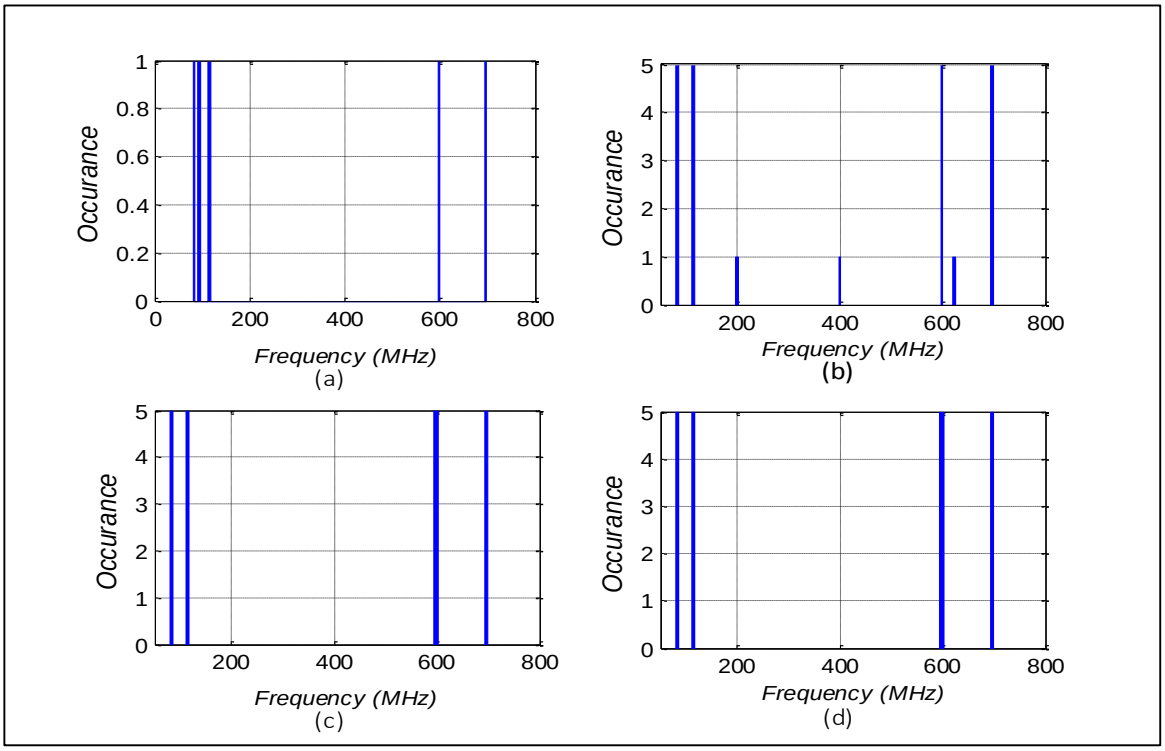

Figure 5-14: Histogram of the detected edges using collaborative edge detection for $k = 5$ SUs using: a) non-collaborative, b) OR (1 out of 5), c) AND (5 out of 5), d) Majority (2 out of 5).

Figure 5-15 shows the number of detected edges within a range of $\pm 5\%$ around the exact edge ($f = 200MHz$), versus the average SNR of the PU occupying the second subband ($f \in [200,400]$MHz) in Figure 5-13 (a) using collaborative edge detection for the three combining rules: OR, AND and Majority. At a scale factor of $s = 2$ and for $k = 5$ collaborative SUs it can be concluded that the number of detected unwanted edges decreases as the average SNR of the PU increases, resulting in more accurate edge detection and hence better detection of the PUs. However, in OR-combining the number of detected edges chosen by the FC to make the final decision regarding the number of subbands and their boundaries, is higher than that of both the Majority-combining and AND-combining. This means that using OR-combining involves more computations and calculations to decide the number and locations of the subbands within the wideband spectrum.

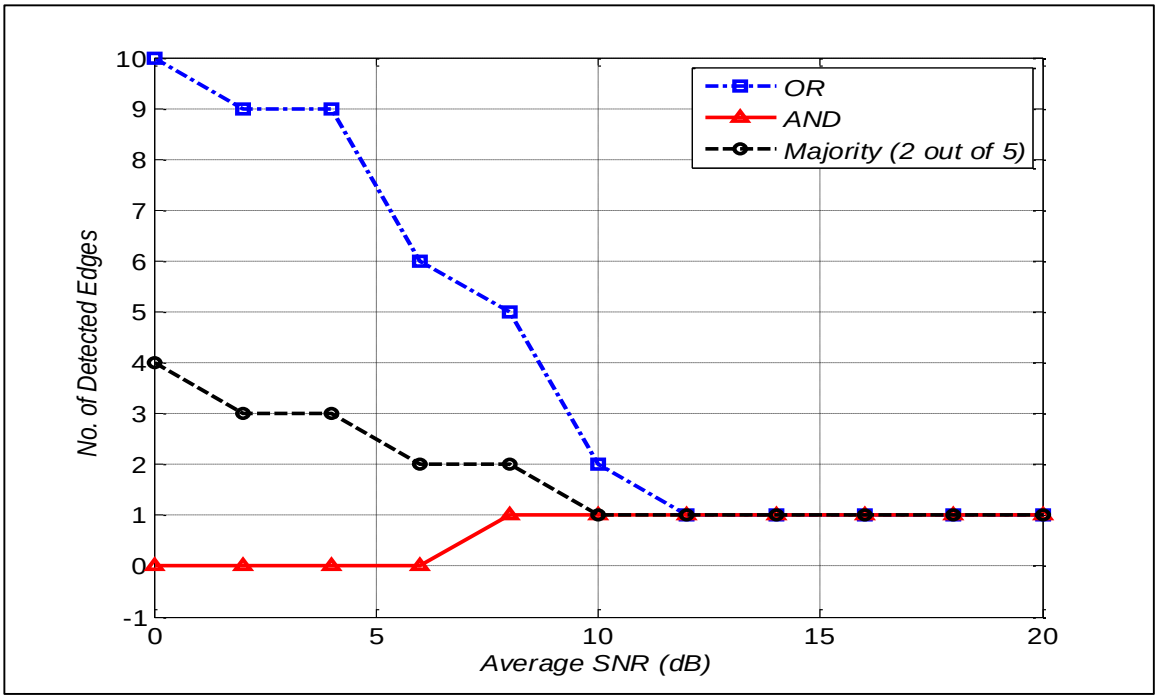

Figure 5-15: Number of detected edges vs. SNR using collaborative edge detection for k = 5 SUs.

Table 5-2: Number of detected edges at different SNR values using collaborative edge detection for k = 5 SUs.

SNR (dB)	Number of Detected Edges		
	OR	Majority	AND
4	9	3	0
10	2	1	1
20	1	1	1

Figure 5-16 depicts the probability of detecting the edges within a range of $\pm 5\%$ around the exact edge $(f = 200MHz)$ versus the average SNR of the PU within the subband $(f \in [200,400])$. It is obvious that the probability of edge detection improved as the average SNR increased from 0dB to 20dB. Moreover, AND-combining outperforms both OR and Majority combining in terms of the probability of edge detection. However, AND-combining fails to detect the edges at a low average SNR (0dB - 6dB), which proves the results shown in Figure 5-14 (c).

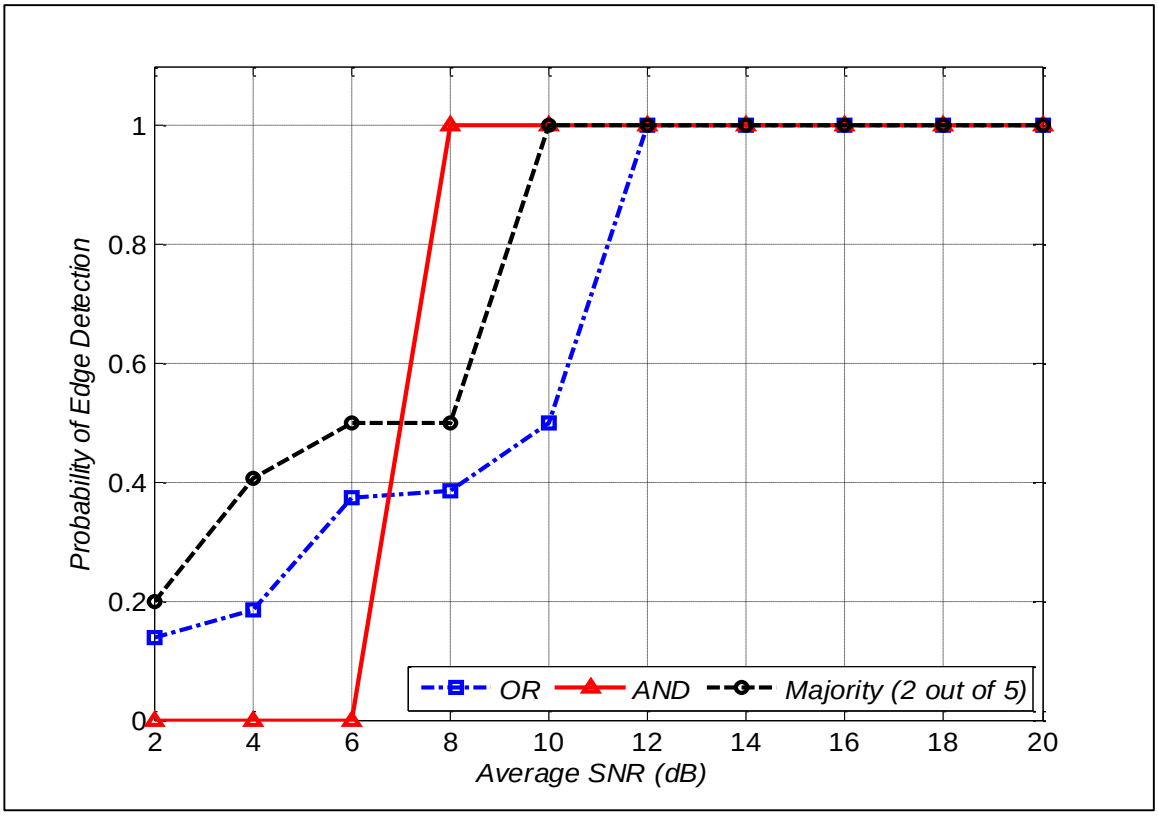

Figure 5-16: Probability of edge detection vs. average SNR using collaborative edge detection for k = 5 SUs.

Table 5-3: Probability of edge detection at different SNR values using collaborative edge detection for k = 5 SUs.

SNR (dB)	**Probability of Edge Detection**		
	OR	**Majority**	**AND**
6	0.375	0.5	0
10	0.5	1	1
20	1	1	1

5.5.3 The Effect of Log-normal Shadowing

The presence of log-normal shadowing results in degradation in the received average power and adds more random variations to the signal. In wideband sensing this will lead to inaccurate edge detection, since these random variation may be interpreted as edges. The signal transmitted by the PU experiences log-normal shadowing due to the presence of an obstacle between this PU and the SU sensing the spectrum. The PSD of the received signal for a PU occupying a frequency band ($f \in [200,400]$) and experiences log-normal shadowing $\sigma_{dB} = 2\text{dB}$ is shown in Figure 5-17. The effect of shadowing on wavelet-based edge detection is shown in Figure 5-18. It is obvious that the number of detected edges increased as the severity of shadowing increased from $\sigma_{dB} = 2\text{dB}$ in Figure 5-18 (b) to $\sigma_{dB} = 12\text{dB}$ in Figure 5-18 (d). These results are confirmed in Figure 5-19 where the number of detected edges within a range of $\pm 25\%$ around the exact edge, $f \in [150,250]$, increases with the increase of σ_{dB} levels.

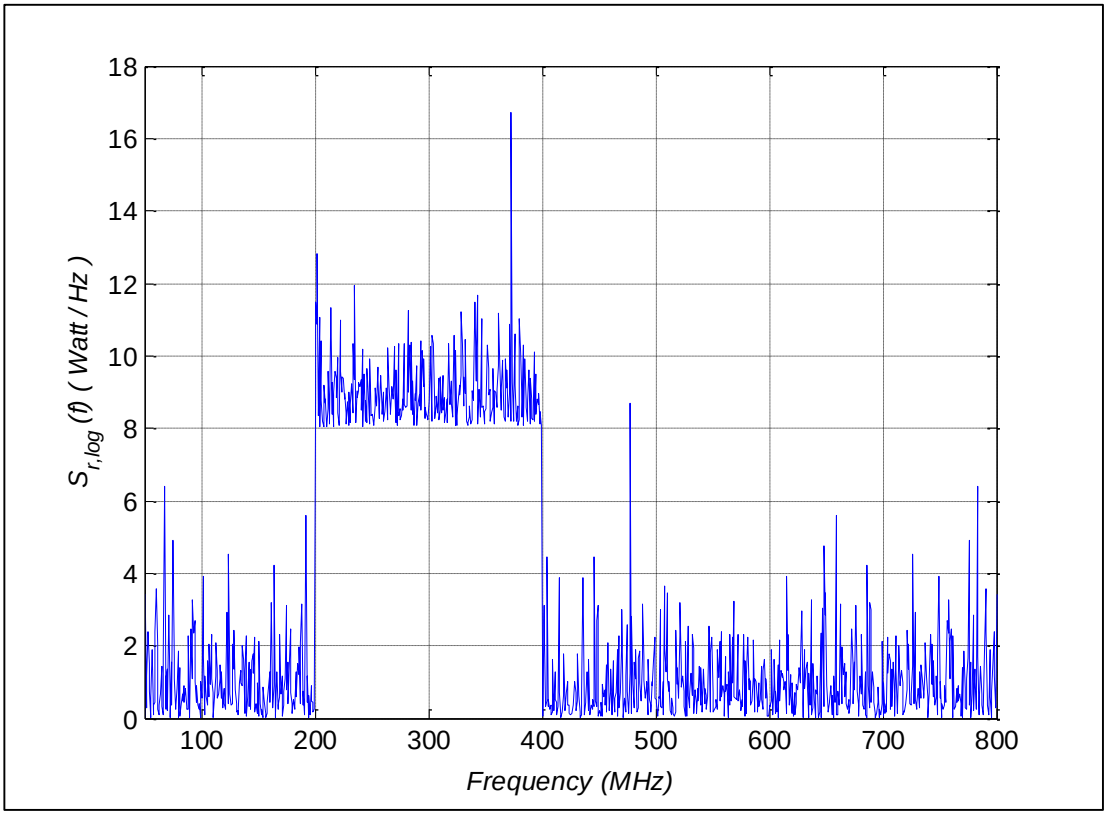

Figure 5-17: PSD of the received wideband signal in log-normal channel for $\sigma_{dB} = 2\text{dB}$, average SNR$= 10dB$.

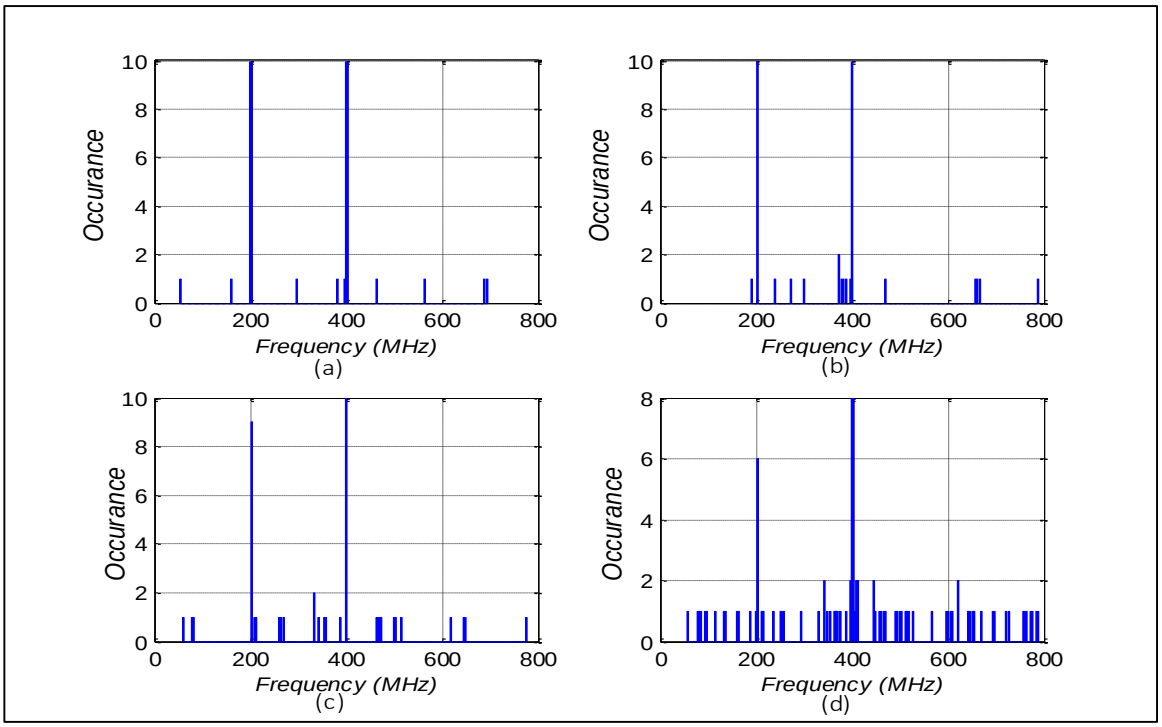

Figure 5-18: Histogram of the detected edges in log-normal channel for 10 simulation runs for different values of σ_{dB}: a) AWGN, b) $\sigma_{dB} = 2$dB, c) $\sigma_{dB} = 6$dB, d) $\sigma_{dB} = 12$dB.

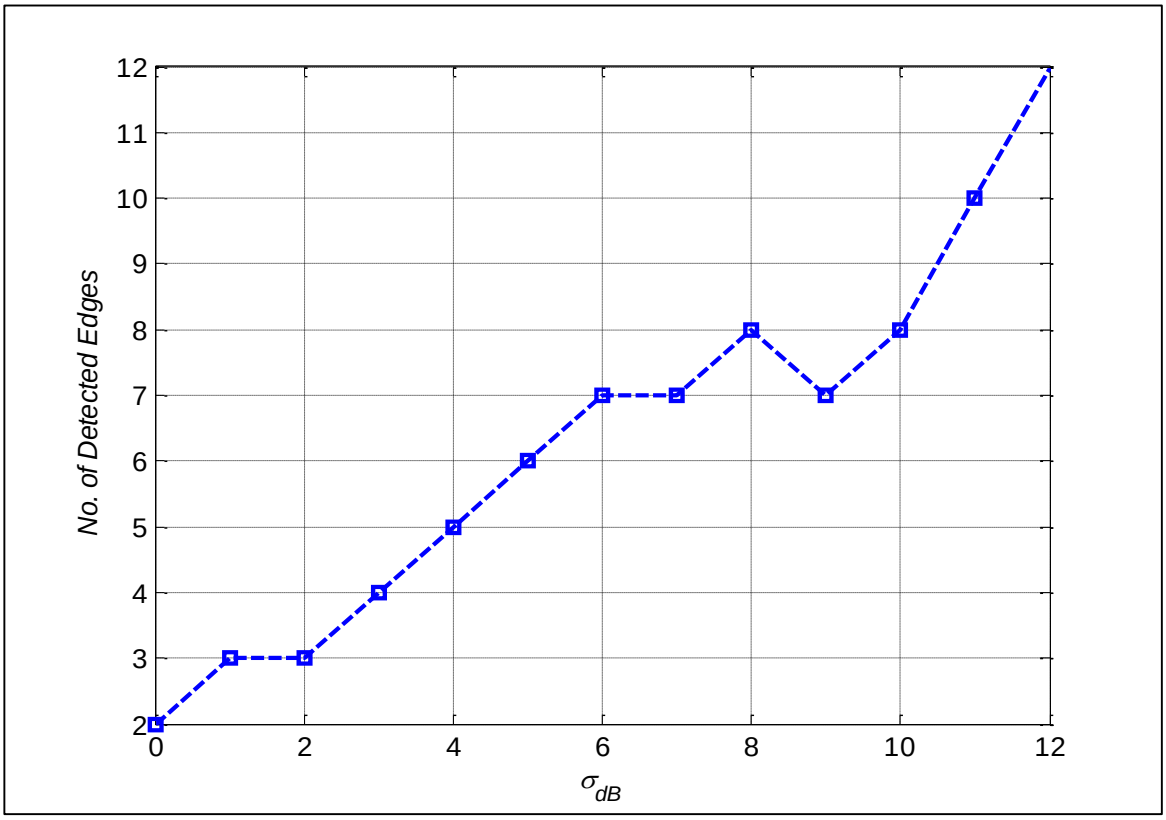

Figure 5-19: Number of detected edges vs. σ_{dB} in log-normal channel.

Table 5-4: Number of detected edges at different σ_{dB} values in log-normal channel.

σ_{dB}	No. of Detected Edges
0	2
2	3
6	7
12	12

The probability of detecting the edges within a range of $\pm 5\%$ around the exact edge $(f = 200MHz)$ of the subband occupied by the PU experiencing shadowing decreases as the level of shadowing increases from 0dB to 12dB, as shown in Figure 5-20. This is because more edges are detected at higher σ_{dB} values, leading to misdetecting the correct edges. In summary, it can be concluded that the presence of log-normal shadowing affects the performance of wavelet-based edge detection.

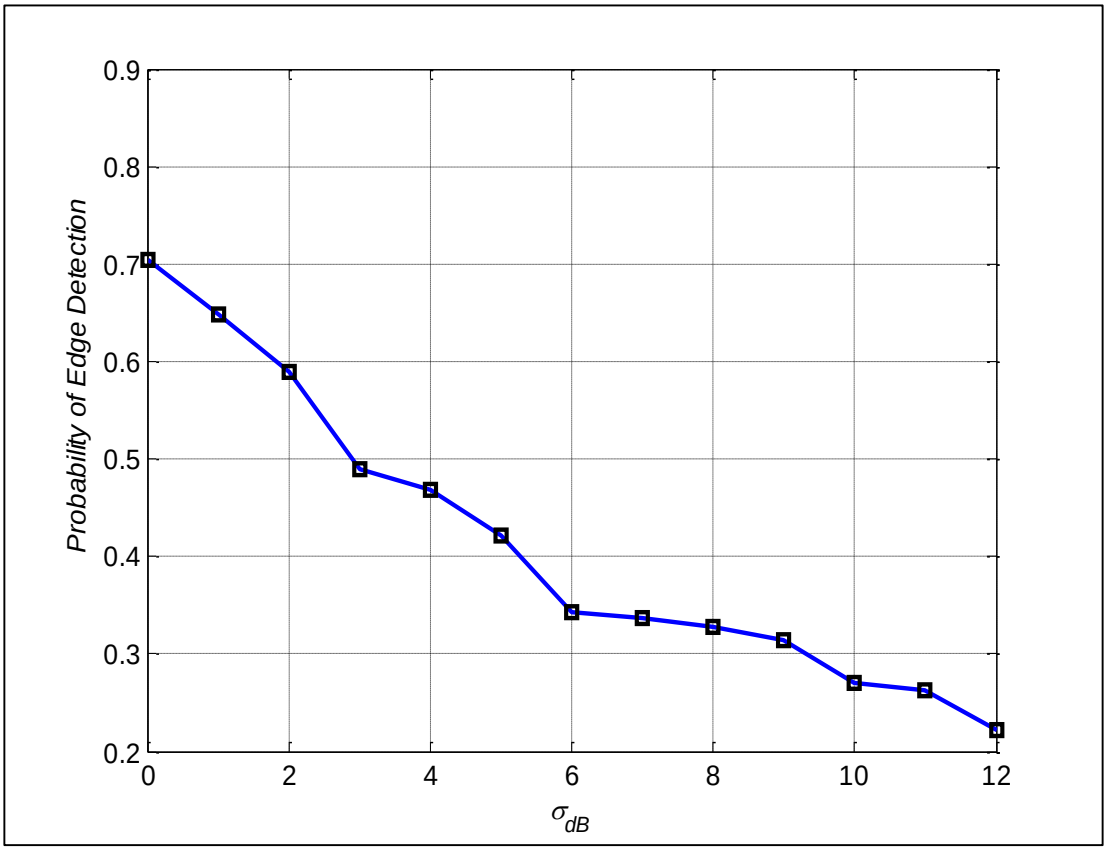

Figure 5-20: Probability of edge detection vs. σ_{dB} in log-normal channel (non-collaborative edge detection) at average SNR$= 10\ dB$, s $= 2$.

Table 5-5: Probability of edge detection at different σ_{dB} values in log-normal channel.

σ_{dB}	**Probability of Edge Detection**
0	0.704
2	0.589
6	0.343
12	0.221

5.5.4 The Effect of Spectrum Shape

The spectrum investigated in the previous section had sharp edges. However, in this section a spectrum with blunt envelopes (slow varying peaks) is addressed. For the wideband signal shown in Figure 5-21, with bandwidth $B = 400\ MHz$ and frequency range $[f_0 = 100\ MHz,\ f_N = 500\ MHz]$, it is obvious that higher scales result in more accurate edge detection. The multiscale product is even better for edge detection as shown in Figure 5-22. However comparing these results with those for the sharp edges spectrum, it can be seen that slow varying peaks are more difficult to identify and detect. Hence, the shape of the wideband spectrum affects the accuracy of wavelet-based edge detection.

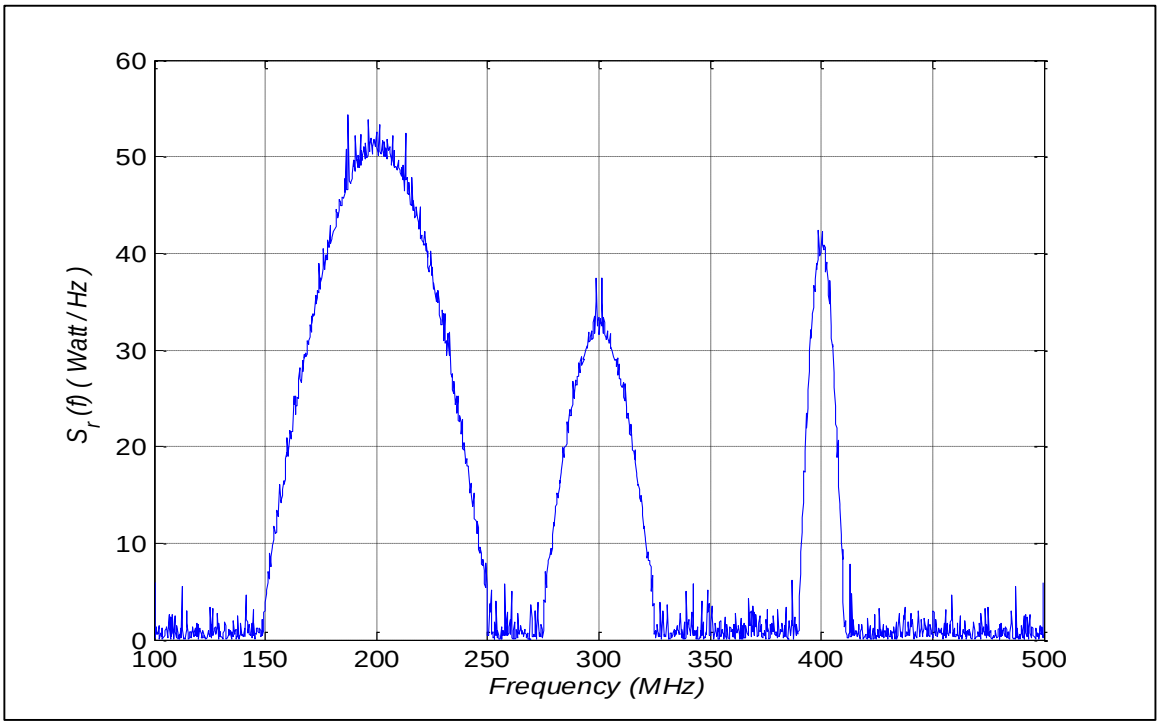

Figure 5-21: PSD of the received wideband signal with blunt envelopes.

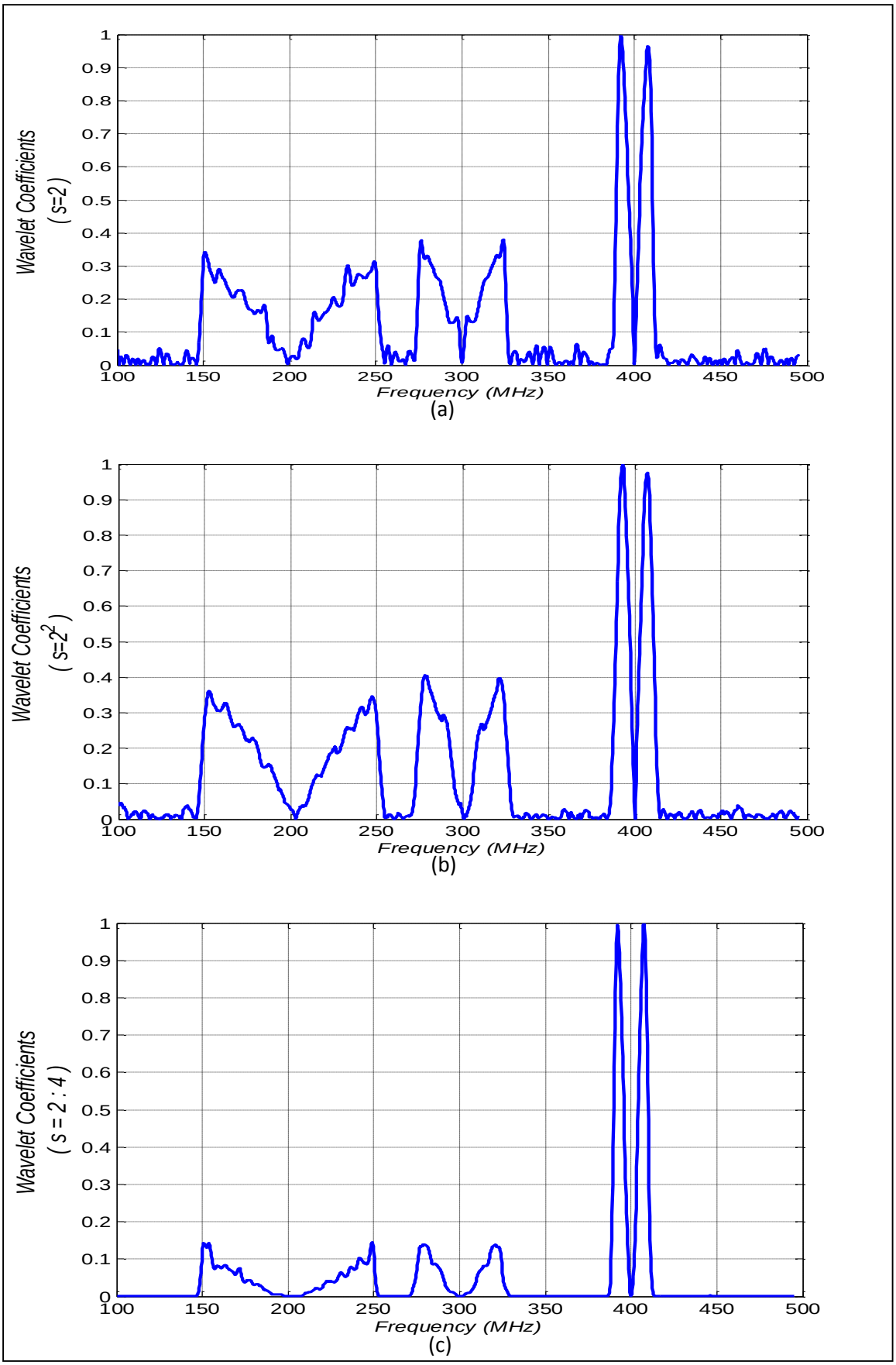

Figure 5-22: Wavelet coefficients at different scales: a) s = 2, b) s = 4, c) multiscale product s = 2: 4.

In conclusion, a wavelet-based edge detection system model for wideband edge detection was studied using MATLAB simulation. The effect of the scale factor of the wavelet function and spectrum shape on edge detection were considered. Also, collaborative wideband edge detection was explored. Results indicated that better edge detection was achieved at higher scale factor values, and the detection of the edges could be enhanced using a multiscale wavelet product. Moreover, collaboration between SUs in edge detection improved detection performance, and better detection was achieved at higher average SNR levels of the primary user occupying the wideband spectrum. The performance of this system model was also tested under log-normal shadowing. The presence of log-normal shadowing resulted in a degradation in edge detection performance, since shadowing reduces the average power of the PU signal received by the SU, and at the same time it adds more random variations to the signal, resulting in more false unwanted edges.

CHAPTER 6: WIDEBAND SPECTRUM DETECTION

In this chapter two approaches for wideband spectrum detection will be investigated and compared. The first approach is the tunable bandpass filter (TBPF) filterbank in which a parallel structure of tunable narrowband bandpass filters is used to sense the spectrum on a wideband level. The second approach is a proposed wideband spectrum detection model using wavelet-based detection.

6.1 Problem Formulation

Assume a primary user (PU) operating over the wideband spectrum portion $f \in [f_0, f_N]$, the center frequency, f_c, and bandwidth, B, of the PU are unknown to the secondary user (SU). Also, they remain unchanged during the sensing interval T, but change from one sensing interval to another as shown in Figure 6-1. Sensing the presence of the PU will be performed using two sensing approaches: the TBPF filterbank approach and the proposed wavelet-based detection approach. System models and performance analysis of both approaches are addressed and discussed in the following sections.

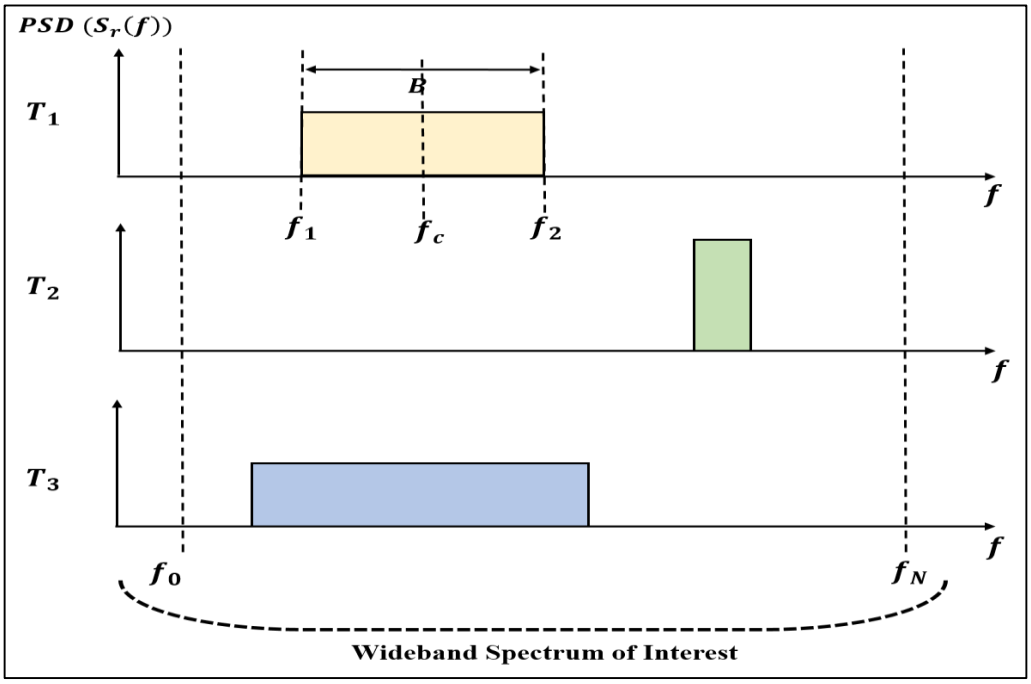

Figure 6-1: Schematic illustration of the primary user activity over the wideband spectrum.

6.2 Wideband Spectrum Detection using TBPF Filterbank

As mentioned in chapter 5, when PU activity details such as the center frequency and bandwidth are known to the SU, then sensing can be performed on a narrowband basis over the frequency band. A tunable bandpass filter is set to the center frequency and bandwidth of the PU, and the traditional sensing techniques listed in chapter one namely, energy detection, match filter detection and cyclostationary detection can be used to decide the status of this frequency band.

However, this is not the case in wideband sensing, where the SU needs to sense the whole spectrum to detect the presence of the PU. In this case, multiple frequency bands should be scanned using multiple tunable bandpass filters (TBPF) forming a filterbank [45]. The block diagram of the TBPF approach is depicted in Figure 6-2, the center frequency $\left(f_{c,n} = (f_{n-1} + f_n)/2 \right)$ and the bandwidth $(B_n = f_n - f_{n-1})$ of each tunable bandpass filter (BPF_n) are preset to scan the frequency subband $(f \in [f_{n-1}, f_n])$ within the wideband spectrum. By switching the tunable BPF, the operating center frequency and bandwidth can change over the wideband spectrum $(f \in [f_0, f_N])$. A schematic illustration of the sensing scenario used in this approach is shown in Figure 6-3. Sensing is performed over fixed frequency subbands, where one subband is scanned at a time and compared with the energy threshold (λ) to decide whether it is busy or free. A summary of spectrum sensing using this approach is proposed in Algorithm 2. Using this architecture for wideband spectrum detection requires large numbers of RF components, additionally, the center frequency and bandwidth of the BPFs are preset which results in increasing the implementation costs and complexity.

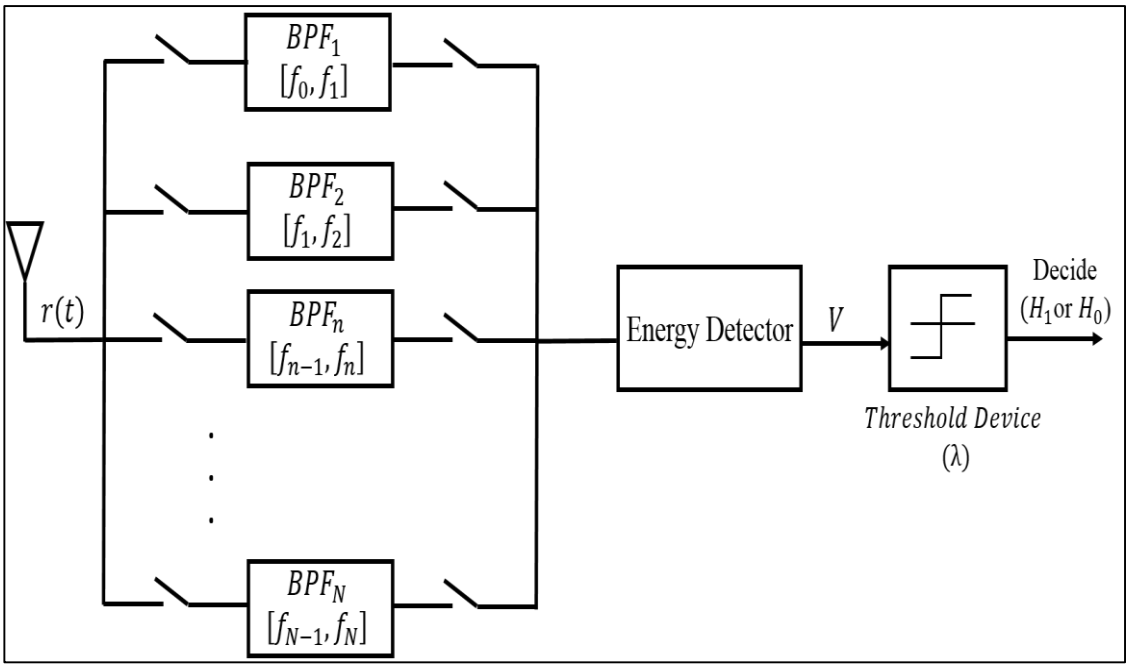

Figure 6-2: Block diagram of wideband spectrum detection using the TBPF filterbank approach.

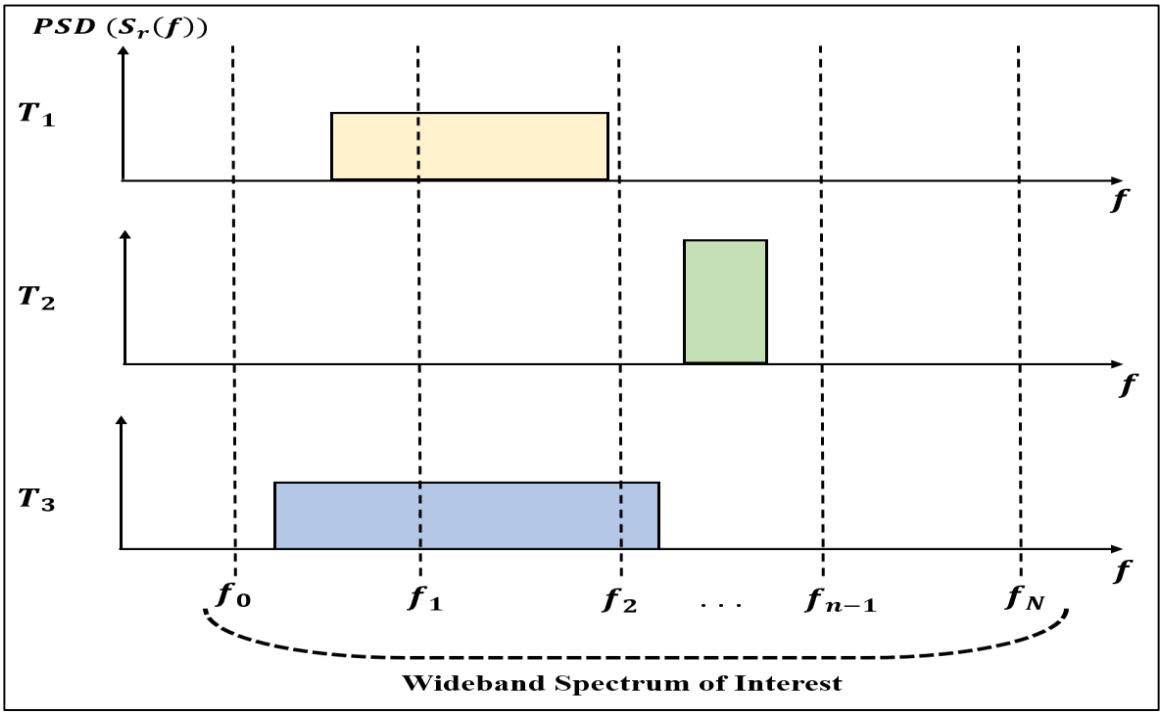

Figure 6-3: Schematic illustration of the sensing scenario using TBPF filterbank approach.

Algorithm 2: Wideband Spectrum Detection using TBPF Filterbank

Input: $f_0, f_N, \{f_n\}_{n=1}^{N-1}, r(t)$

Output: $\{a_n^2\}_{n=1}^{N}, \{P_{d,n}\}_{n=1}^{N}$

$R_r(\tau) \leftarrow E\{r(t)r(t+\tau)\}$

$S_r(f) \leftarrow \mathcal{F}\{R_r(\tau)\}$

for i**= (1) to (**N**) do**

$a \leftarrow f_{i-1}$

$b \leftarrow f_i$

$h = \frac{b-a}{y}$

$\beta_i = 0$

for j**= (1) to (**$y-1$**) do**

$\beta_i \leftarrow \beta_i + hS_r(a+jh)$

end for

$\beta_i \leftarrow \beta_i + \frac{h}{2}S_r(a) + \frac{h}{2}S_r(b)$

end for

$x \leftarrow \min_n \{\beta_n\}_{n=1}^{N}$

for n**= (1) to (**N**) do**

$a_n^2 \leftarrow \beta_n - x$

if $a_n^2 \geq \lambda$ **then**

$P_{d,n} = 1$

else

$P_{d,n} = 0$

end if

end for

6.3 Wideband Spectrum Detection using Wavelet-based Detection

In this section a wideband spectrum detection system model is proposed. The system model described in chapter 5 for wideband edge detection using wavelet-based edge detection, shown in Figure 6-4, is used for detecting the edges (irregularities) within the wideband spectrum. The results are then applied to the

energy detector to perform spectrum detection. The exact operation is described in Figure 6-5. In the first stage wavelet-based edge detection is performed to detect the edges of the wideband spectrum and define the number of non-overlapping frequency subbands (N) and their corresponding center frequency $(\hat{f}_{c,n})$ and bandwidth (B_n). The center frequency of the *n*-th subband is defined as:

$$\hat{f}_{c,n} = \frac{f_{n-1} + f_n}{2} \tag{6.1}$$

$$B_n = f_n - f_{n-1} \tag{6.2}$$

In the second stage the wideband sensing problem turns to narrowband sensing, where the results of the first stage are applied to the energy detector and traditional energy detection is performed on the subbands to classify them into busy and free based on the estimated PSD level within each subband (a_n^2). A summary of spectrum detection using this approach was illustrated earlier in Algorithm 1, in chapter 5. A schematic illustration of the sensing scenario used in this approach is shown in Figure 6-6. The main advantage of using this approach for wideband spectrum detection is its ability to adapt to a dynamic wideband frequency range. However, the high sampling rate of ADC required to perform this technique and the high energy consumption are drawbacks of this technique.

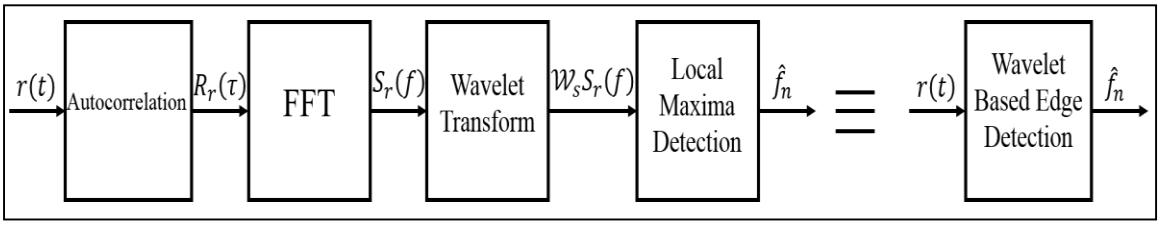

Figure 6-4: Block diagram of the wavelet-based edge detection.

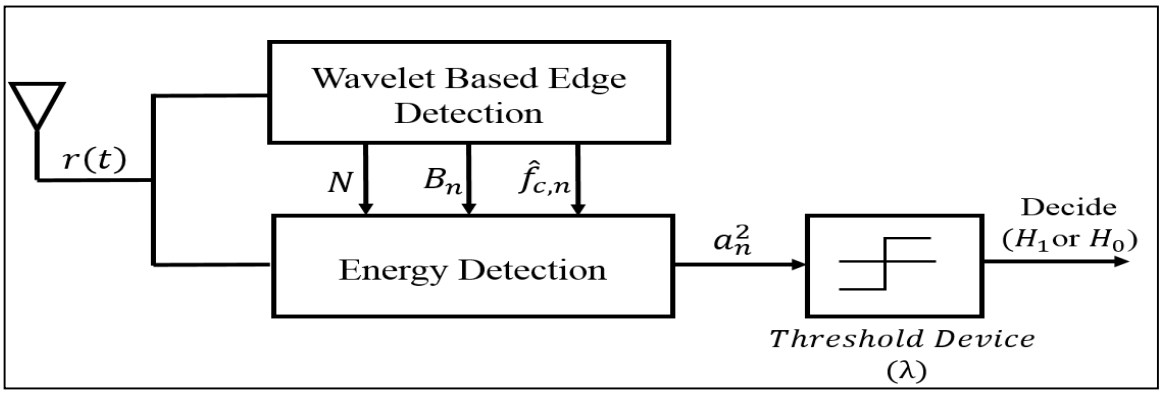

Figure 6-5: Block diagram of the proposed wideband spectrum detection approach using the wavelet-based detection.

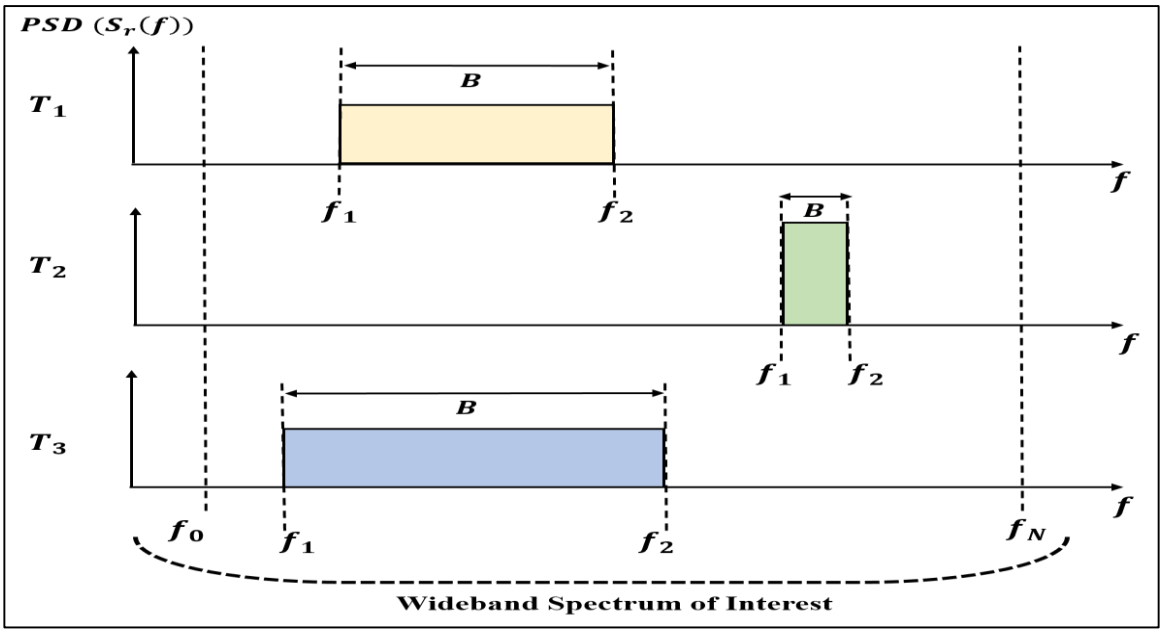

Figure 6-6: Schematic illustration of the sensing scenario using wavelet-based detection approach.

6.4 Simulation Results and Discussion

In this section the performance of the two approaches discussed earlier for wideband spectrum detection is investigated. Their performance is compared in terms of spectrum occupancy, which is an indicator for wideband spectrum detection efficiency.

6.4.1 Spectrum Occupancy

In this section the metric spectrum occupancy is used to study the efficiency of the wideband spectrum detection technique in detecting the presence of the PU within the wideband spectrum. Spectrum occupancy is defined as the ratio of the detected bandwidth occupied by the PU (B) to the total wideband bandwidth i.e.

$$Spectrum\_Occupancy\ [PU] = \frac{B}{B_t} \times 100\% \tag{6.3}$$

where

$$B_t = f_N - f_0 \tag{6.4}$$

1) Case One:

Consider the received PSD of the PU shown in Figure 6-7. The PU occupies a bandwidth equal to $(B = 90\ MHz)$ with center frequency $(f_c = 675\ MHz)$ and exact

spectrum occupancy of (22.5%). The red dashed lines represents the subbands over which the TBPF filterbank performs sensing, each subband has a bandwidth of 80 MHz. Figure 6-8 depicts spectrum occupancy versus the probability of false alarm (P_f) using the TBPF filterbank approach. As shown in the figure, at a low probability of false alarm the spectrum occupancy equals $\left(\frac{80}{400} = 20\%\right)$, which means that the presence of the PU is detected over only one subband. While at a high probability of false alarm, spectrum occupancy equals $\left(\frac{160}{400} = 40\%\right)$. This means that at a low P_f the TBPF filterbank detected the PU over the fully occupied subband ($f \in [640,720]$), while the partially occupied subband ($f \in [550,640]$) was declared as a free band. At a high P_f both subbands were declared as busy bands.

Figure 6-9 shows spectrum occupancy versus the probability of false alarm using the wavelet-based detection approach. This approach gave more accurate results than the TBPF filterbank approach, since it detected the exact spectrum occupancy of the PU. This means that the wavelet edge detector detected the correct edges of the PSD within the wideband spectrum.

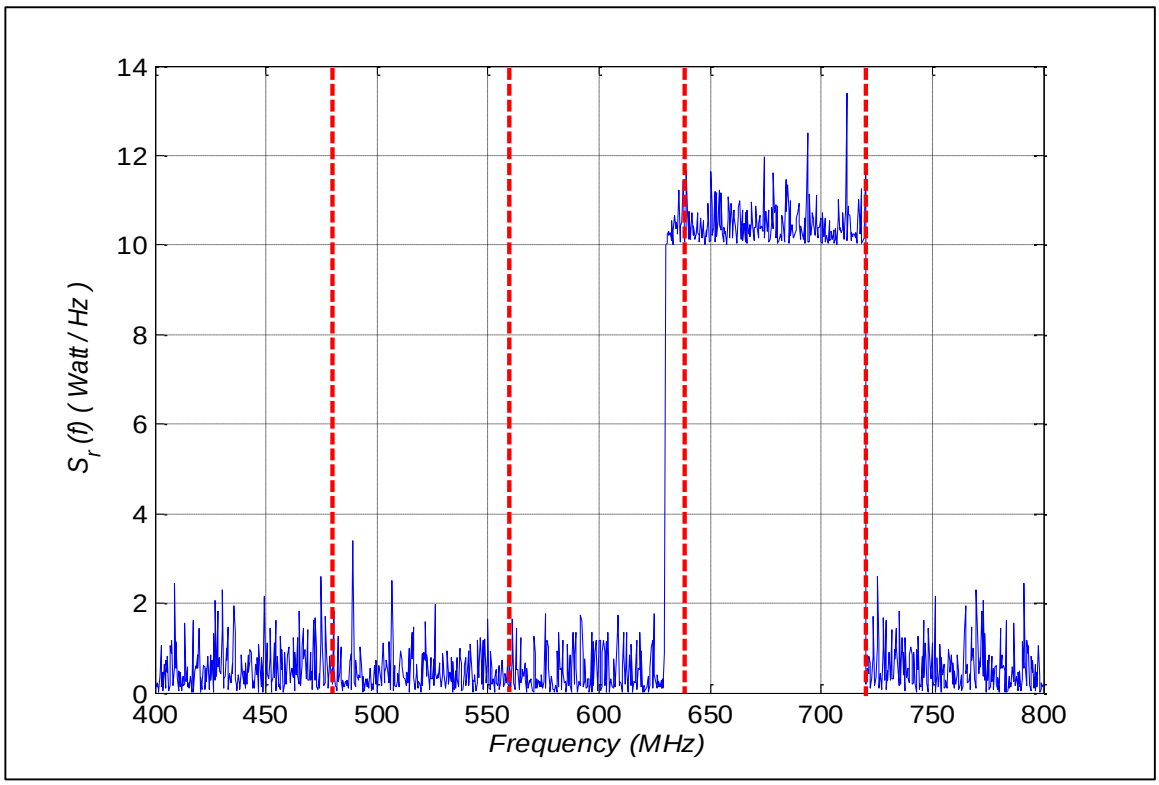

Figure 6-7: Received power spectral density within the wideband spectrum (case 1).

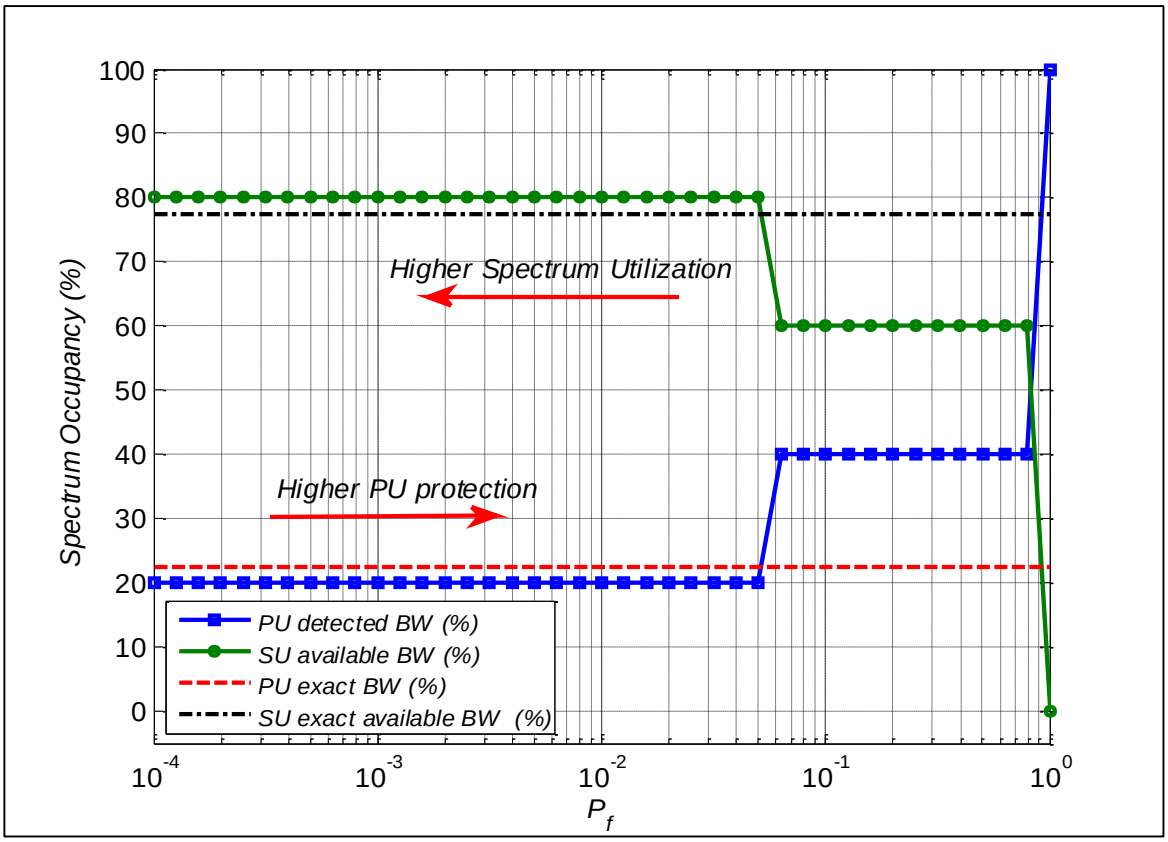

Figure 6-8: Spectrum occupancy using TBPF filterbank (case 1).

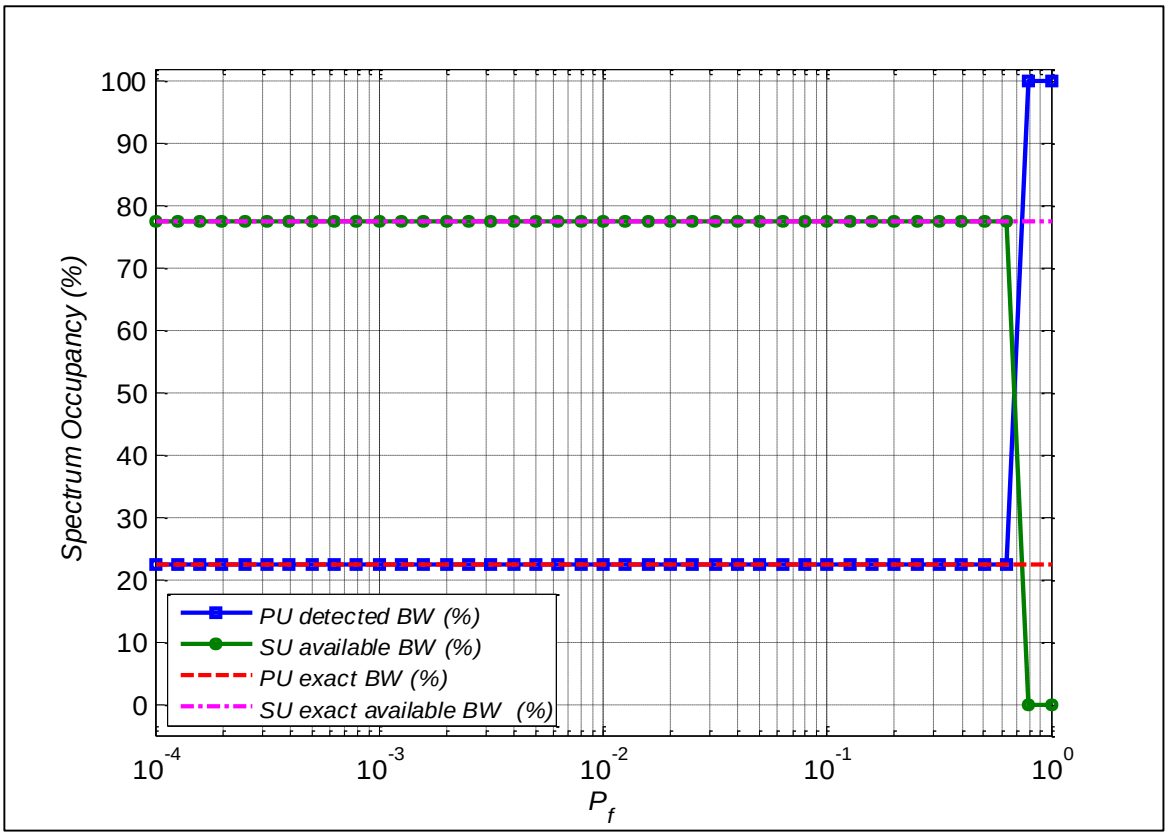

Figure 6-9: Spectrum occupancy using wavelet-based detection (case 1).

2) Case Two:

In Figure 6-10 a PU occupying a bandwidth of $(B = 20\,MHz)$ with a center frequency $(f_c = 520\,MHz)$ and exact spectrum occupancy of (5%) is considered. As before, spectrum occupancy versus the probability of false alarm is calculated using the two approaches. In Figure 6-11 the TBPF filterbank approach is used, and simulation results show that the PU was not detected at a low P_f, which resulted in 0% spectrum occupancy. While at a high P_f the PU was detected and the subband $(f \in [480,560])$ was declared as busy. However, in Figure 6-12 the wavelet-based detection approach resulted in more accurate results.

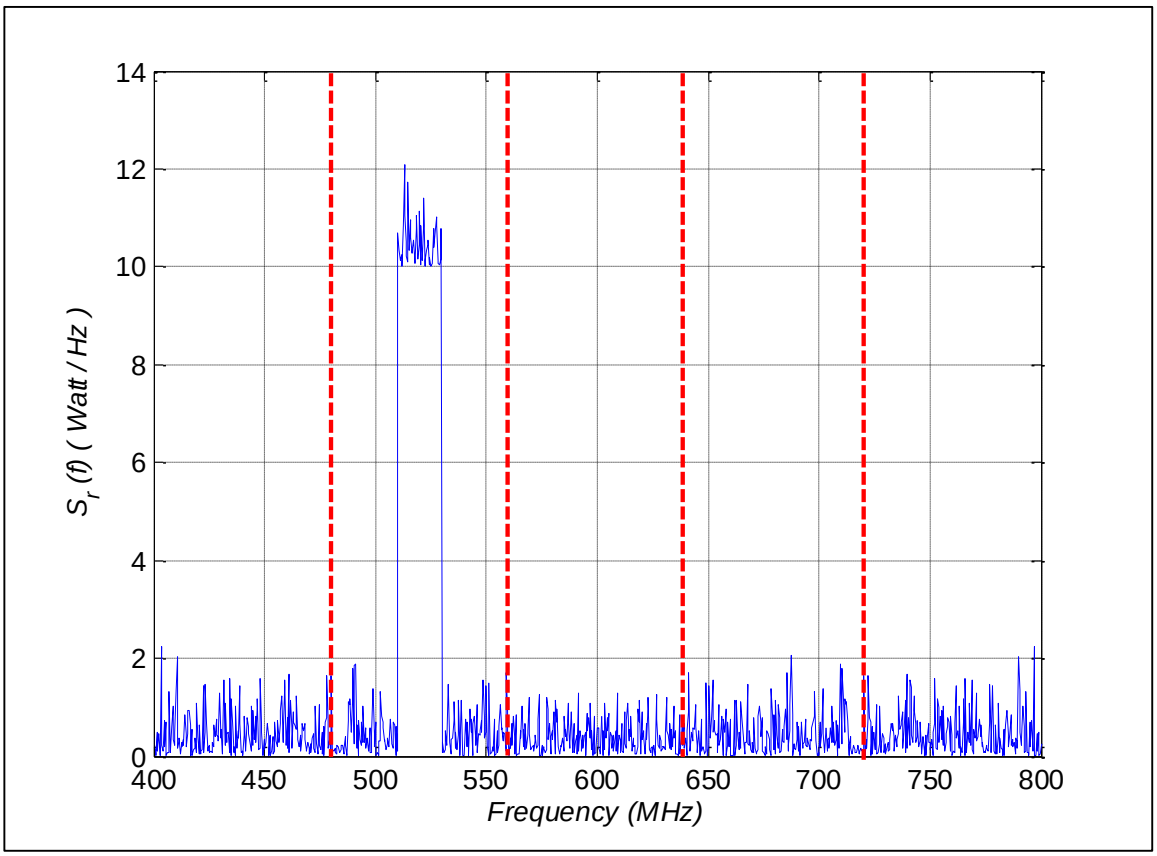

Figure 6-10: Received power spectral density within the wideband spectrum (case 2).

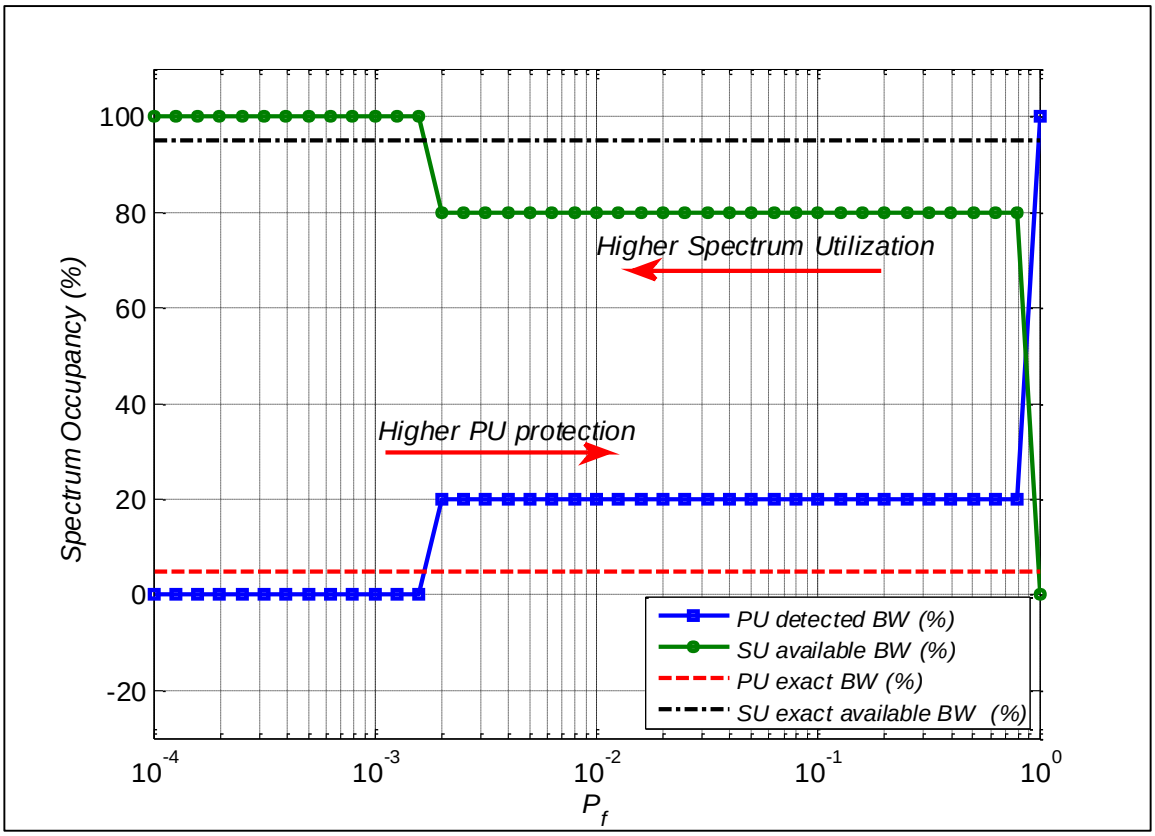

Figure 6-11: Spectrum occupancy using TBPF filterbank (case 2).

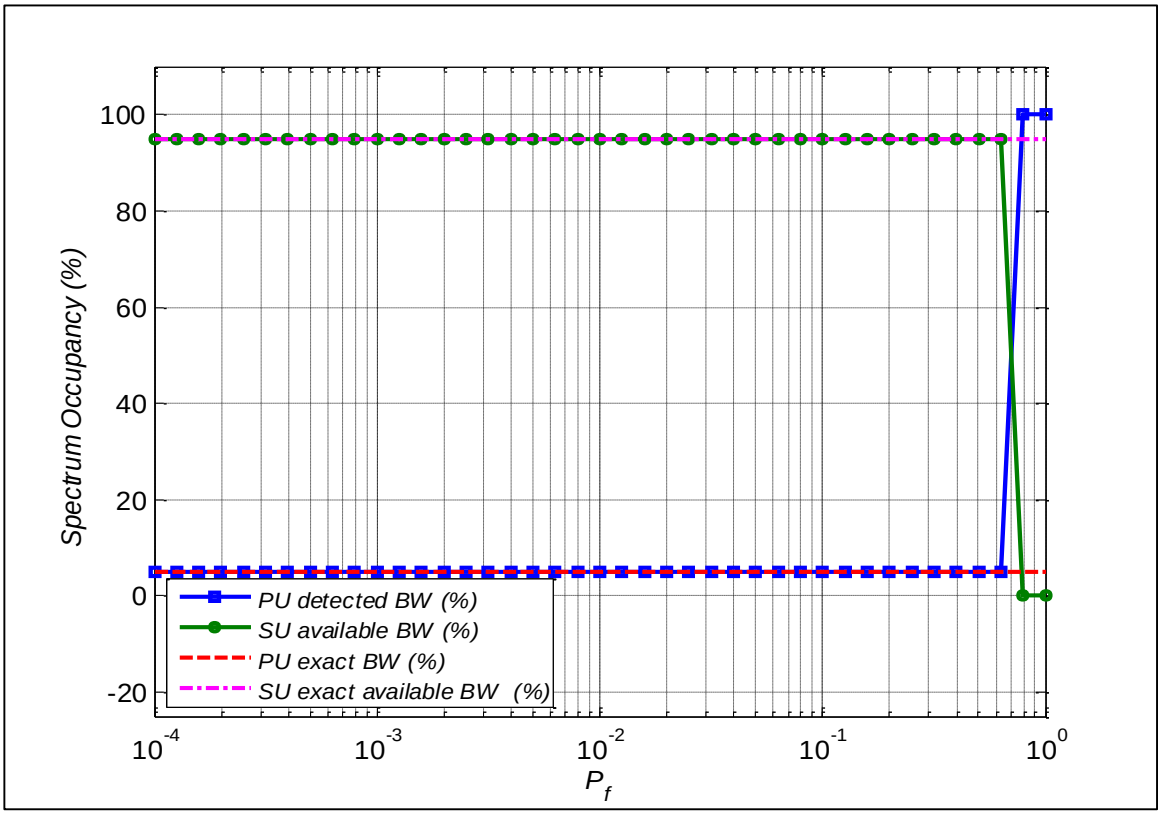

Figure 6-12: Spectrum occupancy using wavelet-based detection (case 2).

3) Case Three (General Case):

In the previous two cases the center frequency of the PU was fixed during the sensing interval. However, a more general case is considered here where the center frequency of the PU is variable with a fixed bandwidth ($B = 100\ MHz$), and fixed average SNR of 10dB. Spectrum occupancy using both approaches is calculated over five sensing intervals, as shown in Figure 6-13.

Figure 6-14 shows spectrum occupancy versus the probability of false alarm using the TBPF filterbank approach. It is obvious that at a low P_f detected spectrum occupancy of the PU is less than the exact one leading to higher interference for the PU and more spectrum opportunities for the SU. While at a high P_f more spectrum occupancy for the PU is achieved resulting in more protection form SU interference, but less spectrum utilization for the SU.

In Figure 6-15 the wavelet-based detection approach is used, from simulation results it can be seen that this approach was able to detect the exact occupancy of the PU resulting in more accurate sensing results. These results proves the results obtained in the previous two cases for a fixed center frequency.

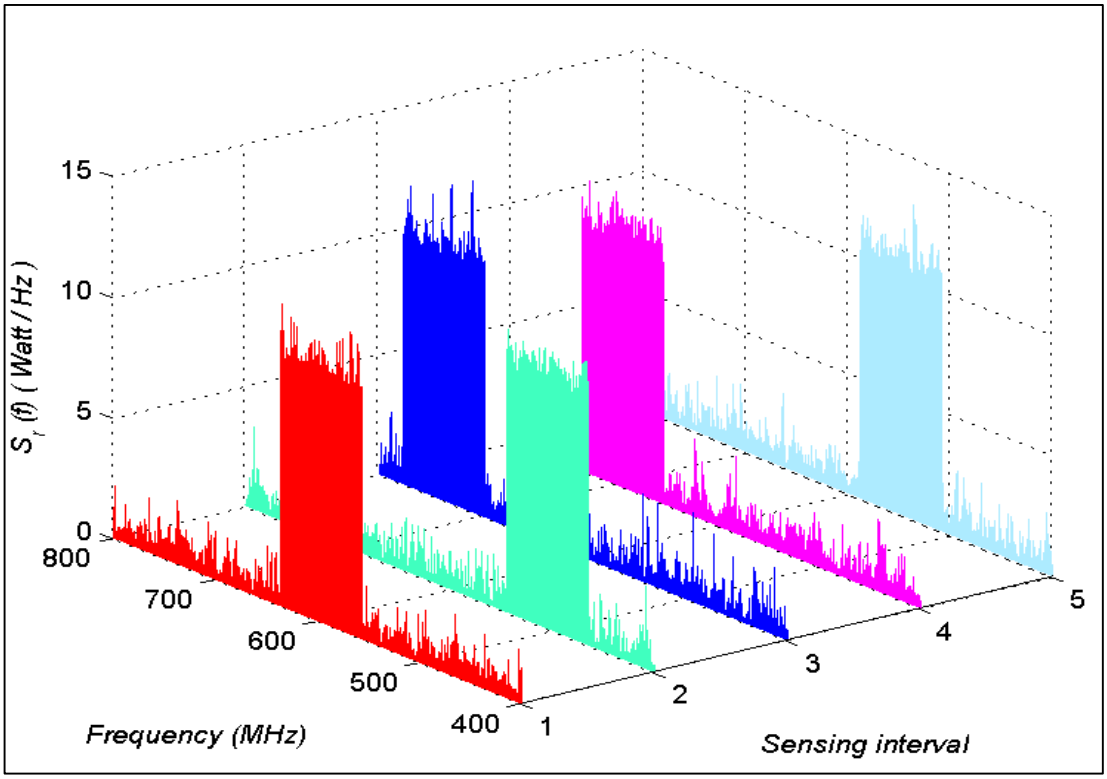

Figure 6-13: Received power spectral density within the wideband spectrum (case 3).

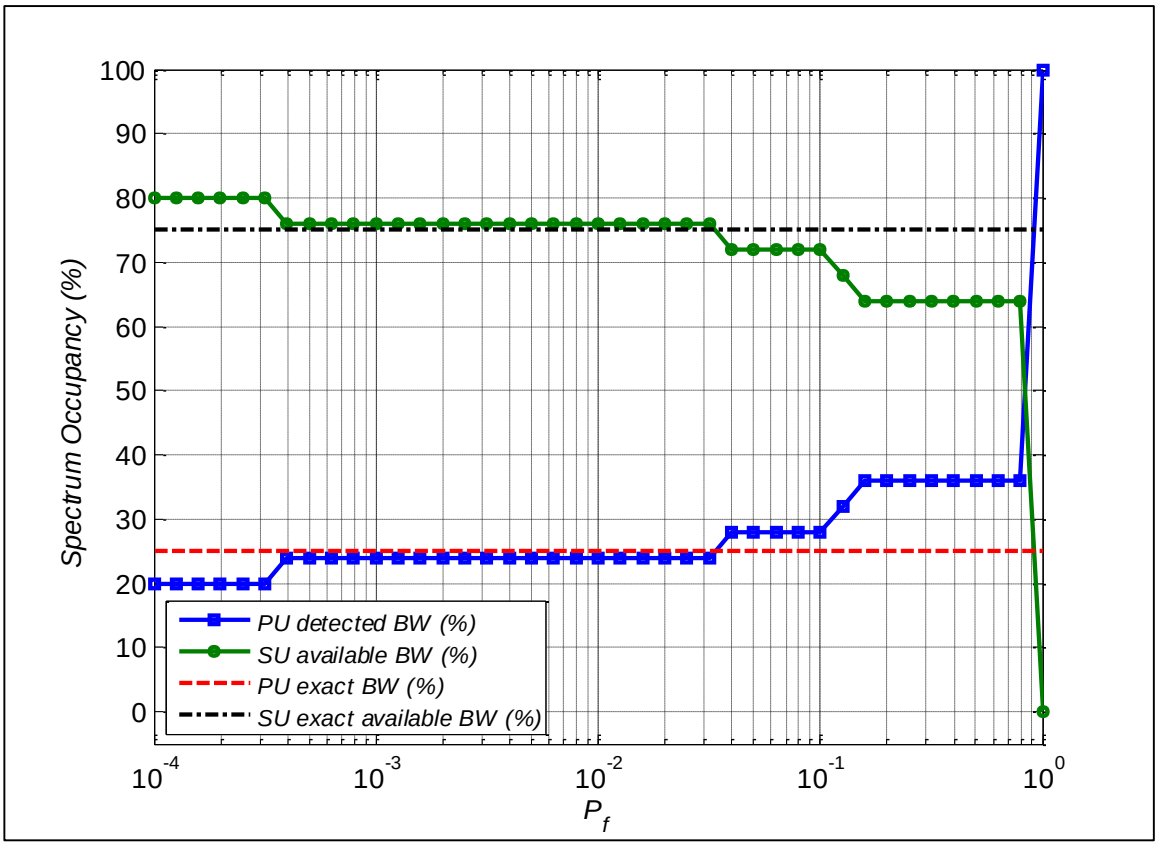

Figure 6-14: Spectrum occupancy using TBPF filterbank (case 3).

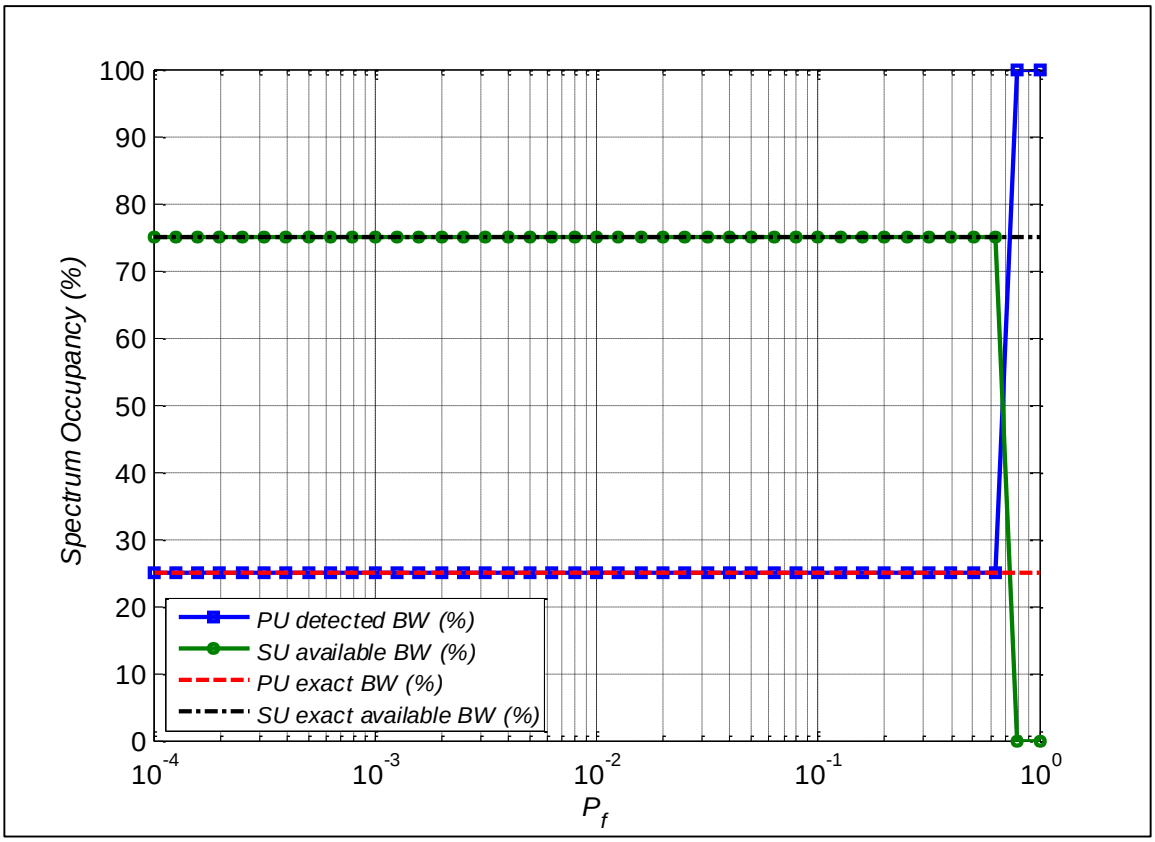

Figure 6-15: Spectrum occupancy using wavelet-based detection (case 3).

It can be concluded that the proposed wideband spectrum detection approach using wavelet-based detection outperforms the TBPF filterbank approach in terms of spectrum occupancy. At a low P_f the TBPF filterbank failed to detect the presence of the PU over the partially occupied subbands and decided that these bands were free, which caused interference to the PU from the SUs using these bands. At a high P_f the PU signal was detected, but this resulted in high spectrum under-utilization as a partially occupied band is considered as busy. However, the wavelet-based detection approach detected the PU more accurately and resulted in spectrum occupancy close to the exact one, which provides better spectrum utilization.

CHAPTER 7: CONCLUSIONS AND FUTURE WORK

In this chapter, concluding remarks are made, and the results obtained are discussed and compared. Also, recommendations for future work are suggested to extend the work presented in this thesis.

7.1 Conclusions

In this thesis, energy based narrowband spectrum sensing in a log-normal shadowing environment was investigated, and collaborative spectrum sensing under shadowing using both soft fusion and hard fusion was evaluated. In addition, wideband spectrum sensing using wavelet-based edge detection was explored.

In chapter 2, an overview of the cognitive radio concept and a summary of different spectrum sensing techniques were presented. Collaborative spectrum sensing models and the difference between narrowband and wideband spectrum sensing were highlighted. In chapter 3 narrowband non-collaborative spectrum sensing, using energy detection, was investigated in both an AWGN channel and a log-normal shadowing channel. A closed-form expression for the probability of detection in a log-normal shadowing channel based on the Gauss-Hermite integration was derived, and the accuracy of this expression was tested in a MATLAB simulation. The degradation in the sensing performance due to the presence of log-normal shadowing was obvious. Moreover, the new expression of the probability of detection under shadowing proved its accuracy in spectrum sensing. The effect of different factors on spectrum sensing, such as the average SNR of the primary user, the number of samples acquired from the signal received by the secondary user and the level of shadowing represented by the dB-spread were studied. In general, better detection of the primary user was achieved at a higher average of SNR values. However, the larger the number of samples acquired during sensing, the lower the probability of detecting the primary user in both an AWGN channel and a log-normal channel. Moreover, severe shadowing represented by higher dB-spread values resulted in worse sensing performance and less probability of detection.

Narrowband collaborative spectrum sensing was performed in chapter 4 to overcome the effect of log-normal shadowing spectrum sensing. Collaborative sensing was executed in a centralized fashion, where k spectrum sensors sense a

certain frequency band and report their sensing information to a fusion center that combines the received information and takes the final decision on the presence of the primary user within that band. The fusion center combines sensing information using either soft (data) fusion or hard (decision) fusion. In this chapter two soft fusion schemes were investigated, the square-law selection (SLS) scheme and the square-law combining (SLC) scheme. In addition, hard fusion using three combining rules: AND, OR and Majority combining was analyzed.

The improvement in sensing performance due to collaboration between secondary users was clear from the simulation results. In soft fusion, the collaborative secondary users send their measured energies to the fusion center, and the secondary user with the highest measured energy is chosen in the SLS scheme, while the energies of all secondary users are added together in the SLC scheme. It was shown that the SLC scheme outperformed the SLS scheme in terms of the probability of detection. Also, using the SLC scheme involves less computational complexity at the fusion center since it adds the energies of the secondary users together, while in the SLS the energy at each secondary user should be estimated to choose the user with the highest energy.

In hard fusion, the fusion center receives a one-bit binary decisions (1 or 0) from each secondary user, and combines the decisions using one of the three main combining rules; AND, OR and Majority. It was shown that OR-combining outperformed both AND-combining and Majority-combining by providing higher probability of detection for a certain probability of false alarm, resulting in higher protection for the primary user from the secondary user interference. However, using AND-combining provided more spectrum opportunities for the secondary users and higher spectrum utilization since it resulted in higher probability of misdetecting the primary user.

A comparison between hard fusion and soft fusion indicated that soft fusion using the SLC scheme outperformed all hard fusion combining rules with better probability of detection. However, using the SLC requires more bandwidth as the secondary user sends its measured energy, while in hard fusion a one-bit binary decision is sent to the fusion center, resulting in fewer bandwidth requirements, and lower computational complexity at the fusion center. Therefore, a trade-off between

the desired level of detection and the available resources should be done when choosing a certain combining scheme.

In chapter 5 wideband spectrum sensing was investigated, and different wideband sensing techniques were addressed. A system model for wideband spectrum sensing using wavelet-based edge detection was studied in a MATLAB simulation. The effect of the scale factor of the wavelet function and spectrum shape on edge detection was considered. Also, collaborative wideband edge detection was explored. Results indicated that better edge detection was achieved at higher scale factor values and the detection of the edges was enhanced using multiscale wavelet products. Moreover, collaboration between secondary users in edge detection improved detection performance and better detection was achieved as the average SNR of the primary user occupying the wideband spectrum increased. The performance of this system model was also tested under log-normal shadowing. The presence of log-normal shadowing resulted in degradation in edge detection performance, since it reduces the average power of the primary user signal received by the secondary user and, at the same time, it adds more random variations to the signal resulting in more false edges.

In chapter 6 two approaches for wideband spectrum detection were investigated and compared: the TBPF filterbank approach and the proposed approach using wavelet-based detection. Simulation results indicated that the proposed approach outperformed the TBPF filterbank in terms of spectrum occupancy and utilization.

7.2 Future Work

The work done in this thesis can be extended, and some suggestions for more research and future work are listed below.

7.2.1 Correlated Log-normal Shadowing

The centralized collaborative spectrum sensing model designed in chapter 4 in the log-normal shadowing channel was based on the assumption that the k collaborative spectrum sensors are i.i.d, which means that they experience i.i.d same shadowing statistics. A general system model where the spectrum sensors are not

i.i.d can be developed. Moreover, correlated log-normal shadowing can be included in the analysis.

7.2.2 Non-ideal Reporting Channel

The reporting channel used for communication between the spectrum sensor and the fusion center is assumed to be a noiseless channel. However, in reality this assumption is not accurate since this channel is subject to noise and shadowing. Therefore, this should be taken into account by introducing the probability of error over the reporting channel in the system design.

7.2.3 Effect of the Mother Wavelet Function

In chapter 5, the wavelet-based edge detection model used for wideband sensing used the Gaussian mother wavelet as the smoothing function. Other types of mother wavelet functions such as the Haar wavelet or Mexican hat wavelet can be used to study the effect of the mother wavelet types on the performance of the edge detection.

References

[1] J. Wang, M. Ghosh, and K. Challapali, "Emerging cognitive radio applications: A survey," *Communications Magazine, IEEE,* vol. 49, pp. 74-81, 2011.

[2] F. C. Commission, "Spectrum policy task force report, FCC 02-155," ed: Nov, 2002.

[3] M. A. McHenry, "NSF spectrum occupancy measurements project summary," *Shared spectrum company report,* 2005.

[4] T. Yucek and H. Arslan, "A survey of spectrum sensing algorithms for cognitive radio applications," *Communications Surveys & Tutorials, IEEE,* vol. 11, pp. 116-130, 2009.

[5] G. Ganesan and Y. Li, "Cooperative spectrum sensing in cognitive radio, part I: Two user networks," *Wireless Communications, IEEE Transactions on,* vol. 6, pp. 2204-2213, 2007.

[6] W. Zhang and K. B. Letaief, "Cooperative spectrum sensing with transmit and relay diversity in cognitive radio networks," *IEEE Trans. Wireless Commun,* vol. 7, 2008.

[7] B. Farhang-Boroujeny, "Filter bank spectrum sensing for cognitive radios," *Signal Processing, IEEE Transactions on,* vol. 56, pp. 1801-1811, 2008.

[8] B. Farhang-Boroujeny and R. Kempter, "Multicarrier communication techniques for spectrum sensing and communication in cognitive radios," *Communications Magazine, IEEE,* vol. 46, pp. 80-85, 2008.

[9] A. Feldster, Y. P. Shapira, M. Horowitz, A. Rosenthal, S. Zach, and L. Singer, "Multi-rate asynchronous sampling of bandwidth-limited signals," *arXiv preprint arXiv:0806.2039,* 2008.

[10] Y. Hur, J. Park, W. Woo, K. Lim, C.-H. Lee, H. Kim, *et al.*, "A wideband analog multi-resolution spectrum sensing (MRSS) technique for cognitive radio (CR) systems," in *Circuits and Systems, 2006. ISCAS 2006. Proceedings. 2006 IEEE International Symposium on*, 2006, p. 4 pp.

[11] M. Mishali and Y. C. Eldar, "Blind multiband signal reconstruction: Compressed sensing for analog signals," *Signal Processing, IEEE Transactions on,* vol. 57, pp. 993-1009, 2009.

[12] M. Mishali and Y. C. Eldar, "Wideband Spectrum Sensing at Sub-Nyquist Rates," *arXiv preprint arXiv:1009.1305,* 2010.

[13] Y. L. Polo, Y. Wang, A. Pandharipande, and G. Leus, "Compressive wide-band spectrum sensing," in *Acoustics, Speech and Signal Processing, 2009. ICASSP 2009. IEEE International Conference on*, 2009, pp. 2337-2340.

[14] Z. Tian and G. B. Giannakis, "A wavelet approach to wideband spectrum sensing for cognitive radios," in *Cognitive Radio Oriented Wireless Networks and Communications, 2006. 1st International Conference on*, 2006, pp. 1-5.

[15] Z. Tian and G. B. Giannakis, "Compressed sensing for wideband cognitive radios," in *Acoustics, Speech and Signal Processing, 2007. ICASSP 2007. IEEE International Conference on*, 2007, pp. IV-1357-IV-1360.

[16] K. R. Liu and B. Wang, "Cognitive radio networking and security," *A Game-Theoretic View, ISBN*, pp. 978-0, 2011.

[17] L. Lu, X. Zhou, U. Onunkwo, and G. Y. Li, "Ten years of research in spectrum sensing and sharing in cognitive radio," *EURASIP Journal on Wireless Communications and Networking*, vol. 2012, pp. 1-16, 2012.

[18] N. S. Shankar, C. Cordeiro, and K. Challapali, "Spectrum agile radios: utilization and sensing architectures," in *New Frontiers in Dynamic Spectrum Access Networks, 2005. DySPAN 2005. 2005 First IEEE International Symposium on*, 2005, pp. 160-169.

[19] S. D. Jones, E. Jung, L. Xin, N. Merheb, and I. J. Wang, "Characterization of Spectrum Activities in the U.S. Public Safety Band for Opportunistic Spectrum Access," in *New Frontiers in Dynamic Spectrum Access Networks, 2007. DySPAN 2007. 2nd IEEE International Symposium on*, 2007, pp. 137-146.

[20] J. Marinho and E. Monteiro, "Cognitive radio: survey on communication protocols, spectrum decision issues, and future research directions," *Wireless Networks*, vol. 18, pp. 147-164, 2012.

[21] H. Urkowitz, "Energy detection of unknown deterministic signals," *Proceedings of the IEEE*, vol. 55, pp. 523-531, 1967.

[22] H. Tang, "Some physical layer issues of wide-band cognitive radio systems," in *New frontiers in dynamic spectrum access networks, 2005. DySPAN 2005. 2005 first IEEE international symposium on*, 2005, pp. 151-159.

[23] P. Kolodzy, "Next generation communications: Kickoff meeting," in *Proc. DARPA*, 2001.

[24] D. B. Rawat and G. Yan, "Spectrum sensing methods and dynamic spectrum sharing in cognitive radio networks: A survey," *International Journal of Research and Reviews in Wireless Sensor Networks*, vol. 1, pp. 1-13, 2011.

[25] S. Haykin, "Cognitive radio: brain-empowered wireless communications," *Selected Areas in Communications, IEEE Journal on*, vol. 23, pp. 201-220, 2005.

[26] A. Ghasemi and E. S. Sousa, "Opportunistic spectrum access in fading channels through collaborative sensing," *Journal of communications,* vol. 2, pp. 71-82, 2007.

[27] I. S. Gradshteyn and I. M. Ryzhik, *Table of Integrals, Series, and Products*: Acamedic Press, 1963.

[28] S. Atapattu, C. Tellambura, and H. Jiang, "Energy Detection Based Cooperative Spectrum Sensing in Cognitive Radio Networks," *Wireless Communications, IEEE Transactions on,* vol. 10, pp. 1232-1241, April 2011.

[29] A. H. Nuttall, "Some integrals involving the Q_M function (Corresp.)," *Information Theory, IEEE Transactions on,* vol. 21, pp. 95-96, Jan 1975.

[30] Q. Zhao and B. M. Sadler, "A survey of dynamic spectrum access," *Signal Processing Magazine, IEEE,* vol. 24, pp. 79-89, 2007.

[31] Y.-C. Liang, Y. Zeng, E. C. Peh, and A. T. Hoang, "Sensing-throughput tradeoff for cognitive radio networks," *Wireless Communications, IEEE Transactions on,* vol. 7, pp. 1326-1337, 2008.

[32] A. Goldsmith, *Wireless communications*: Cambridge university press, 2005.

[33] A. Papoulis and S. U. Pillai, *Probability, random variables, and stochastic processes*: Tata McGraw-Hill Education, 2002.

[34] A. J. Goldsmith, L. J. Greenstein, and N. B. Mandayam, *Principles of Cognitive Radio*: Cambridge University Press, 2012.

[35] N. B. Mehta, J. Wu, A. F. Molisch, and J. Zhang, "Approximating a Sum of Random Variables with a Lognormal," *Wireless Communications, IEEE Transactions on,* vol. 6, pp. 2690-2699, 2007.

[36] M. Abramowitz and I. A. Stegun, *Handbook of mathematical functions: with formulas, graphs, and mathematical tables*: Courier Dover Publications, 2012.

[37] S. Nallagonda, S. D. Roy, and S. Kundu, "Performance of Cooperative Spectrum Sensing in Log-normal Shadowing and Fading under Fusion Rules," *International Journal of Energy, Information & Communications,* vol. 3, 2012.

[38] D. Teguig, B. Scheers, and V. Le Nir, "Data fusion schemes for cooperative spectrum sensing in cognitive radio networks," in *Communications and Information Systems Conference (MCC), 2012 Military*, 2012, pp. 1-7.

[39] F. F. Digham, M.-S. Alouini, and M. K. Simon, "On the energy detection of unknown signals over fading channels," *IEEE Transactions on Communications,* vol. 55, pp. 21-24, 2007.

[40] L. Fenton, "The sum of log-normal probability distributions in scatter transmission systems," *Communications Systems, IRE Transactions on*, vol. 8, pp. 57-67, 1960.

[41] S. C. Schwartz and Y.-S. Yeh, "On the Distribution Function and Moments of Power Sums With Log-Normal Components," *Bell System Technical Journal*, vol. 61, pp. 1441-1462, 1982.

[42] M. Fleyer, A. Linden, M. Horowitz, and A. Rosenthal, "Multirate synchronous sampling of sparse multiband signals," *Signal Processing, IEEE Transactions on*, vol. 58, pp. 1144-1156, 2010.

[43] A. P. Ying Wang, Y. L. Polo, and G. Leus, "Distributed Compressive Wide-Band Spectrum Sensing."

[44] H. Sun, "Collaborative spectrum sensing in cognitive radio networks," 2011.

[45] A. Sahai and D. Cabric, "Spectrum sensing: fundamental limits and practical challenges," in *Proc. IEEE International Symposium on New Frontiers in Dynamic Spectrum Access Networks (DySPAN)*, 2005.

List of Publications

Part of the material in this thesis was published as:

1. Nedaa Al Hussien, Mohammed Abdel-Hafez, Khaled Shuaib, "Collaborative Sensing for Cognitive Radio under Log-Normal Shadowing", accepted in the *8th IEEE GCC Conference and Exhibition (GCC 2015) - Communication & Signal Processing 4*, February 1-4, 2015, Muscat, Oman.
2. Nedaa Al Hussien, Mohammed Abdel-Hafez, Khaled Shuaib, "A Comparison of Fusion Rules for Collaborative Sensing under Log-Normal Shadowing", accepted in the *10th International Conference on Innovations in Information Technology (IIT 2014) - Intelligent and Software Systems*, November 9-11, 2014, Al Ain, United Arab Emirates.